ERDA/JPL-954614-77/1
Distribution Category UC-63

LIFETIME AND DIFFUSION LENGTH MEASUREMENTS ON SILICON MATERIAL AND SOLAR CELLS

Final Report

16 December 1976 – 31 October 1977

by
Siegfried Othmer and Susan C. Chen

for
JET PROPULSION LABORATORY
Pasadena, California

Contract No. 954614

This work was performed for the Jet Propulsion Laboratory, California Institute of Technology, under NASA Contract NAS7-100 for the U.S. Energy Research and Development Administration, Division of Solar Energy.

The JPL Low-Cost Silicon Array Project is funded by ERDA and forms part of the ERDA Photovoltaic Conversion Program to initiate a major effort toward the development of low-cost solar arrays.

NORTHROP RESEARCH AND TECHNOLOGY CENTER
One Research Park
Palos Verdes Peninsula, CA 90274

NRTC 77-42R

Distribution Category UC-63
ERDA/JPL-954614-77/1

LIFETIME AND DIFFUSION LENGTH MEASUREMENTS ON SILICON MATERIAL AND SOLAR CELLS

Final Report

16 December 1976 – 31 October 1977

by
Siegfried Othmer and Susan C. Chen

for
JET PROPULSION LABORATORY
Pasadena, California

Contract No. 954614

This work was performed for the Jet Propulsion Laboratory, California Institute of Technology, under NASA Contract NAS 7-100 for the U.S. Energy Research and Development Administration, Division of Solar Energy.

The JPL Low-Cost Silicon Solar Array Project is funded by ERDA and forms part of the ERDA Photovoltaic Conversion Program toward the development of low-cost solar arrays.

NORTHROP RESEARCH AND TECHNOLOGY CENTER
One Research Park
Palos Verdes Peninsula, California 90274
(213) 377-4811

ABSTRACT

Experimental methods were evaluated for the determination of lifetime and diffusion length in silicon intentionally doped with potentially lifetime-degrading impurities found in metallurgical grade silicon, impurities which may be residual in low-cost silicon intended for use in terrestrial flat-plat arrays. Results obtained by these methods were compared for mutual consistency. Lifetime measurements were made using a steady-state photoconductivity method, which was compared with a photoconductivity decay technique. Diffusion length determinations were made using short-circuit current measurements under penetrating illumination. This method was compared with a direct measurement of diffusion length using a scanning electron microscope. Mutual consistency among all experimental methods was verified, but steady-state photoconductivity was found preferable to photoconductivity decay at short lifetimes and in the presence of traps. The effects of a number of impurities on lifetime in bulk material, and on diffusion length in cells fabricated from this material, were determined. Results were compared with those obtain by others on the same material and devices using different techniques. General agreement was found in terms of the hierarchy of impurities which degrade the lifetime

TABLE OF CONTENTS

CONTENTS (Continued)

LIST OF ILLUSTRATIONS

ILLUSTRATIONS (Continued)

LIST OF TABLES

SECTION 1.0
INTRODUCTION

The diffusion length is one of the fundamental parameters governing the quality of a solar cell in that it determines the effective collection volume for generated carriers in the neutral bulk of the cell. The corresponding quantity in the time domain is the minority-carrier recombination lifetime, which is related to the diffusion length via the carrier mobility. Among the factors which govern solar cell efficiency, the diffusion length is the one most sensitive to the quality of the material, in terms of both crystal imperfections and concentrations of certain impurities.

The purpose of this program was to perform measurements of minority-carrier recombination lifetime in bulk silicon, and diffusion length in solar cells fabricated from the same material, in order to assess the sensitivity of these parameters to the presence of certain intentional dopant impurities. The set of impurities chosen was that found in metallurgical grade silicon as well as other elements which are likely to be residual in the silicon production and purification processes being considered in the materials task of the Low-cost Silicon Solar Array (LSSA) Project.

A number of different techniques were required to cover the ranges of material resistivity and lifetime anticipated, and the initial task under this contract consisted of verifying their mutual consistency. Minority-carrier lifetime was determined using the method of transient photoconductivity decay (PCD) as well as steady-state photoconductivity (SSPC). Diffusion lengths were determined on solar cells and other test structures by means of short-circuit current measurements using either point-source excitation from a scanning electron microscope or uniform generation derived from a Co^{60} gamma source or bandedge light.

The photoconductivity decay method is attractive in that it yields the minority-carrier recombination lifetime directly by monitoring the return to equilibrium of an excess minority-carrier population. Its simplicity has led to its exclusive use in several exhaustive studies of lifetime as it is affected

by radiation-induced defects Such studies have yielded successful characterization of recombination centers In the presence of traps, however, the decay of photoconductivity may not be governed by the recombination process, but rather by the "detrapping" time In that event, a measurement under a single set of experimental conditions at a single temperature may be insufficient to establish whether the observed decay time is in fact indicative of recombination rather than trapping This feature constitutes the principal shortcoming of the PCD method Ameliorative strategies will be discussed further in Section 2 3 of this report.

Lifetime may also be determined by means of the conductivity change induced by a steady-state excitation, the duration of which is much longer than the lifetime so that carrier populations are in equilibrium This technique is attractive for the case of low resistivity and short lifetime where the PCD method may suffer from inadequate signal-to-noise ratio due to the limited conductivity change which can be induced with the available generation rate. A disadvantage of the method is that a number of parameters determine the relation between steady-state photoconductivity signal and carrier lifetime, and all of these have to be determined for each sample with precision The susceptibility of the technique to the effects of trapping constitutes both a limitation and an asset, vis-a-vis the PCD technique, as will be discussed in Section 2 3. The experimental implementation of the steady-state photoconductivity technique which was used in this program has been employed previously in a study of radiation effects on solar cells and frequent reference will be made to that work [1, 2]

Diffusion lengths were determined on devices principally by using penetrating light to effect uniform carrier generation throughout the semiconductor Short-circuit current measured under such conditions is related to the diffusion length in a simple way The generation rate prevailing under experimental conditions was determined by comparison with the known generation rate of a Co^{60} gamma source An independent check on the Co^{60} value of diffusion length was provided by direct measurement of this quantity using a scanning electron

microscope. Consistency was found between these two methods. This is discussed in Section 3.1. With confidence established in the diffusion length measurement methods, comparison of diffusion length and lifetime methods was also of interest. After determination of the diffusion length, junctions were removed from several solar cells and the lifetime measured via PCD. Reasonable agreement was obtained. These same cells were therefore used to determine the generation rate prevailing in the SSPC technique, as discussed in Section 2.5.

Results of SSPC and diffusion length determinations for silicon doped with various impurities, supplied to us from Westinghouse and Monsanto, are presented in Section 4.0. Implications of these results for the LSSA materials task and suggestions for future studies are addressed in Section 4.3.

SECTION 2.0
EXPERIMENTAL PROCEDURES

2.1 PHOTOCONDUCTIVITY DECAY

In the PCD technique, the exponential decay time of an excess carrier population is monitored directly. In our implementation, excess carriers are produced by means of a Field Emission flash x-ray of 100 or 150 keV energy. This energy is sufficiently high that generation is reasonably uniform throughout the sample. The available dose is on the order of 1 rad(Si) (1 rad = 100 ergs/gm). Pulse duration is on the order of 50 ns. Significantly, there is no "tail" in the pulse waveform so that short lifetimes can in principle be measured. The induced conductivity change is monitored on a storage scope under constant-current conditions. Sample bias is maintained sufficiently low to avoid carrier sweepout, in the case of long lifetimes, and sufficiently low to avoid sample heating in the case of low-resistivity samples. Constant-current conditions are assured by use of a series resistor which is larger than the sample resistance by a factor of about 100.

The photoconductivity decay transient is complicated by the presence of the surface, the effect of which is expressed in terms of a surface recombination velocity. This gives rise to a net enhanced recombination rate, particularly at early times following a pulse. Quantitative determinations of the decay times must therefore await the dissipation of these higher spatial modes of the recombination process. In practice, the criterion that the lowest spatial mode is being observed is simply that the decay be exponential. The effect of the surface in this mode yields an effective lifetime, as described in Section 2.4. A second consideration is that observation take place under low-injection condition since the lifetime is in general dependent on injection level above a certain level. In practice, measurements are made in the range of $\Delta\sigma/\sigma = 10^{-3}$, and extending down to the level where signal-to-noise ratio or trapping effects are limiting. The finding of exponential decays over more than a decade in dynamic range is taken as evidence that the low-injection limit of lifetime is being observed.

In the present study, the PCD method served principally as a calibration tool for the SSPC technique, which was employed in the bulk of the measurements. The generation rate g prevailing in SSPC was taken to be that which yielded the same lifetime as had been measured via PCD. As long as the fundamental spatial mode is observed in PCD, the effect of the surface is assumed to be the same in both the transient and steady-state measurements, and is thus irrelevant insofar as the determination of generation rate is concerned. This g-determination will be discussed in Section 2.5 following a description of the SSPC method.

2.2 STEADY-STATE PHOTOCONDUCTIVITY TECHNIQUE

The steady-state photoconductivity method was the standard method employed in this study for determination of lifetime. It is based on the relationship of steady-state excess carrier density Δn to lifetime of $\Delta n = g\tau$, where g is the generation rate. Δn was determined experimentally under constant-current conditions, for which the following equation holds

$$\Delta n = \frac{\Delta V}{e V_o \sigma (\mu_e + \mu_h)} . \qquad (1)$$

Here V_o is the voltage drop across the illuminated portion of the sample, ΔV the voltage change in the presence of generation rate g, and the other quantities have their usual meaning. $\Delta V/V_o << 1$ is assumed.

The experimental apparatus has been described previously.[2] It employs penetrating light for relatively uniform excitation. The light is derived from an incandescent source and passed through a silicon filter which is much thicker than the sample so that only relatively penetrating light reaches the sample. A Corning 7-57 prefilter is employed to keep the silicon filter from heating up. It is critical for the maintenance of g-calibration that the sample and silicon filter are maintained at the same temperature so that the bandgap, and thus the wavelength dependence of absorption coefficient, is the same in both. (The question may be raised here as to whether this condition is in fact met when the resistivity of the sample differs greatly from that of the filter.

It was previously demonstrated[2] that the generation rate is independent of resistivity down to 0.1 Ω-cm (p-type) at a minimum. This covers the range of resistivities of the present samples.)

To facilitate detection, the light was chopped at a frequency (277 Hz) much lower than the reciprocal lifetime, and the signal was coherently detected using an Ithaco 395 lock-in amplifier. Signal recovery capability was enhanced by employing a transformer (Triad geoformer G-10) for noise-free gain of a factor of about 100 and an approximate impedance match to the sample. The circuit is shown in Figure 2-1. For Westinghouse samples, which were typically in the 3 to 5 Ω-cm range, a geoformer input impedance of 277 Ω was employed (voltage gain including amplifier was 454), whereas for Monsanto samples, which were typically about 0.5 Ω-cm, 66-Ω input impedance was used (and corresponding voltage gain was 910). The light amplitude was monitored by means of a PIN diode optimized for long-wavelength detection (EGG SGD-40), and this signal was likewise phase-sensitively detected (Ithaco 391

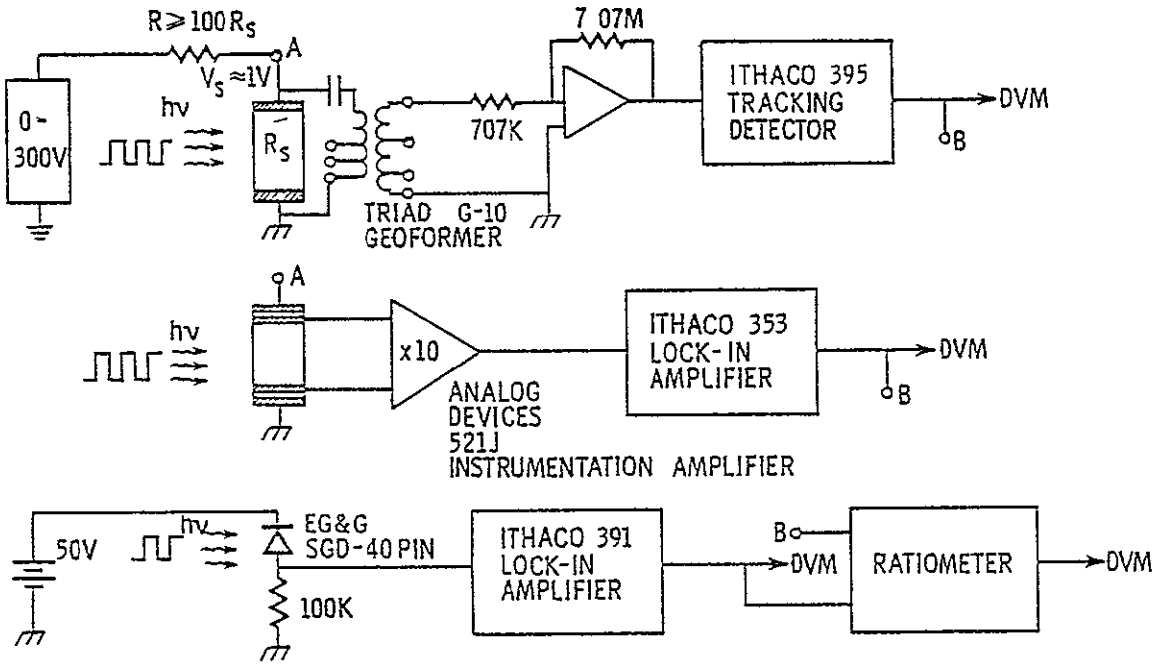

Figure 2-1. Schematic representation of the signal recovery electronics of the steady-state photoconductivity (SSPC) experiment. Two alternative methods are shown, one using a 2-point measurement method optimized for low-noise signal recovery, and a second one using a 4-point method for immunity to contact effects.

lock-in). The experimental arrangement is illustrated schematically in Figure 2-2. The incandescent lamps (55C3) shown within the sample chamber are used to provide dc background light of an intensity sufficient to fill traps so that these do not contribute to the conductivity modulation. This is discussed further in Section 2.3.

The generation rate employed for all measurements was determined to be 8.1×10^{16} cm^{-3} sec^{-1} (see Section 2.5). A 1-μs lifetime, then, would give rise to an excess density Δn of about 10^{11} cm^{-3}. For 3.5 Ω-cm p-type material and an applied voltage of 1V, the observed ΔV would be about 40 μV and the injection ratio $\Delta n/p_o$ would be about 2×10^{-5}.

Tractability of the experimental method required that a fixed generation rate be used for all samples. Prudence further required that the lamp be operated conservatively for stability. Hence, the maximum generation rate which could be achieved in this experiment was necessarily quite limited. If it is merely required to establish the low-injection-level limit of the carrier lifetime, then this is of little concern as long as the light intensity is sufficient from the standpoint of signal-to-noise considerations. In the present program it was also of interest to observe the injection level dependence of lifetime by performing measurements at three different injection levels. Since the injection level scales directly with lifetime under conditions of constant generation

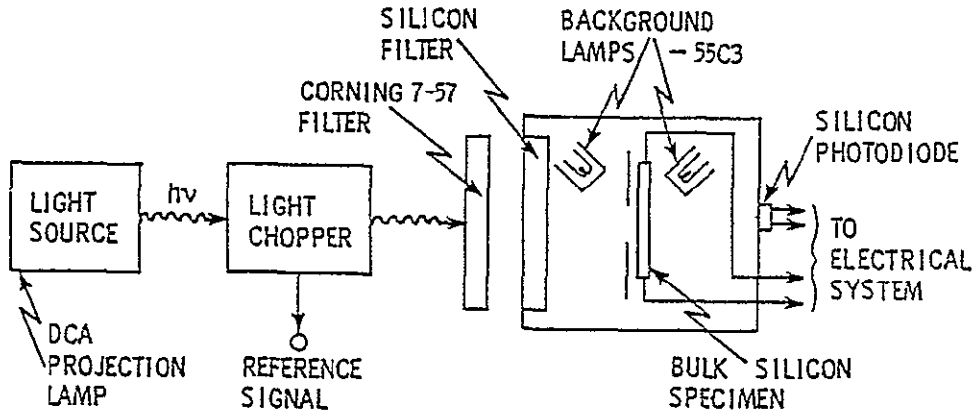

Figure 2-2. Schematic representation of the steady-state photoconductivity apparatus employed to measure minority-carrier lifetime in bulk silicon specimens.

rate, the maximum generation rate which could be achieved in our apparatus was insufficient in the case of low lifetimes to reveal any injection-level dependence. Nevertheless, measurements were made on all samples with generation rates which bracketed the standard value, with ratios of 1.93 and 0.50 with respect to that value. Even in the case of low lifetimes this was useful in that it served to confirm the value measured under standard conditions.

The samples to be measured under this program had already been characterized by other contractors of the LSSA project via the PCD technique. To make the comparisons with our own determinations most meaningful, therefore, it was desirable to avoid any sample processing whatever which might change the lifetimes. Since even moderate heat treatment is known to be capable of affecting the carrier lifetime, an effort was made to employ deposited contacts in an unsintered state. The experimental method just outlined was therefore modified to make it insensitive to the expected high contact resistance. An instrumentation amplifier of 10^9-Ω input impedance and high common mode rejection was employed to measure the conductivity modulation signal at two voltage probes which were provided in addition to the current-carrying contacts. This configuration is also illustrated in Figure 2-1.

The evaporated aluminum contacts were found to exceed the sample resistance by about three orders of magnitude at a sample bias of 1V, being on the order of 10^5 to 10^6 Ω. The contact resistance was also found to be extremely photosensitive. Over the range of background light intensity available, the resistance varied over an order of magnitude under conditions of constant sample voltage (1V), and over four or more orders of magnitude under constant current conditions. No significant improvement in these respects was found when contact evaporation followed immediately upon etching of the sample surface to remove the native oxide layer. Samples were prepared for us in this way by JPL.

SSPC measurements were attempted with contacts under as-evaporated conditions Even with the voltage probes ostensibly shielded from the chopped

light, the observed signal was dominated by modulation of the contact resistance. A second test was performed with the current-carrying contacts made ohmic by ultrasonic soldering. Under these conditions, the signal resulting from contact resistance modulation was of magnitude comparable to that of the desired signal. If it is recognized that the sample conductivity modulation is on the order of one part in 10^5, whereas the contact resistance modulation may exceed a factor of 10^2 under the same illumination (direct), then it is clear that even a small amount of scattered light to the region of the voltage contacts can compromise the results. The attempt to use unsintered evaporated contacts was therefore abandoned and the decision made to return to the use of conventional ultrasonically soldered contacts. Since the additional complexity of the 4-point measurement scheme no longer offered compensating advantages, it was abandoned simultaneously in favor of the orginal 2-point measurement method. However, the use of such a contact geometry, in which contacts were soldered to the top, or broad, surfaces of the samples rather than on the end surfaces, does raise a question as to the effective electrical length of the sample, for purposes of determining the applied voltage across the illuminated portion of the sample.

The effective electrical length of the samples was determined by resistivity profile in a number of specimens. A typical profile is illustrated in Figure 2-3. In obtaining such profiles, a digital voltmeter of greater than 10^{10} Ω input impedance was used and a 1V bias was established across the sample, as in the actual lifetime measurements. The effective electrical length was found not to differ significantly from the true length of the sample, and therefore the voltage across the illuminated portion was given simply by the applied sample voltage and the ratio of illuminated length (1.067 cm) to total sample length (2.00 cm). The sum of carrier mobilities was taken to be 1700 cm^2/V-sec in the case of the higher-resistivity Westinghouse samples, and 1150 cm^2 in the case of the lower-resistivity Monsanto specimens. These values were derived from Gartner,[3] and were not independently checked.

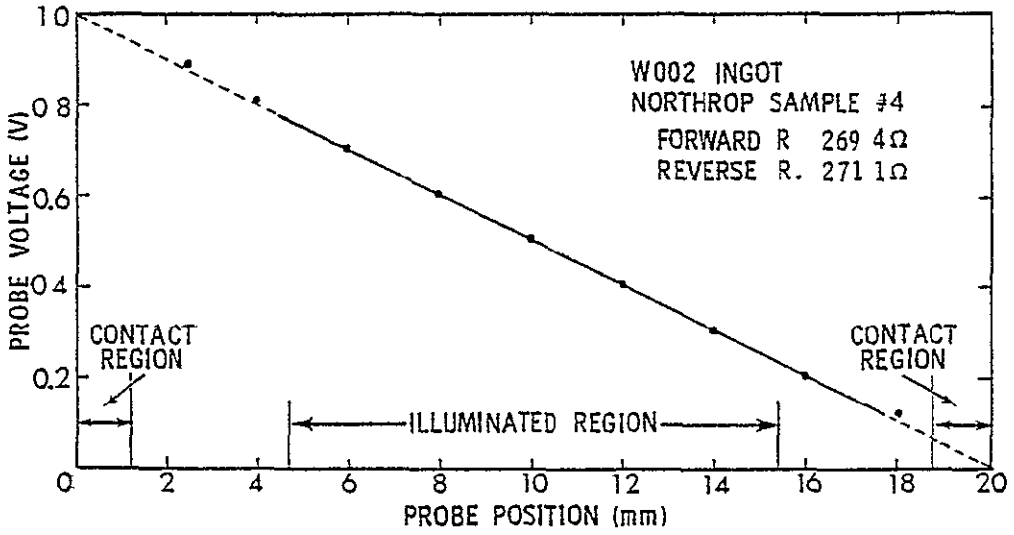

Figure 2-3. Resistivity profile of a standard-geometry 1 x 2 cm sample showing the effective electrical length of the sample and the region of illumination.

The resistivity of all samples was determined in two ways. A 4-point probe measurement was made, corrected for the prevailing sample geometry of 1 x 2 cm^2, and the resistivity was also determined from the measured sample resistance, together with the sample dimensions. The average of these two values was used to determine Δn (Eq.(1)).

It is clear from the above that there are numerous sources of independent error in the SSPC method and that its utilization has to be justified on grounds other than directness and simplicity. The justification in fact rests on the higher signal recovery capability afforded by a CW technique as opposed to a pulse technique, a factor which becomes important at low resistivities and at the low lifetimes that we expected to encounter. An additional justification, however, lies in the steady-state response in the presence of traps, and to this topic we now turn our attention.

2.3 THE EFFECT OF TRAPS ON THE PCD AND SSPC LIFETIME MEASUREMENT METHODS

All photoconductivity methods of determining carrier lifetime may be influenced by the presence of traps. As minority carriers are trapped, to be subsequently released to the minority-carrier band prior to recombination,

this temporarily fixed charge is compensated by majority carriers, thus enhancing the local conductivity. In the case of PCD, the measured decay time may be affected by a detrapping time which is on the same order of magnitude as the lifetime. Alternatively, the decay time may be completely determined by a trapping process and not by the carrier recombination lifetime at all. In the former case, the decay is generally observed to be nonexponential. A potential remedy in this case is to fill traps by the application of a steady background light of an intensity just sufficient to yield an exponential decay. In the event that the observed decay time is completely dominated by a single trapping process, the decay will be observed to be quite exponential, thus giving no evidence that the recombination lifetime is not being observed. The effect of background light in this case would be to change the amplitude of the observed pulse rather than the time constant of the decay. A remedy for this state of affairs would be to extend measurements over a range of experimental conditions, such as temperature and injection level, which would reveal unambiguously whether trapping or recombination is being observed. However, if measurement is restricted to a single set of experimental conditions, a certain ambiguity must remain. Whether this is a significant limitation on the utility of room temperature lifetime measurements for present purposes should be resolved by the present work in that it facilitates comparison of measurements performed by various contractors using techniques which differ in their susceptibility to trapping. We now address the effect of trapping on steady-state methods.

The SSPC technique is in one sense more profoundly influenced by trapping than transient methods. If one considers a trap population characterized by long detrapping times, for example, then this would result simply in a baseline offset in the case of transient decay, whereas in the steady-state method it would contribute far more to the observed conductivity modulation than some short recombination lifetime. The use of background light to fill traps is therefore crucial in the case of steady-state methods since such traps appear to be ubiquitous in samples of the present study and in previous work.[2]

The typical response observed in SSPC as a function of background light intensity is illustrated in Figure 2-4 A plateau in the response is reached at high light intensities and this is taken to be the conductivity modulation which arises strictly from the recombination process The virtue of the SSPC technique vis-a-vis PCD with regard to trapping is that this direct experimental test of the influence of traps is available In every case, the SSPC measurement was performed as a function of background light level in order to determine the plateau region If the background light intensity were to be increased significantly beyond this region, the injection-level dependence of lifetime would assert itself and the observed signal would once again increase (typically, though not necessarily)

The effect of trapping on steady-state photoconductivity has previously been treated in certain special cases [4] An example is illustrated in Figure 2-5

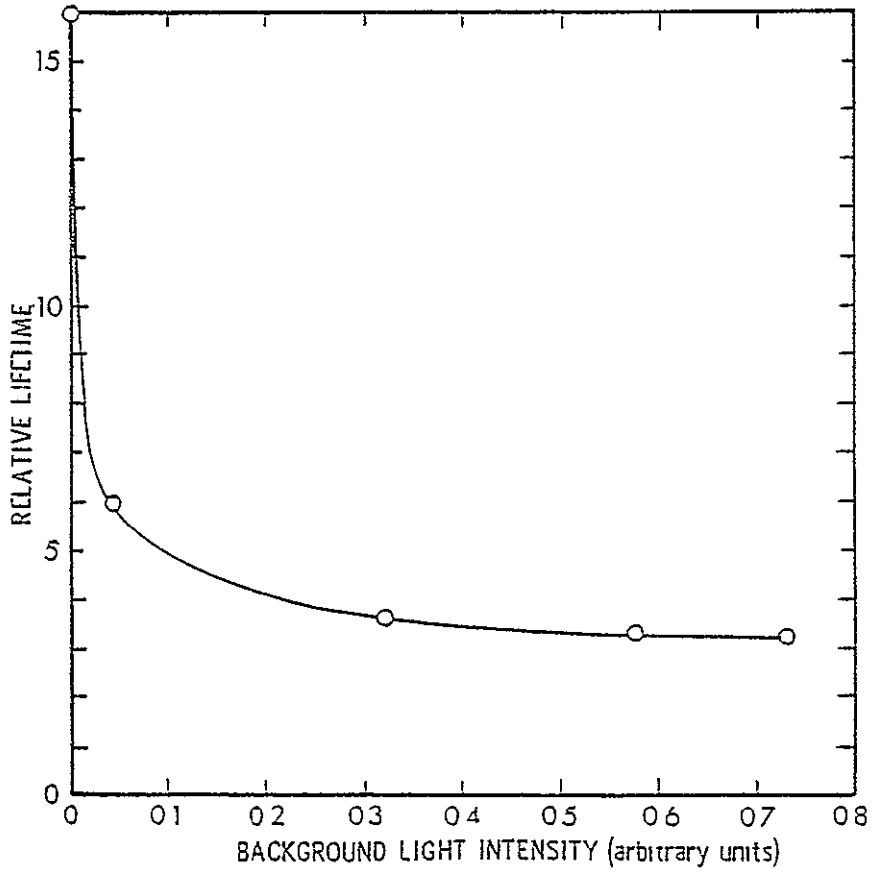

Figure 2-4 Conductivity modulation amplitude (SSPC signal voltage) as a function of background light intensity A plateau region is observed at high intensities which is taken to be the modulation arising from the recombination process

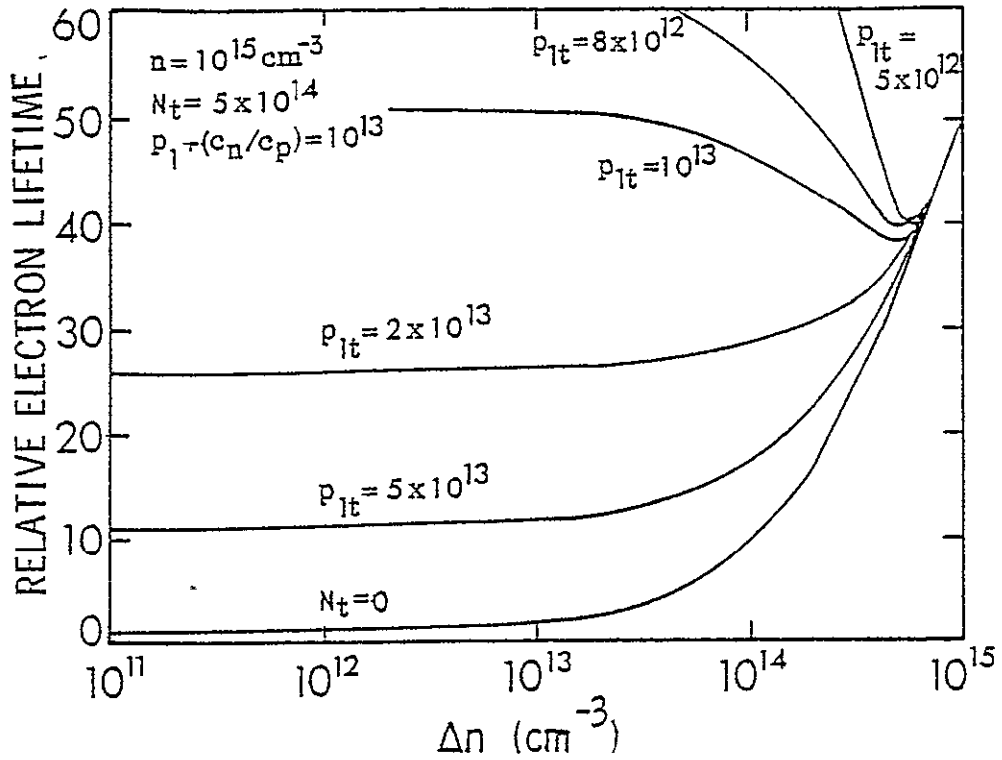

Figure 2-5 Theoretical dependence of steady-state photoconductivity lifetime in the presence of traps for various trap energy levels (from Ref 4) The parameter p_{1t} is the hole concentration which would prevail if the Fermi level were coincident with the trap energy level.

Here the electron lifetime which would be observed in the presence of a single trap level is shown as a function of injection level for several positions of the trap energy level. The quantity p_{1t} is the hole concentration which would exist if the Fermi level were at the trap energy level position The profound effect of the trap on relative lifetime is apparent Present experimental conditions are intended to yield the lifetime which would prevail in the absence of traps, i e , the curve for $N_t = 0$ The intensity which is required to accomplish this may, however, entail an injection level which is too high to yield the low-injection level limit of lifetime Rigorous treatment would therefore require full characterization of the recombination process, in terms of injection level and of temperature Ambiguities must remain if measurements are restricted to single set of experimental conditions In the present case, a protocol of measurement was decided upon in which three intensities of chopped light were employed to reveal injection level effects This is sufficient if in fact the chopped light, rather than the background light, governs the injection level

2.4 THE EFFECT OF SURFACE RECOMBINATION ON LIFETIME MEASUREMENTS

The existence of a high surface recombination velocity can have profound influence on the measured lifetime for sample geometries employed in the present program (sample thicknesses ranging from 0.022 to 0.034 cm). The surface recombination velocity therefore has to be determined and suitable corrections applied. In past studies of minority-carrier lifetime, it has been our experience that etched samples exhibit unstable surfaces. Sandblasted surfaces, by contrast, were found to yield a stable, high surface recombination velocity, and such surfaces were generally used. In the current program it was of interest to maintain surface conditions (polished and etched) unchanged from those which existed at the time that the samples were characterized by the other contractors involved in this aspect of the materials study (Westinghouse and Monsanto). This required that we make an independent determination of the surface recombination velocity for such surface treatment.

For the sample geometries employed in this study, the thickness is considerably less than the other dimensions and the only one comparable to the diffusion length. Consequently, a one-dimensional treatment of diffusion toward a surface is adequate. The relationship which holds between measured (effective) lifetime, bulk lifetime, and diffusion length L is given by

$$\tau_{eff}/\tau = \left[1 - \frac{(sL/DT)\sinh(T/L)}{(1/L)\sinh(T/L) + (s/D)\cosh(T/L)}\right]. \qquad (2)$$

where s is the surface recombination velocity, T the half-thickness of the sample, and D the diffusivity.[5] This equation was employed to find L and τ for a given value of τ_{eff} using a programmable calculator. The relationship may be illustrated graphically for a typical value of s, as shown in Figure 2-6 for a typical sample thickness. It is apparent that for even moderate lifetimes the effect of the surface is dramatic. For example, an experimental uncertainty of ±10% in a measured lifetime of 2.5 μs implies an uncertainty of +25%, -17% in the actual lifetime of 10 μs, under the conditions given in the figure. The importance of having stable, reproducible surface conditions is apparent.

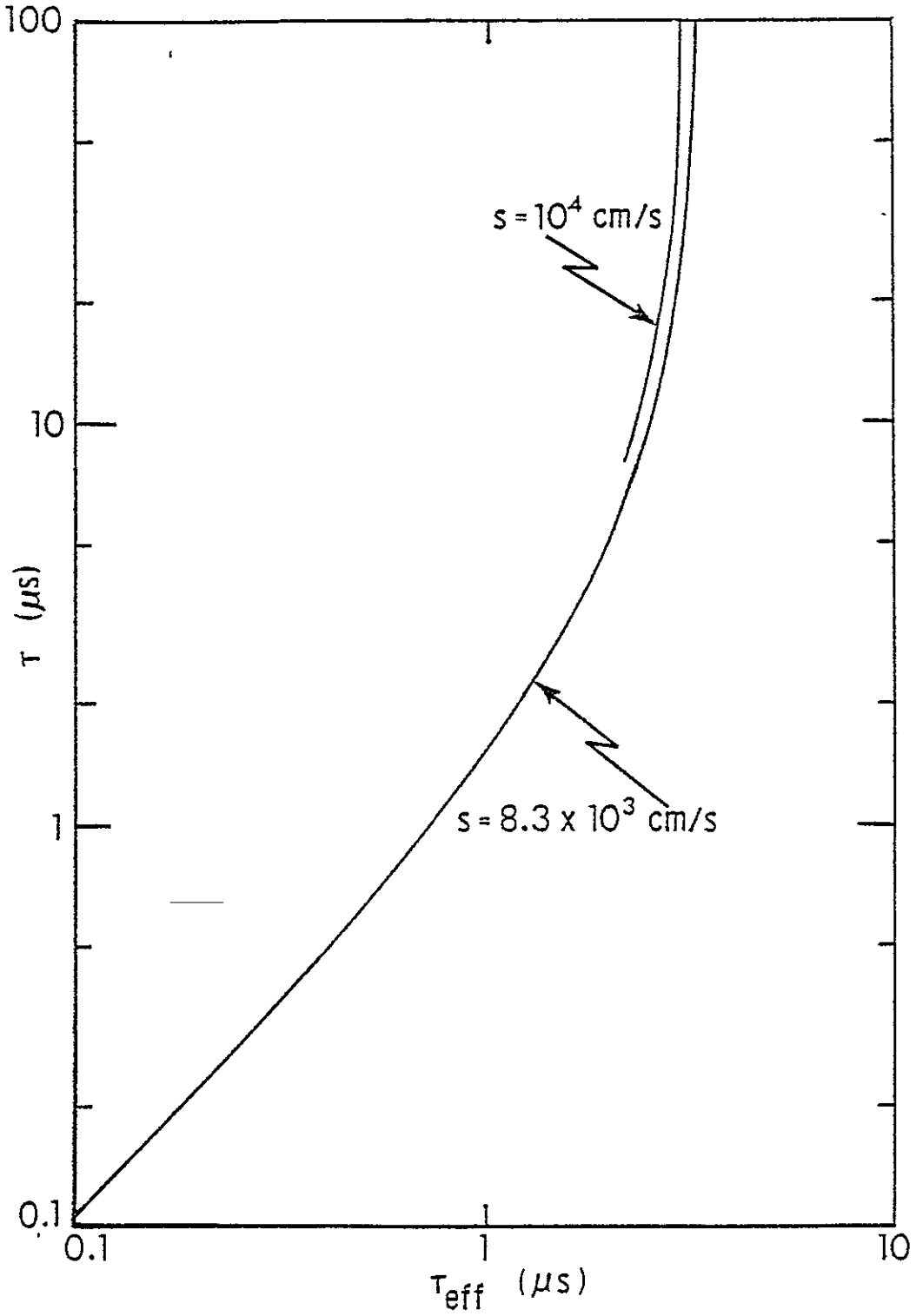

Figure 2-6. Relationship of measured lifetime (τ_{eff}) to bulk lifetime for a sample of 260 μm thickness and of given surface recombination velocity.

The most desirable way of determining the surface recombination velocity is to start with a sample of known long lifetime and to examine it under conditions in which the surface dominates. This avenue was not open to us since we were not in a position to reproduce others' surface treatments. Instead, we employed an indirect approach in which certain samples were sandblasted and effective lifetimes before and after the treatment were compared. Since the surface recombination velocity had been previously established for sandblasted surfaces,[2] this comparison would permit the appropriate value for the initial surface condition to be derived. The PCD method was used since the generation rate applicable in SSPC would be affected by the sandblasting. Results for two Westinghouse specimens from the undoped ingot W002 are shown in Table I.

Table I. Photoconductivity lifetime measurements on baseline Westinghouse samples to determine effect of sandblasting on surface recombination velocity. Two independent measurements are shown for each sample.

Sample Designation	Photoconductivity Decay Lifetime (μs)		
	Prior to Sandblasting	Sandblasted One Side	Sandblasted Both Sides
W002 Sample #4	2.37	2.51	2.42
	2.54	2.57	2.54
W002 Sample #7	2.19	2.31	2.16
	2.25	2.31	2.16

No systematic changes in PCD lifetime were observed outside the range of experimental uncertainty. The implication is that the surface recombination velocity is substantially the same in the two cases. Specifically, we have assumed a value of 8.3×10^3 cm/sec for our sandblasted surfaces, on the basis of the earlier work.[2] The probable error in the lifetime measurements above, namely about 2%, corresponds to a range in s of 7.8 to 8.9×10^3 cm/sec. If we assume a 10% uncertainty in the assumed value of s for sandblasted surfaces, then the range in s which would be consistent with the above measurement

is 7.4 to 9.3 x 10^3 cm/sec, or ±12%. This range encompasses the value of 9 x 10^3 cm/sec determined by the Westinghouse group for their samples.[6]

A check on the value of s is available a posteriori in that all the measured lifetimes must be less than or equal to the "surface lifetime", i.e., that lifetime at which the τ vs. τ_{eff} curve diverges. This test merely places an upper bound on the possible values of s. A more refined test of the appropriateness of the determination of s may be based on the expectation that calculated bulk lifetimes, based on measured effective lifetimes, should be uncorrelated with the sample thickness, whereas the existence of any error in s, or in the generation rate, should manifest itself in finite correlation. Such a statistical analysis of the data was performed and the resulted are presented in an Appendix.

2.5 DETERMINATION OF THE GENERATION RATE IN STEADY-STATE PHOTOCONDUCTIVITY

The generation rate prevailing in the SSPC technique may be determined most effectively by simply defining it to be that which yields the correct lifetime for a sample of known lifetime, as determined via PCD. Calibration samples are preferably made from material that has been fully characterized and found to be unaffected by trapping at room temperature. Such a calibration had in fact already been performed,[1] but it referred to the case of sandblasted surfaces, which yield a different generation rate than polished surfaces. Consequently, we decided to employ the actual samples for determination of of the generation rate. Westinghouse baseline material from ingot W002 was used. In retrospect, this was not a good choice for the purpose since that ingot exhibited considerable trapping. However, the study turned out to be illuminating for that very reason.

The samples exhibited nonexponential decays in PCD, indicative of a distribution of trapping time constants, or of trapping on the time scale of the lifetime. To suppress the trapping contribution, background lights of the same type as those employed in the SSPC fixture were added to the experimental

apparatus. The light intensity was adjusted until quite exponential decays were observed. The decay was monitored over more than two decades in dynamic range. Typical data, taken on one of the baseline comparison standards, are shown in Figure 2-7. At the highest signal levels, the decay constant is somewhat reduced due to the presence of the higher spatial modes, whereas at the highest sensitivity, a slight increase in decay constant is observed, presumably due to residual trapping. Decays were not always observed to be exponential to this degree; however, it was found that if the light intensity was further increased, an undershoot in the waveform would appear, indicative of a suppression of conductivity below the quiescent value. Such negative photoconductivity has been seen before by others, and is explanable in terms of multiple trap energy levels, under the influence of extrinsic excitation, as discussed by Milnes.[7] Despite the fact that excitation is both extrinsic and intrinsic in the present case, the same explanation is presumed to hold. Operationally, the light intensity was increased until the trace was found to be exponential, or to the limit consistent with a good baseline.

Data were taken in this way on several samples from the same ingot (W002). Some confirmation was desirable, however, that the data obtained were unaffected by the presence of trapping. For this reason, measurements were made on two of the samples over a range of temperatures. It was anticipated that trapping would influence the two measurements differently, so that correspondence of the respective temperature dependences would confirm the absence of trapping effects on the measured values. The SSPC apparatus had never been employed previously for absolute lifetime measurements as a function of temperature so it was necessary as a preliminary task to determine the temperature dependence of the generation rate. This temperature dependence arises from the fact that the absorbed light intensity is determined by the product of the filter spectral transmittance and the sample absorptance. This product is nonvanishing only near the bandedge and it is extremely sensitive to any changes in the wavelength dependence of the absorption coefficient in that range.

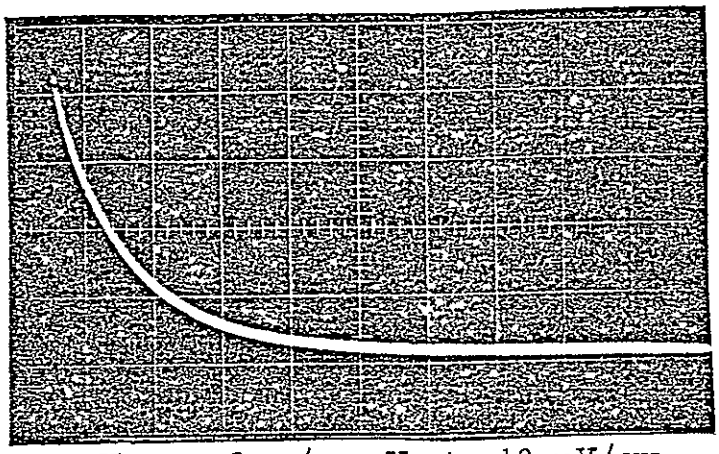

Horiz.: 2 μs/cm, Vert.: 10 mV/cm

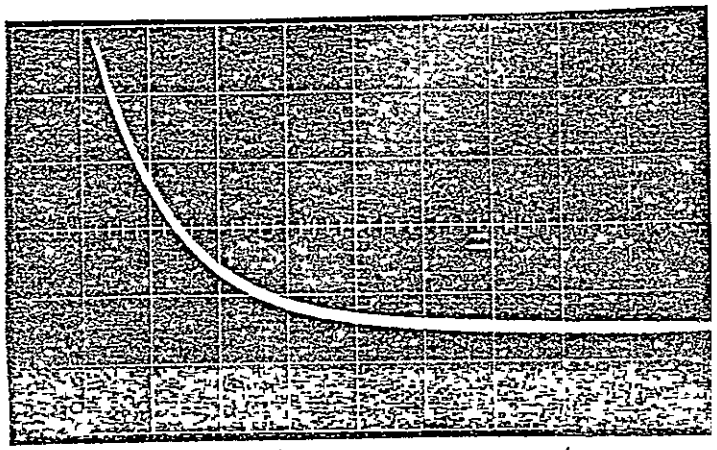

Horiz. 2 μs/cm, Vert. 5 mV/cm

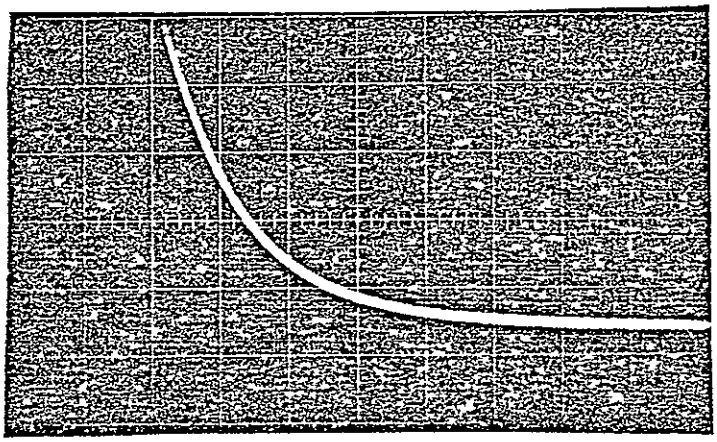

Horiz. 2 μs/cm, Vert. 2 mV/cm

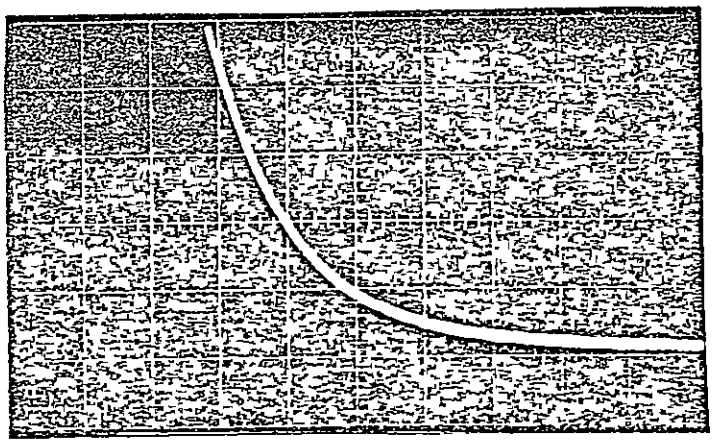

Horiz. 2 μs/cm, Vert. 1 mV/cm

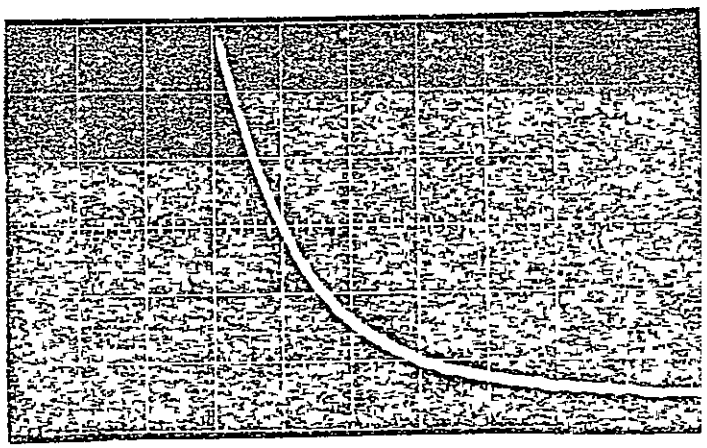

Horiz. 2 μs/cm, Vert. 0.5 mV/cm

Figure 2-7. Photoconductivity decay response under constant current conditions for baseline Westinghouse sample. Sample voltage 4.2V.

The generation rate temperature dependence was determined by means of a PIN diode placed inside the temperature-controlled sample chamber. In preface to this, the temperature dependence of generation rate was determined for the PIN diode which normally monitors the light transmitted through the sample chamber and which remains at room temperature. The results could be fitted empirically with an exponential which could be expressed in terms of an equivalent activation energy (ΔE) in the form

$$g(T) = g_o \exp(\Delta E / kT), \qquad \text{where } \Delta E = 0.084 \text{ eV}.$$

The observed ΔE of 0.084 eV places an upper limit on the temperature dependence of the generation rate which would prevail for a sample held at the same temperature as the filter.

The direct measurement of the generation rate temperature dependence was performed with the same type of PIN diode (EG&G SGD-40) as used above. Results of this determination are shown in Figure 2-8. The number of data points are minimal because of long thermal time constants. The filter was contained in a massive stainless steel housing and required about 2 hours to come to sample temperature. The data of Figure 2-8 correspond to a ΔE of 0.05 eV.

Comparison of the respective temperature dependences of PCD and SSPC further requires knowledge of the temperature dependence of the electron and hole mobilities. Here we derived values appropriate to our dopant concentration by interpolation from those given by Gartner.[3] They are shown in Figure 2-9.

The results of SSPC lifetime determinations, corrected for temperature dependences of carrier mobility and generation rate, are shown in Figure 2-10, along with PCD lifetime values taken on the same sample. The data reveal a difference in temperature dependences at low temperature, indicating that trapping is influencing the PCD measurements. The temperature dependences converge at high temperature, however, as would be expected. The SSPC data were therefore scaled to correspond to the PCD data at high temperature,

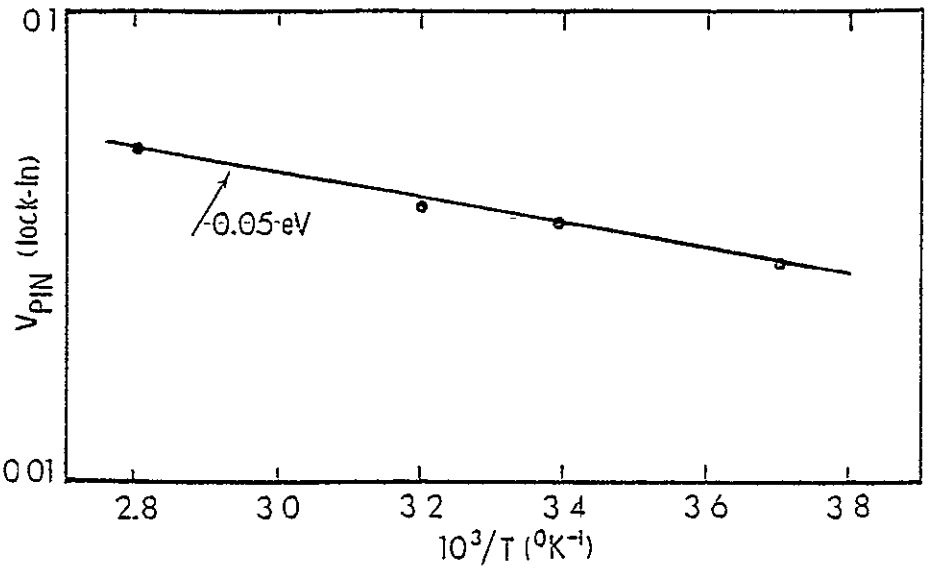

Figure 2-8. Temperature dependence of the generation rate of the SSPC measurement apparatus, as determined by means of a PIN diode at the sample position, and controlled at sample temperature.

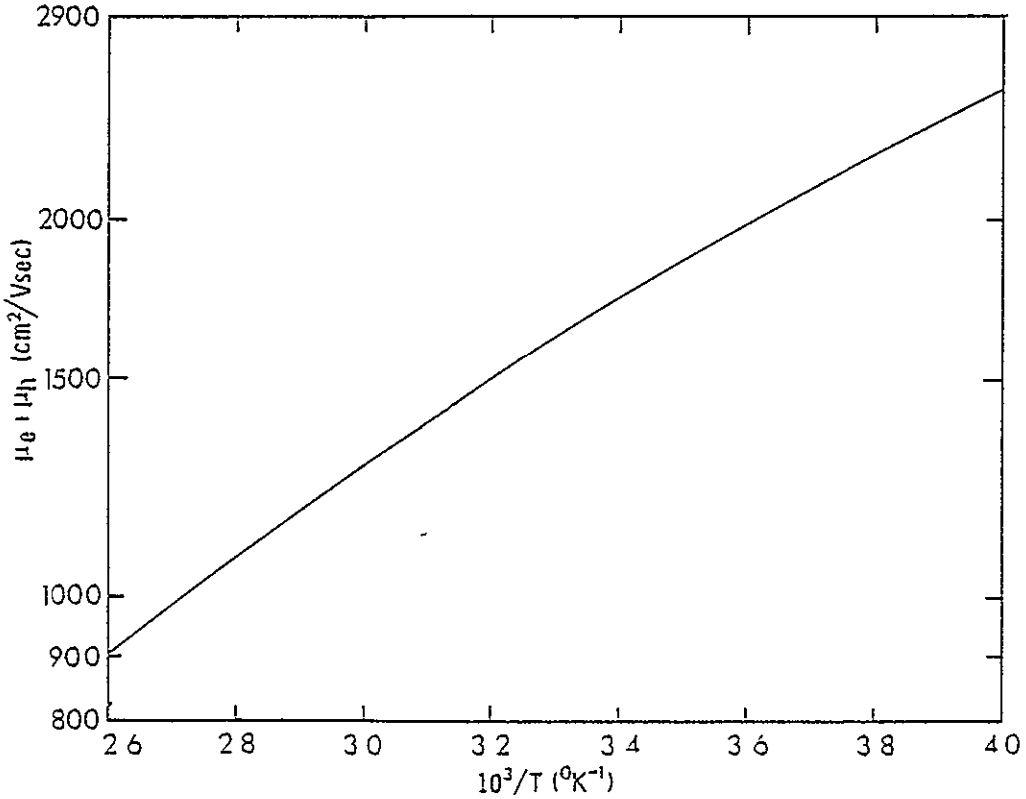

Figure 2-9. Assumed temperature dependence of mobility for the Westinghouse baseline samples used to determine the temperature dependence of steady-state photoconductivity.

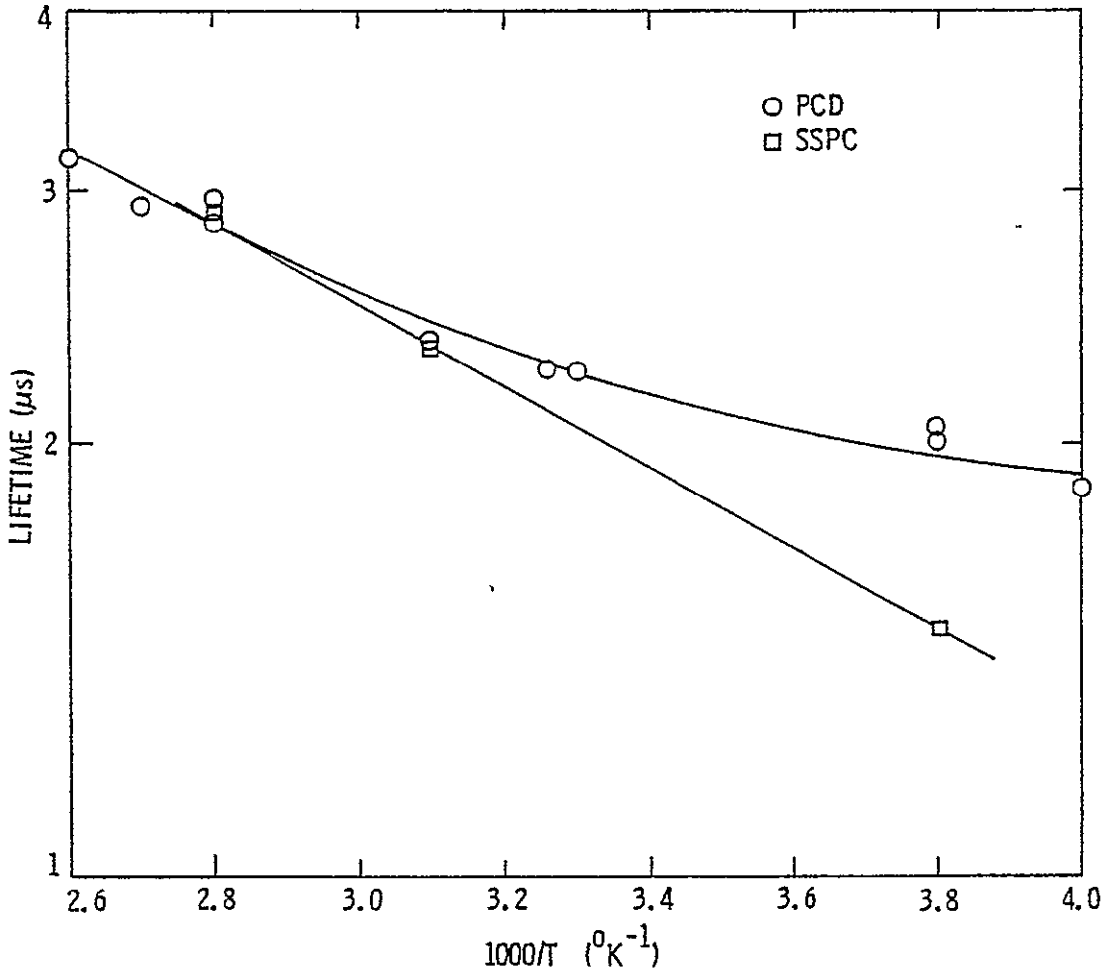

Figure 2-10. Steady-state and photoconductivity decay lifetime measured as a function of temperature on a baseline Westinghouse sample. SSPC data have been arbitrarily displaced to correspond to the PCD data at high temperature.

which yielded a generation rate of 5.3×10^{16} $cm^{-3} sec^{-1}$. It was our expectation that the generation rate determined in this way would be relatively free of the effects of trapping.

The above generation rate was therefore assumed for all calculations of lifetime for both Westinghouse and Monsanto samples. It was subsequently recognized, however, that quite a number of the measured, or effective, lifetimes were in excess of the "surface lifetime" for our assumed surface recombination velocity. The data seemed well-behaved, so an error in the assumed generation rate was indicated.

Two approaches were therefore undertaken to determine the generation rate in a different manner from that used above, and using samples which did not exhibit trapping. These methods, which will be discussed below, yielded generation rates which were in reasonable agreement with each other but differed from the one deduced from the above measurements performed on the W002 ingot. The cogent implication of this finding is that in the presence of severe trapping, as observed in PCD, the experimental method employed for the PCD measurements was not adequate to yield values of lifetime which were insensitive to presence of traps. On the one hand, it appears to be inadequate to employ background light to fill traps, in an amount sufficient to yield exponential decays. On the other hand, it appears to be inadequate to utilize the temperature dependences of SSPC and PCD lifetime in the manner we have, at least if measurements are restricted to such a narrow range.

The first alternative method of determining the generation rate was based on the previous study[2] in which the generation rate was determined for sandblasted surfaces, using samples which did not exhibit trapping. Thirteen samples, ranging in resistivity from 0.1 Ω-cm to 13 Ω-cm, had been measured via PCD and SSPC and a generation rate determined. No sample exhibited a deviation greater than 8% from the PCD values, based on this generation rate. The standard deviation was 5% of the mean, giving a standard error of the generation rate of 1.4%. The generation rate therefore appears to be well established for this surface condition.

Comparison with the present samples is made possible by reference to the samples which were used to establish the surface recombination velocity, which were also sandblasted (Section 2.4). These were measured via SSPC as well as with PCD. Results of measurements before and after sandblasting are given in Table II. The generation rate is found to increase as one or both surfaces are sandblasted, due to the enhanced scattering of the incoming beam. This scattering gives rise to a larger path length of the light within the sample

Table II. Relative SSPC generation rate for polished and sandblasted surfaces.

Sample Designation		Relative SSPC Lifetime		
		Prior to Sandblasting	Sandblasted One Side	Sandblasted Both Sides
W002	Sample #4	1.00	1.84	2.01
	Sample #7	1.00	1.83	1.90
	Sample #8	1.00	1.94	1.88
			Mean Ratio	1.93

and thus a higher probability of interaction. The difference in generation rates before and after sandblasting was found to be a factor of 1.93 ±0.04. Applying this scale factor to the generation rate determined in the previous study should yield a value of acceptable accuracy appropriate to the present case of polished surfaces.

The second alternative method of determining the generation rate refers to the solar cells employed in a comparison of diffusion length and lifetime measurements to determine their mutual consistency (Sec. 3.0). Lifetimes were measured on these cells using both PCD and SSPC, after removal of the junctions. The generation rate which yielded the best agreement between the two sets of measurements was similar to the one determined in the earlier program, differing by 9%. Sandblasted surfaces were used in this comparison as well.

On the basis of these results, a final choice of generation rate was based on an equal weighting of the above determination and that obtained in the previous program. For the case of polished surfaces, then, the generation rate was determined to be 8.1×10^{16} $cm^{-3} sec^{-1}$ under standard conditions. The statistical basis for estimating the precision of this g is unfortunately modest. There is in addition to the uncertainty of g for sandblasted surfaces also the possible error in g-ratio between polished and sandblasted surfaces. A conservative estimate of the former uncertainty is 7%, whereas the probable error of the latter is 2%. The net uncertainty is just over 7%.

It is unfortunate that in the interest of preserving the surface conditions of the samples as furnished, both the determination of surface recombination velocity and the determination of the generation rate were compelled to be indirect, increasing the error margin in both cases.

2.6 SHORT-CIRCUIT CURRENT MEASUREMENTS OF DIFFUSION LENGTH

In this program, diffusion lengths were to be determined on solar cells and similar test structures furnished by other contractors of the LSSA project. Lifetimes had already been determined on these devices by the open-circuit voltage decay method. The principal method employed for the measurement of diffusion length utilizes the simple relationship which prevails between the carrier collection volume, governed by the diffusion length, and the short-circuit current. For uniform, low-level carrier generation and with sample boundaries far removed, the equation in the one-dimensional case is

$$I_{sc} = q\,g\,A\,(L_p + W + L_n) \qquad (3)$$

Here g is the generation rate, A the junction area, W is the depletion region width, and L_p and L_n are the p- and n-region diffusion lengths. In the practical case of a shallow junction, with heavily doped surface layer, carrier collection from that region is usually neglected. Loss due to surface recombination is quite high and lifetimes in heavily doped regions may be reduced by the predominance of higher-order recombination processes. The measured short-circuit current therefore reflects the sum of neutral base diffusion length and width of the depletion region. Carrier collection from the latter is essentially complete. However, for the present devices, it is one micron or less in magnitude and makes a negligible contribution for typical diffusion lengths.

The above method of determining diffusion lengths has been treated by Rosenzweig,[8] and more recently by Reynolds and Meulenberg.[9] For application to solar cells, the above formulation needs to take explicit account of recombination at the rear surface of the cell. This is treated in the latter reference. The general solution is

$$I_{sc} = q A g L \left[\frac{D \exp(-w/L) + s L \{\exp(-w/L) - 1\}}{s L \sinh(w/L) - D \cosh(w/L)} + 1 \right], \qquad (4)$$

where s is the surface recombination velocity, D the diffusivity, and w the cell width. For solar cells without a back surface field (the assumption of a neutral base has been made throughout), it is a good assumption to take $s = \infty$. The above equation then assumes a simpler form

$$I_{sc} = q A g L \left[\frac{\cosh(w/L) - 1}{\sinh(w/L)} \right] . \qquad (5)$$

This can be rewritten as

$$\frac{I_{sc}}{q A g w} = \frac{1}{x} \left[\frac{\cosh x - 1}{\sinh x} \right], \text{ with } x = \frac{w}{L} , \qquad (6)$$

and the equation was used in this form to obtain a solution for L from experimental values of short-circuit current.

We have employed this method of determining diffusion lengths in our study using penetrating, bandedge light to achieve uniform generation throughout the specimen. The generation rate employed in this facility was calibrated with respect to the known generation rate of a Co^{60} gamma source. Finally, the calibration of the Co^{60} gamma source, as well as the validity of the method, were checked independently using a scanning electron microscope to determine the bulk diffusion length directly. These experimental methods and their verification will be discussed in more detail in the following sections.

2.7 DIFFUSION LENGTH MEASUREMENTS USING Co^{60} IRRADIATION

The use of Co^{60} gamma irradiation for determination of solar cell diffusion lengths is attractive for two reasons. First, once it has been initially determined, the generation rate is predictable at later times on the basis of the known half-life. Second, the gamma energies of 1.17 and 1.33 MeV are so high that absorption coefficients in silicon are fairly small ($\mu \approx 0.065$ cm^{-1}), yielding very uniform generation with typical samples. Nonuniformity is less than 0.5% in a 30-mil sample on this account. These reasons make it attractive to employ Co^{60} gammas as a standard measurement method.

Disadvantages of the technique are that (1) radiation damage of the cell cannot be totally avoided, (2) the method is time-consuming, and (3) the cell metallization may cause the dose rate to be spatially varying within the cell. The method is time-consuming in that only a small number of cells can be measured within the volume in which the generation rate is known, and radiation safety requirements make the sample cycle time about one hour. Radiation damage can be minimized by making prompt measurements and removing the sample quickly from the source. It can also be taken into account by recording the short-circuit current graphically for a short period of time and extrapolating back to time before exposure. For the purpose of establishing calibration standards, the effect can be minimized by choosing a sample of low diffusion length where defects introduced during measurement would produce little change.

For unirradiated samples, it may be assumed that the increase in recombination rate effected by the radiation varies linearly with dose. Thus,

$$\frac{1}{\tau} - \frac{1}{\tau_o} = K\phi \tag{7}$$

where τ_o and τ are the pre- and post-irradiation lifetimes, respectively, ϕ is the ionizing radiation fluence, and K is commonly referred to as the lifetime damage constant. In terms of diffusion length, this equation takes the form

$$1/L^2 - 1/L_o^2 = \frac{K}{D}\phi \, . \tag{8}$$

We have, therefore,

$$\frac{dL}{d\phi} = -\frac{K}{2D} L^3 \, . \tag{9}$$

It is evident that degradation of the diffusion length is far more significant for the longer diffusion lengths. The in-out dose received by the sample in our Co^{60} source was determined to be about 7×10^3 rads(Si) and the dose received by the sample during a one-minute measurement interval about 4×10^3 rads(Si).

Typical damage constants are such that this dose may result in a 10% degradation of a 200-μm diffusion length. Correspondingly, the change in a 40-μm diffusion length would be about 0.4%.

The question of dose nonuniformity produced by nonhomogeneous specimen environment was addressed at some length in the course of this program since we considered it to be the remaining uncertainty affecting the accuracy of the technique. Some background discussion of this general topic of dose enhancement is probably in order.

Gamma rays in the MeV range interact with matter via the photoelectric effect, Compton scattering, and to a small degree, via pair creation. Whereas the initial absorption or scattering process occurs reasonably uniformly throughout the specimen, the recoil electrons distribute their energy very anisotropically. Uniformity of carrier generation therefore follows from uniformity in gamma absorption only in a homogeneous material environment. Equilibrium of pair generation per unit volume with energy absorbed out of the beam is established beyond the maximum recoil electron range from an interface. At an interface between two dissimilar materials, the same criterion for homogeneity applies. Near the interface, the nonuniformity in dose profile arises principally from three sources. First, the photoelectric absorption cross section is strongly dependent on atomic number (Z^5) as well as on gamma energy ($E_\gamma^{-7/2}$). Second, the energy loss rate via electron-electron interaction scales roughly with atomic number as well as density of the material. Third, Compton scattering depends on the density of scattering centers (electrons), and thus roughly on the material density. Compton scattering dominates the photoelectric effect at these high gamma energies. The secondary gamma ray emitted in a Compton process can lead to dose buildup within the irradiated sample. However, this effect may be disregarded for the present thin sample geometry.

In consequence of these considerations, the sample holder previously employed for Co^{60} measurements was modified to bring about a condition of dose equilibrium within the solar cell.[2] The cell was sandwiched between

layers of 30-mil aluminum which is sufficiently close in atomic number and density to silicon to reduce dose enhancement effects to insignificance. All materials of high atomic number were eliminated. Additionally, we considered the problem of secondary electron emission from the aluminum sandwich as well as the matter of low-energy electrons from the surroundings impinging on the sample holder, leading possibly to errors in the measurement of short-circuit current when the latter is small. To deal with this potential problem, the sample holder was encased in an enclosure which was likewise composed of 30-mil aluminum. The forward current emitted from the enclosure and reaching the sample holder was expected to be comparable to the back-scattered current from the sample holder reaching the enclosure

The remaining outstanding question with regard to dose enhancement concerned the effect of the cell metallization which may be composed of such elements as titanium, palladium, silver, tin, and lead. We have attempted to estimate the magnitude of this effect on the basis of dose enhancement studies made by Wall and Burke et al.[10,11,12] on interfaces between heavy metals and aluminum, which may be taken as representative of silicon. The authors employed ionization chamber measurements for these studies and confirmed these with solar cell measurements. Both thick and thin layers of high-Z material were tested under conditions of normal incidence from either side of the interface. The case of a thick gold layer on aluminum is typical and we have reproduced the results of their ionization chamber measurements for Co^{60} irradiation in Figure 2-11 (Ref. 12). Whereas a dose enhancement is observed at the interface when the direction of beam incidence is from the aluminum side, a dose suppression is seen when beam incidence is from the high-Z side. The effect is clearly significant in magnitude and it extends over distances comparable to solar cell thicknesses (100 mg/cm^2 corresponds to about 370 μm Al). What is perhaps surprising is that the effect is not negligible even in the case of fairly thin layers. We have used data for a 6-μm layer of gold on aluminum from the same references to assess the relative dose effectiveness in this case compared to a thick layer. To facilitate this

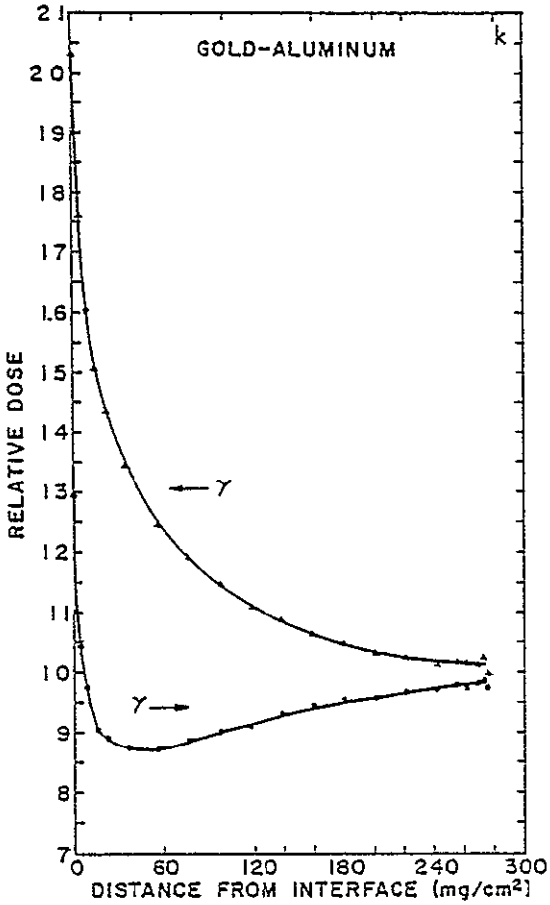

Figure 2-11. Ionization chamber measurements of relative dose in aluminum adjacent to gold for Co^{60} gammas Arrows show direction of incidence Figure taken from Reference 12.

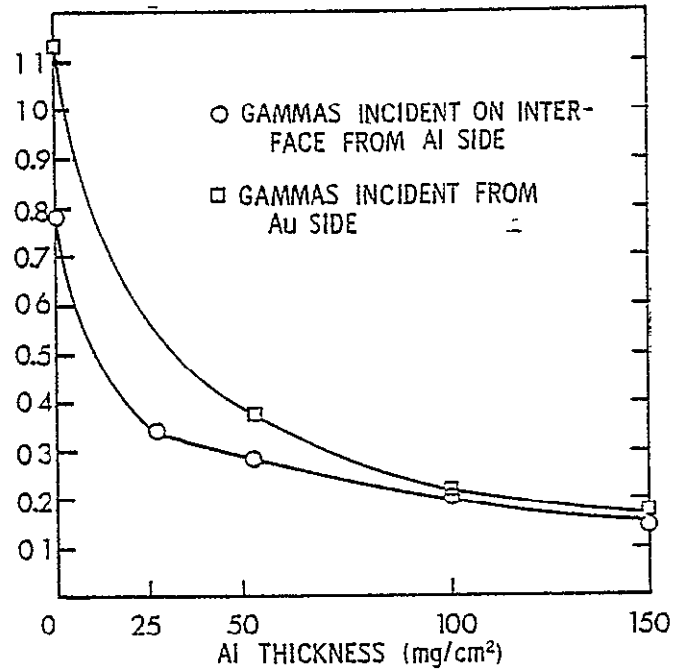

Figure 2-12. Ratio of dose enhancement factors for 6 μm thickness of gold to that for a thick layer of gold, adjacent to aluminum, as a function of aluminum thickness

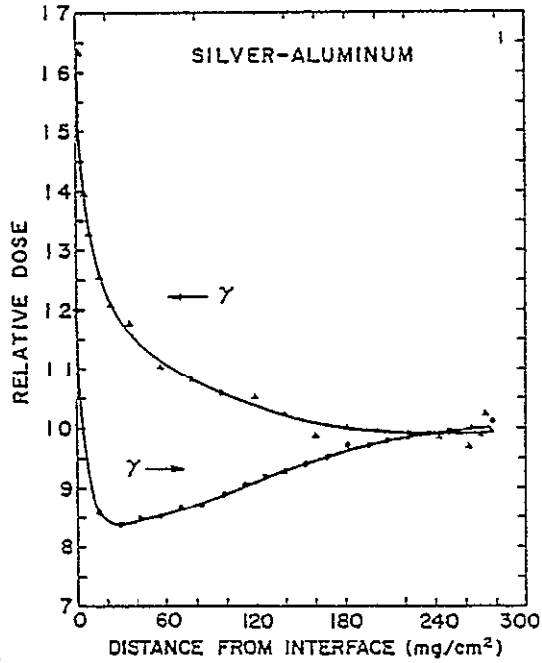

Figure 2-13. Ionization chamber measurements of relative dose in aluminum adjacent to silver for Co^{60} gammas Arrows show direction of incidence. Figure taken from Reference 12.

comparison, we define the quantity

$$\text{Dose enhancement factor} = \frac{\text{Actual dose in aluminum}}{\text{Equilibrium dose in aluminum}} - 1.$$

In terms of this quantity, the relative effectiveness of a 6-μm layer compared to that of a thick layer of gold is given in Figure 2-12 where the ratio of dose enhancement factors for the two cases is illustrated as a function of depth into the aluminum for both directions of incidence of the beam. It is apparent that even thin layers can give rise to dose enhancement factors that are comparable to those for thick layers. On this basis, we have estimated that if solder-reflow metallization is employed on a solar cell, a Co^{60} measurement of diffusion length would involve unacceptable uncertainties in generation rate. Consequently, we have concerned ourselves only with the case of titanium-palladium-silver metallization where 4 to 6 μm of silver may typically be used. Results for dose enhancement in the case of the silver-aluminum interface for a thick layer of silver are reproduced in Figure 2-13 from Ref. 12. If we assume the findings of Figure 2-12 to be applicable here, then we may estimate the dose enhancement factors for a 6-μm layer of silver base metallization. For the case in which beam incidence is on the front surface of the cell, it is estimated that dose enhancement near the junction may amount to 2%. For large diffusion lengths, where significant carrier collection from deep in the bulk is expected, the effective dose enhancement would be somewhat larger. The effect of the front surface metallization is considerably more difficult to estimate since there is partial cancellation of the dose enhancement and dose suppression contributions. In view of the fact that there is only partial metal coverage on the front surface, we estimate the net dose enhancement to be totally negligible.

Since dose enhancement produced by cell metallization was found to be a potential problem, an experimental test of this was desirable for the cells which were to be used in the calibration of the penetrating light apparatus as well as those to be used in the verification of the Co^{60} method with the SEM bulk measurement technique. Additional tasks which were relevant to these

objectives were a redetermination of the gamma flux and calibration of the dose rate prevailing at each of three test positions within the source. We now turn to a discussion of these tests.

The sample holder provides for the simultaneous calibration of three solar cells, placed at the axis of symmetry of the Co^{60} source, which is arranged in a cylindrical array of cobalt rods 14 inches in length. The source was upgraded in 1975 and in that context the cylindrical symmetry of the source was broken. The rods were arranged in a 93-degree arc on a 4.5-inch radius. The three cell positions thus see slightly different generation rates. Two positions are equidistant from the source and the third somewhat farther removed. The difference in dose rate between the near and far positions may be estimated by assuming a 1/r-dependence of flux from each of the rods. This analysis yielded values of generation rate differing by ±4% from the value on axis. The latter value had been determined for us by EG&G using cobalt-glass after upgrading of the source, and the derived April 1977 value was determined to be 62.5 rads(Si)/s. The pair creation energy in silicon has been determined by a variety of methods and typical values range from 3.60 to 3.65 eV. The latter value yields the widely accepted conversion constant of 4×10^{13} pairs/cm^3-rad(Si). We thus determine a generation rate of 2.5×10^{15} pairs/cm^3-sec. A second determination of the gamma flux was made in May, using EG&G cobalt-glass calibration services, and an April 1977 value of 67.9 rads(Si)/s was determined. This value was quoted to within 2% accuracy, yet our two independent determinations differ by 7%. Having no basis for preferring one over the other, the average of the two was assumed. We may take the generation rate to be known to within 5%.

Experimental determination of the dose rate variation among the solar cell test positions and of the effect of cell metallization on generation rate was pursued using two techniques. In the first experiment, several solar cells were measured in different sample positions and with different orientations with respect to the source. By comparing results for the two orientations in the same sample position, the dose enhancement/suppression effect will be

bracketed These tests were performed with solar cells made for us by Optical Coating Laboratory, Inc. (OCLI) in connection with another, earlier program. With respect to the precision that was sought for these tests, the results were compromised by cell degradation during the run and by other experimental difficulties. Nevertheless, the data indicated an 8% difference in dose rate between the near and far positions, as well as a 2 to 3% dose enhancement effect Since one of these same cells had been employed in the earlier study already referred to,[1] it was interesting to observe that the diffusion length agreed with the earlier determination to within 2% The former measurement was made with the cylindrically symmetric source, and with the earlier sample holder. The close agreement of the two values must be regarded as somewhat fortuitous, given the respective uncertainties of the measurements However, the agreement does suggest that the sample holder was not responsible for any significant dose enhancement in the earlier study, unless there was an accidental cancellation of effects (The relevance of the earlier study will become apparent in the discussion of Section 3.3.)

A second test of the dose rate variation among sample positions and of dose enhancement effects was performed using nominally identical cells and permitting them to degrade in diffusion length due to gamma exposure The damage constant, according to Eq. (8), was assumed to be the same in these cells, which were phosphorus-doped 2 3 Ω-cm solar cells fabricated by OCLI Differences in rate of degradation would then be a direct indication of the differences in dose rate seen by the respective samples Cells were mounted in opposite orientations with respect to the source in the proximal position, and one was mounted facing the source in the distal position. Results for one of the cells are shown in Figure 2-14 The data show some scatter at early times due to finite resolution The data fit a unity-slope curve, as expected, except at later times where a reverse annealing process becomes important. Damage constants were determined for all three samples and results indicated a 2% difference in generation rate between the cells in the forward position, and an 8% difference between the front and rear positions

We estimate that the damage constants were determined with one-percent precision. The data confirm that for these cells dose enhancement effects are relatively small, making them suitable as calibration standards. The cells were therefore employed for the calibration of the penetrating light apparatus as well as for the comparison with the SEM measurement method.

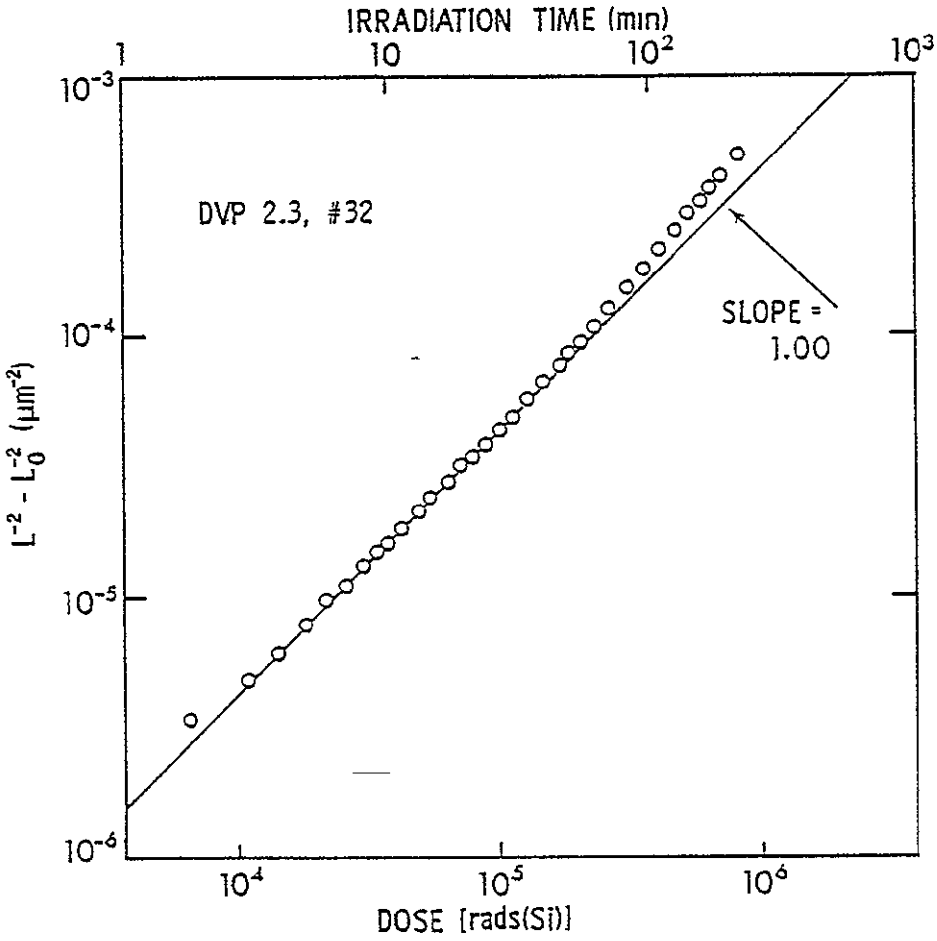

Figure 2-14. The quantity ($L^{-2} - L_o^{-2}$) as a function of gamma dose, or irradiation time. A unity-slope curve is fitted, consistent with the expectation of a linear increase in radiation-induced recombination rate.

2.8 DIFFUSION LENGTH MEASUREMENT USING PENETRATING LIGHT

The standard method of measuring diffusion lengths in this program was the use of penetrating light derived from an incandescent source and passed though a thick silicon filter to yield a spectrum of low absorption coefficient in silicon. The generation rate of this apparatus was determined by means of standard cells calibrated in the Co^{60} source.

At the beginning of this program, a penetrating light setup was available for use. However, it had provision only for 1 x 2 cm cells. Since all of the Monsanto test samples were to be furnished as 2 x 2 cm cells, the decision was made to build a new apparatus which, in addition to allowing measurement of the larger cells, would make provision for testing under conditions of several generation rates, closed-loop temperature control, and adaptability to unconventional test structures such as those which were furnished by Westinghouse.

The experimental facility is illustrated in Figure 2-15. The samples are mounted on aluminum plates which fit into slots in the aluminum enclosure. Illumination is furnished by a DCA projection lamp, used in conjunction with converging optics, which are configured to yield a slightly diverging beam for increased uniformity at the sample position. The light source and sample holder are mounted on a 1.2 m optical bench. To avoid heating the filters, the light is first passed through a 45-degree cold mirror. It is then passed through some neutral density filters which can be rotated into place to yield four different generation rates. Within the sample holder itself, an IR transmitting filter is mounted, the function of which is to assure temperature uniformity within the sample holder by providing an emitting surface at sample temperature. The light then passes through the 2.5-mm thick silicon filter to yield the highly penetrating beam.

The degree to which uniformity in generation rate is achieved with such a filter has previously been tested by comparing the generation rates in 0.5 mm and 1.0 mm bulk samples. They differed by 15%. Since all of the samples tested in the present study had only a narrow spread in sample

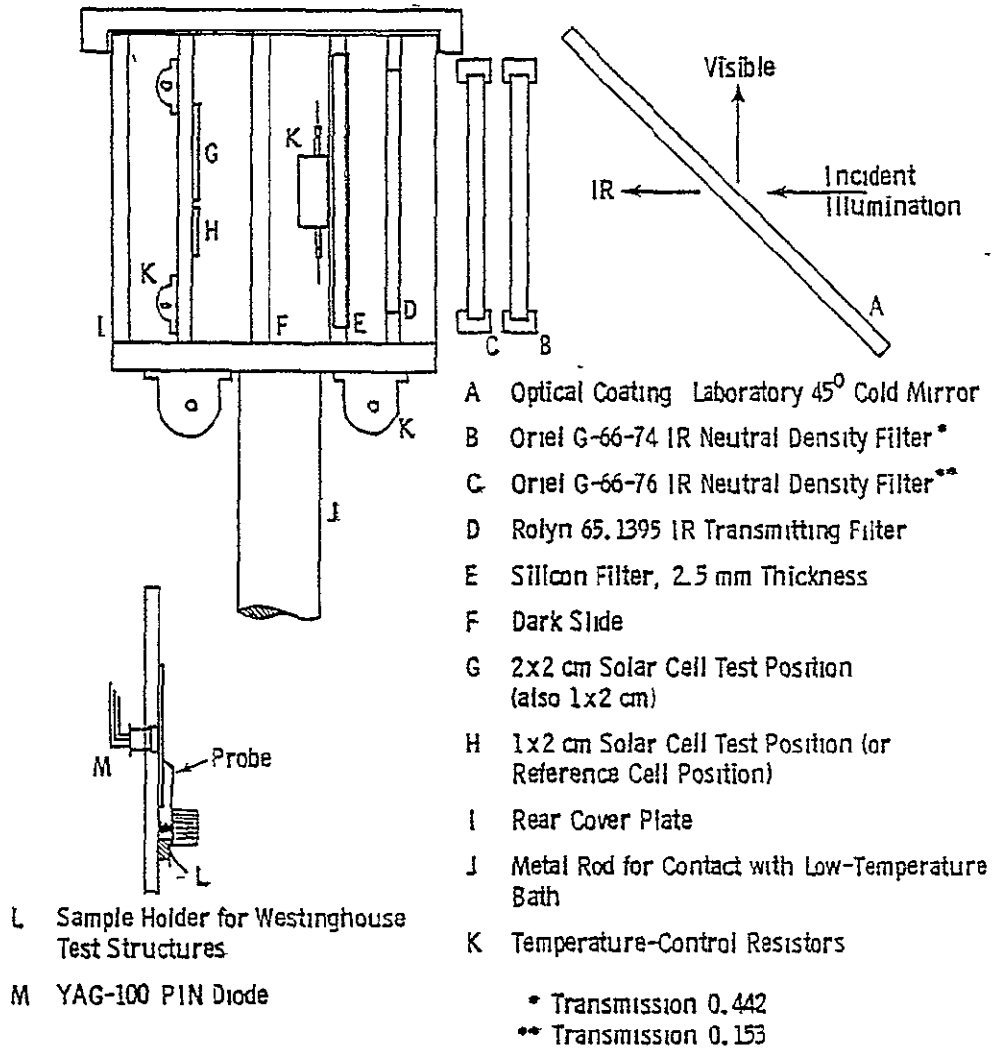

A Optical Coating Laboratory 45° Cold Mirror

B Oriel G-66-74 IR Neutral Density Filter*

C Oriel G-66-76 IR Neutral Density Filter**

D Rolyn 65.1395 IR Transmitting Filter

E Silicon Filter, 2.5 mm Thickness

F Dark Slide

G 2x2 cm Solar Cell Test Position (also 1x2 cm)

H 1x2 cm Solar Cell Test Position (or Reference Cell Position)

I Rear Cover Plate

J Metal Rod for Contact with Low-Temperature Bath

K Temperature-Control Resistors

L Sample Holder for Westinghouse Test Structures

M YAG-100 PIN Diode

* Transmission 0.442

** Transmission 0.153

Figure 2-15. Schematic representation of the diffusion length measurement apparatus employing penetrating bandedge illumination.

thickness and the maximum thickness was no greater than 340 μm, uniformity in generation rate among samples may be estimated to be within 2%.

Ratiometric measurement of two solar cells is provided for one sample holder. In general, however, intensities were monitored with a YAG-100 PIN diode mounted on another sample holder. The latter was designed to be used with the unconventional Westinghouse test samples. The YAG-100 PIN diode is made from high-resistivity silicon so that the depletion depth is comparable to our typical sample thickness It therefore approximates the spectral responsivity of the samples extremely well.

In the course of preliminary testing of the experimental apparatus, it was discovered that the responsivity of the PIN diode was time-dependent. A decrease by about 2% in responsivity was observed (with a decay time of about 2.5 minutes) after the onset of illumination at the generation rates typically used in this study. Since the light exposure history of the PIN diode was variable during the course of the experiments, the calibrations which employed the PIN diode consequently incurred an uncertainty in the range of ±1% from this source.

Resistors were provided for temperature control using resistive heating. The design was for use with an Artronix 5301-D temperature controller. The sample holder was equipped with a heat sink to a cold bath. No temperature control was used in the present work but the sample holder temperature was stabilized at mean room temperature by use of a water bath.

Signal recovery electronics are illustrated in Figure 2-16. Short-circuit current was measured by means of current-to-voltage converters. Chopper-stabilized amplifiers were used for this because of their good offset voltage characteristics. It has been our experience that deviation from short-circuit conditions may influence results in cases of short diffusion length. If the solar cell impedance is low, the input offset voltage is multiplied by the resultant high voltage gain of the amplifier circuit, giving significant output errors. The offset voltage and bias current were independently compensated for in these circuits. The PIN diode circuit, by contrast, uses a FET operational amplifier for current-to-voltage conversion and also provides for compensation of the diode leakage current.

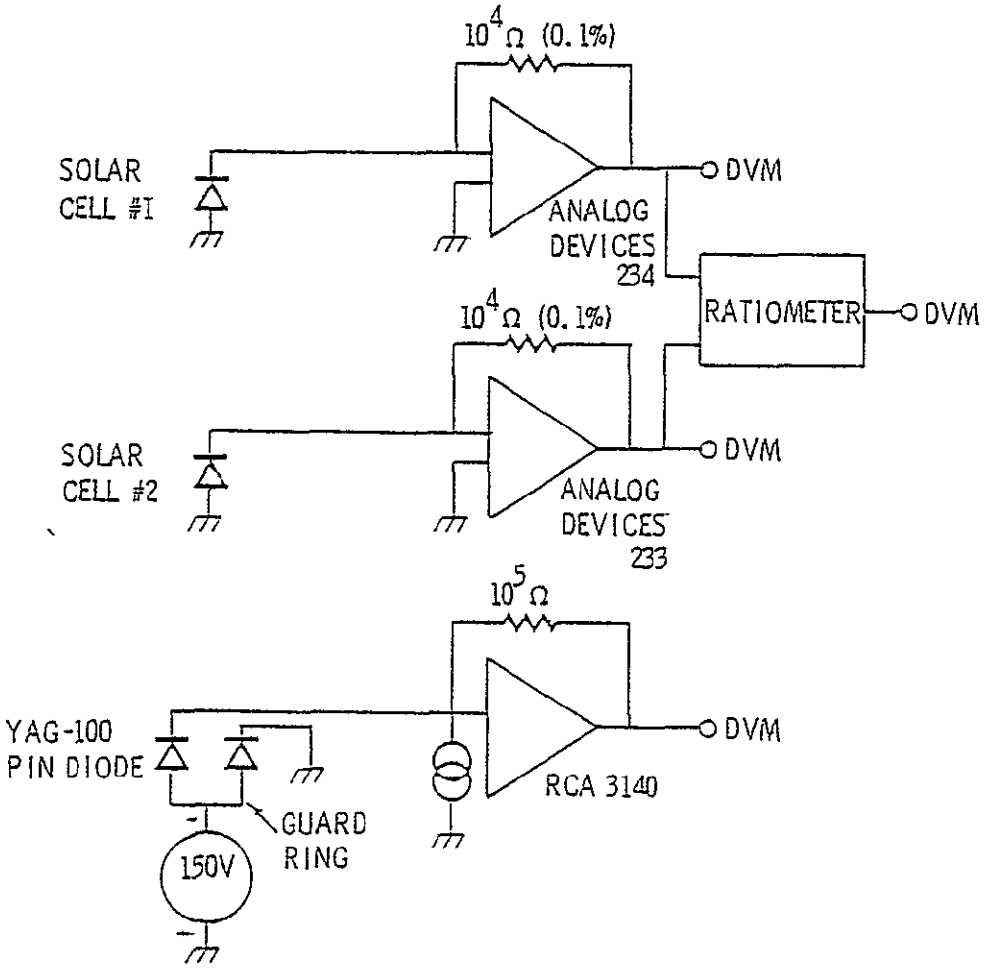

Figure 2-16. Schematic representation of signal recovery electronics for the penetrating light diffusion length measurement method. This apparatus was also employed for the Co^{60} measurements.

2.9 DIFFUSION LENGTH MEASUREMENTS USING THE SCANNING ELECTRON MICROSCOPE

The SEM method of measuring diffusion lengths on solar cells yields a direct measurement of the bulk diffusion length devoid of any device effects. It also offers reasonable precision as well as good spatial resolution. It is therefore an excellent calibration tool for other, more convenient methods of measuring diffusion lengths and it was employed here for that purpose.

The experimental method has been described previously.[13,14] The SEM beam is used for point-source excitation and the steady-state minority-carrier concentration is monitored by means of a reverse-biased junction. The reverse current is measured as a function of distance of the point of injection from the junction, which traces out the minority-carrier concentration profile. In the case of an infinite solid, the profile has the form

$$n(r) = \frac{n(0)}{r} \exp(-r/L) \tag{10}$$

whereas in the one-dimensional case we have

$$n(x) = n(0) \exp(-x/L), \tag{11}$$

where $n(0)$ is an assumed source strength.

The experimental arrangement is shown in Figure 2-17. If the bevel geometry is employed, as illustrated, with a large area junction, the one-dimensional case is obtained. Surface recombination effects on the measured current are also negligible with this geometry. Low-injection level conditions may be assured by operating at low beam currents (10 to 100 pA) and slightly defocusing the beam. The relevant injection level in this experiment is that which prevails just outside the collecting junction. (High injection conditions always exist in the vicinity of the point of beam impact.) The appropriate injection level may be estimated directly from the measured current. For a one-dimensional case, the diffusion current is given by

$$I = \frac{q n D A}{L}, \tag{12}$$

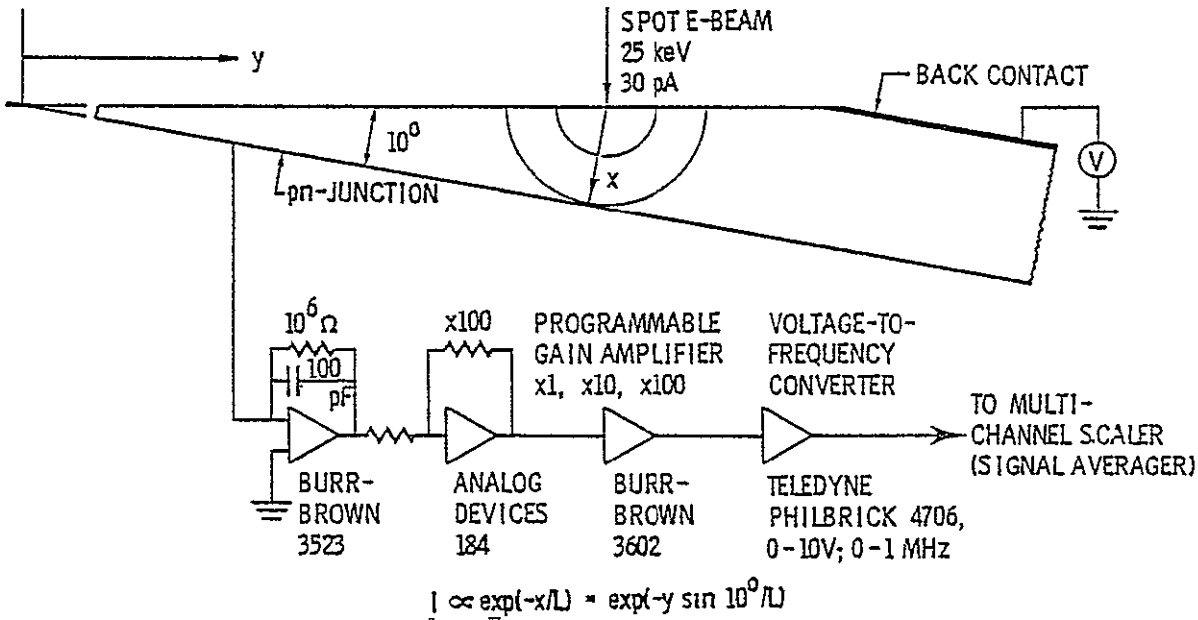

Figure 2-17. Schematic diagram of diffusion length measurement technique using bevel geometry. It offers enhanced spatial resolution, an approximation to one-dimensional geometry (using defocused beam), and reduced sensitivity to surface recombination. It is particularly suitable to determination of ac-diffusion length and drift mobility.

where n is the minority-carrier concentration just outside the depletion region. For the case at hand, in which the concentration is not invariant over the junction area, this equation can still be used for estimation purposes. A precise injection level cannot be defined for this type of experiment.

To provide the needed sensitivity for measurements under low-injection conditions, signal averaging methods are employed. In our implementation, a multichannel scaler is used in conjunction with a voltage-to-frequency converter. The latter has the advantage of infinite resolution over alternative A-D converters but it is relatively inefficient (or grainy) even at a conversion rate of 100 kHz/V. To improve its efficiency, the V-F converter is preceded by a programmable gain amplifier. This arrangement has been used successfully to recover signals which were several orders of magnitude below the noise level, which arises from the reverse leakage current of the large-area junction To minimize this noise current, reverse-bias conditions on the device are held to a modest 4 kT/q or so, just sufficient to provide a large dynamic junction impedance.

SECTION 3.0
VERIFICATION OF MUTUAL CONSISTENCY OF EXPERIMENTAL METHODS

3.1 COMPARISON OF Co^{60} AND SEM METHODS OF DIFFUSION LENGTH DETERMINATION

Ideally, the comparison of the two reference standard methods of measuring diffusion lengths should take place under conditions in which the respective limitations of the techniques are minimized. For this reason, the comparison was undertaken with the solar cells whose diffusion length had been degraded in the Co^{60} source. With regard to the Co^{60} test, it was preferable to use a diffusion length sufficiently short that its determination did not depend strongly on assumptions about recombination at the rear surface. With regard to the SEM method, it was likewise preferable to choose a diffusion length which was short compared to the sample thickness so that the spatial measurement extended over several diffusion lengths (i.e., over more than a decade in current). On this basis, a diffusion length of 30 to 40 μm was chosen and the diffusion length degradation (Section 2.7) was undertaken with this objective in mind. A second reason for using radiation-damaged cells was the expectation that the spatial uniformity of diffusion length would be improved. Since the two techniques perform very different spatial averaging, such uniformity was important for the validity of the comparison. We had in fact started with cells showing very good uniformity in solar cell performance, but it was felt that this uniformity could only be improved upon by gamma irradiation. Such irradiation has the characteristic of creating isolated defects which are, in addition, fairly stable thermally. They should be uniform throughout the silicon. Typical isochronal annealing curves for gamma- and electron-irradiated material, which is similar in these respects to gamma-irradiated silicon, are shown in Figures 3-1 and 3-2.[15] After an initial small anneal, or reverse anneal, the defect population is stable to fairly high temperature. We had seen evidence of such a reverse anneal already during irradiation (Figure 2-14), and this was confirmed by remeasurement after two days at room temperature.

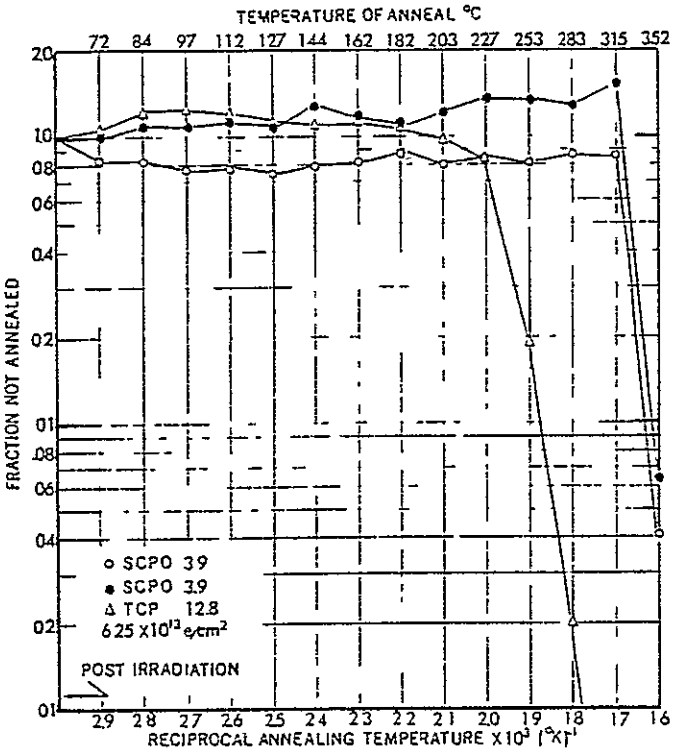

Figure 3-1. Isochronal annealing of reciprocal lifetime at 30°C in electron-irradiated P-doped silicon.[15]

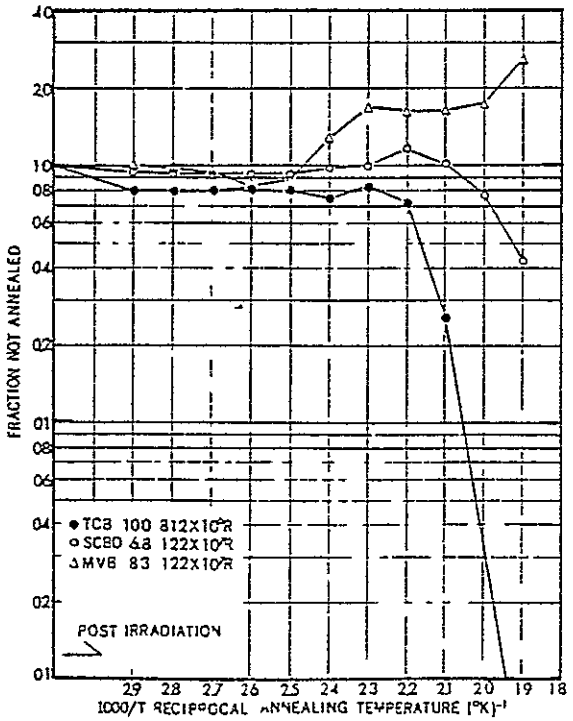

Figure 3-2. Isochronal annealing of reciprocal lifetime at 30°C in Co^{60} γ-irradiated B-doped silicon.[15]

An anneal of the degraded samples for a period of two hours at about 100°C was performed to stabilize the defect population and the cells were then re-measured in the Co^{60} source.

One of these standard cells was used for measurement in the SEM. A 20-degree bevel was ground (of somewhat marginal quality - the knife edge had a tendency to crumble, leaving scratches in the polished surface). Measurements were made on this sample under a variety of experimental conditions, including different regions of the beveled surface, and different beam energies. Because of the poor surface quality, it was found desirable to use high beam energies, which were more penetrating. Results taken at beam energies of 32 and 45 keV are shown in Figures 3-3 and 3-4. Shown is the log of the count per channel of the multichannel scaler, after baseline subtraction. Two traces

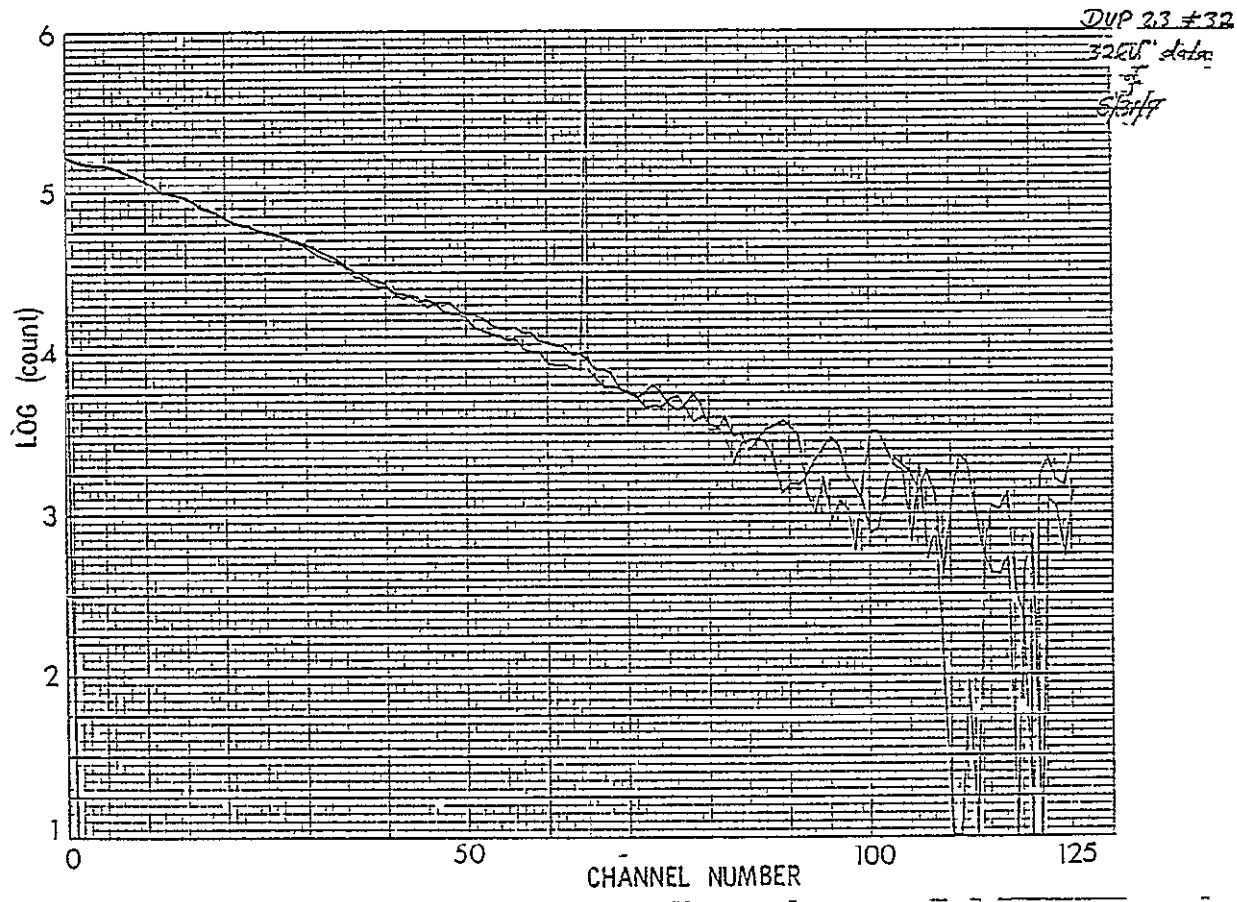

Figure 3-3. Logarithm of sample current as a function of distance of the point of injection from the junction, for a beam energy of 32 kV. One "glitch" in data reduction should be ignored. Shown is the logarithm of the count resulting from digitization and multiple summation for each of 128 channels.

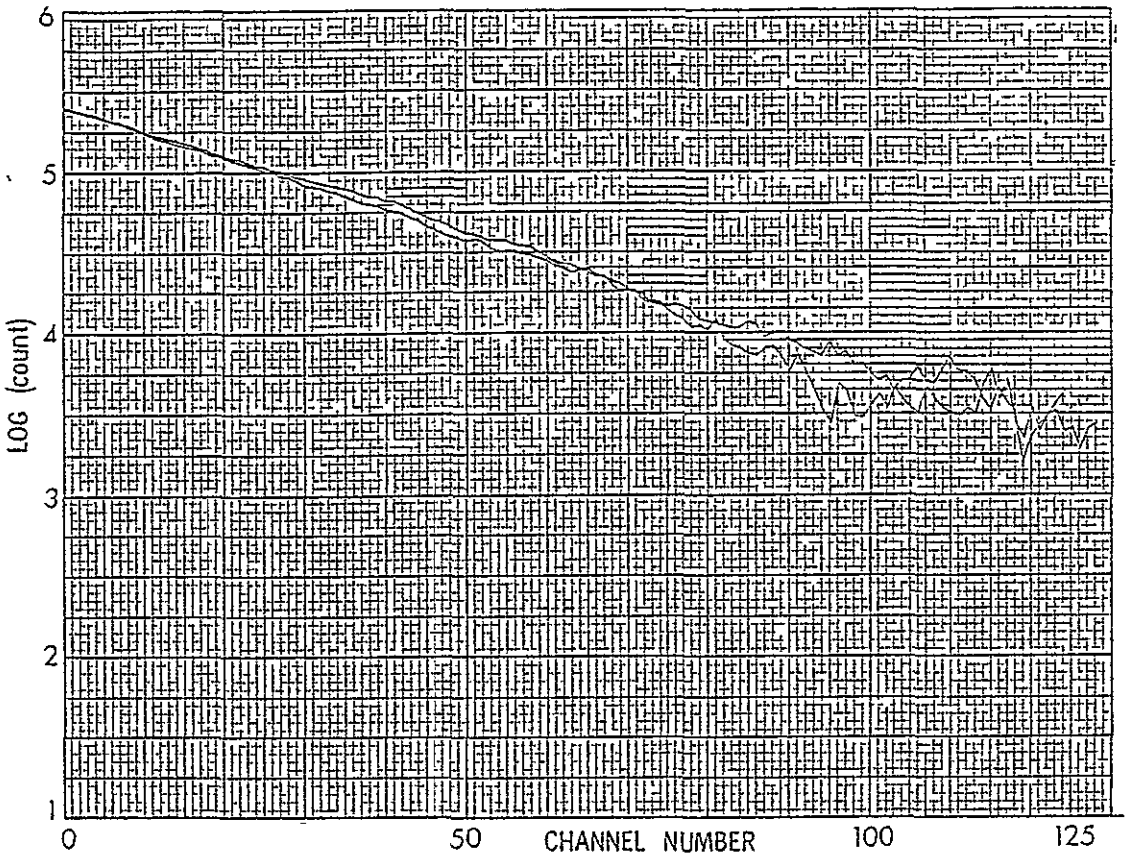

Figure 3-4 Logarithm of sample current as a function of distance of the point of beam incidence from the junction, for a beam energy of 45 kV

are shown in each case, corresponding to the two successive sweeps over the samples which were recorded in memory each time An order of magnitude range of acceptable data was obtained in both cases The signal current was larger in the case of the 45 kV run, giving somewhat cleaner data, and the greater effect of surface irregularities is apparent in the 32 kV data where the curve is not as smooth even where the noise level is not a factor

Diffusion lengths determined using the 45-keV beam were 45 1 μm and 43 5 μm Using 32 kV, the measured values were 39 6 μm and 38 μm It is possible that the 45 kV values may be influenced by the higher injection level prevailing in that case The 32 kV values, on the other hand, may be influenced by the higher noise level in that case, which may lead to underestimates of the diffusion length Taking all the data together, the mean diffusion length is

41.6 μm, the standard deviation is 3.3 μm, and the probable error is 2 μm. The Co^{60} measurement yielded a value of 42.4 μm. The agreement between the two values is most satisfying, although the closeness of the agreement must be regarded as fortuitous in view of the sources of random error and potential sources of systematic error in the two measurement methods.

We regard this test a satisfactory mutual corroboration of the two measurement methods, although admittedly the comparison was made under conditions which were optimal for both.

3.2 COMPARISON OF DIFFUSION LENGTH AND LIFETIME MEASUREMENTS

Having established confidence in our methods of measuring diffusion length, it was also of interest to compare diffusion length with lifetime measurements. This was done by first determining the diffusion length in several solar cells using the penetrating light apparatus. The diffused regions were then removed by etching, the surfaces sandblasted, and the lifetimes determined via PCD. SSPC measurements were also made and these were employed in establishing the generation rate for that apparatus. Consequently, they do not constitute an independent test.

Two 2.3 Ω-cm n-type solar cells and one 2 0 Ω-cm p-type solar cell were characterized in this manner. They were of the same type as those used in other aspects of the calibration program, namely those fabricated for us previously by OCLI. Results of the comparison are shown in Table III

Table III. Comparison of diffusion length and bulk lifetime measurements on solar cells

	L (μm)	D (cm^2/s)	τ (μs)	$(\tau_{eff})_L$ (μs)	$(\tau_{eff})_{PCD}$ (μs)
DVP 2.3 - 8	141	11.1	17.9	6 8	7.0
DVP 2.3 - 13	181	11.1	29.5	8.0	8.8
DVB 2.0 - 34	131	27.0	6 35	3.0	4.3

The first column shows the diffusion lengths determined using the assumption of infinite surface recombination velocity at the back surface. The second column indicates the diffusion coefficient which was assumed in conversion of these diffusion lengths to lifetime The third column shows the equivalent lifetime and the fourth lists the effective lifetime which would be expected for a sample of such diffusion length, given the thickness of the bulk sample, the diffusivity of column 2, and a surface recombination velocity of 8.3×10^3 cm/s. The fifth column shows the effective lifetime measured on the bulk sample via PCD.

Good agreement between the derived lifetime values and the PCD values was found in the case of the n-type specimens (3 and 10%), whereas the correspondence in the case of the p-type sample was only within 43%, or 30%, depending on the point of reference. The PCD lifetime is longer than the diffusion length-derived lifetime, which would be expected if trapping influenced the results. Indeed, background light was required to achieve exponential decays in the case of both DVP 2.3 - 13 and DVB 2.0 - 34. On the basis of the discussion in Section 2.5, perhaps this measure was insufficient to make the determination insensitive to trapping.

Further comparisons would, of course, be of interest in the case of p-type material However, it would be preferable if such studies could be made on thicker material where surface conditions would not have such a profound effect on the derived values.

3.3 DISCUSSION OF CONSISTENCY TESTS

In the previous sections we have reported excellent agreement between a bulk measurement and device measurement of diffusion length performed on the same device, and moderate agreement of diffusion-length equivalent lifetime and that measured by means of photoconductivity decay. The considerable interest in having such consistency checks performed arose from several sources On the one hand, past comparisons of lifetime measurements made by different investigators have shown little

correspondence On the other hand, there is a large body of data in the radiation effects community (quite a lot of it unpublished) which yields higher values for radiation susceptibility when device measurements of diffusion length are employed than when bulk lifetimes are used. This discrepancy was dealt with in two studies performed in our own laboratory,[1,16] and an additional one[13] was directed specifically to making such a comparison Explanations of the discrepancy generally tended to postulate trapping effects and injection-level dependences of lifetime In this state of affairs, it is of great interest to establish the mutual consistency of the measurement methods under ideal conditions This having been done, the range of validity of the various experimental methods can be explored by increasing the data base and performing appropriate statistical analyses This work serves both of these purposes

In the study already referred to,[1,2] damage constants were determined on p-type bulk samples and solar cells over a wide range of resistivities Measured on solar cells, diffusion lengths tended to be shorter than those derived from bulk lifetimes by the factor 1 7, with essentially all of the data being encompassed in the range 1 4 to 2, regardless of the magnitude of the diffusion length. Techniques used were SSPC for lifetime and penetrating light for diffusion length. The same factor (and range) was observed in a large number of unirradiated bulk samples when compared to solar cells fabricated from the same material PCD lifetimes were measured here A systematic error in one of the measurement methods seems a likely possibility Tending to support this view was the finding by Weizer[17] of a disagreement of a factor of 1 9 between his SEM bulk measurement of diffusion length and the standard x-ray method used at NASA-Lewis This discrepancy was not resolved in that the x-ray generation rate was simply redefined in that case to give agreement

An earlier study, which was undertaken to explore device-bulk differences by comparing neutron damage constants determined via PCD and SEM diffusion length, found bulk diffusion lengths to be lower than PCD lifetime by the factor of 1.66, with a standard deviation of 0 15 [13] Differences were postulated to be due to trapping effects on the post-irradiation PCD lifetime measurements

The persistent and systematic discrepancy between device and bulk data, as well as Weizer's finding, motivated the particular attention that we gave the diffusion length measurement methods. As a result, they now appear to have adequate credibility. Moreover, agreement was established between the Co^{60} method as used here and in the earlier study[2] (for calibration). The burden must therefore fall upon systematic processing effects on radiation sensitivity, which is difficult to defend, or upon the bulk lifetime measurement methods. That these methods are subject in principle to errors in the presence of traps is well known and has been the basis of much criticism of their use. We have found evidence of trapping effects on our measurements, despite the use of background light to fill traps, in the course of establishing the generation rate in the SSPC method. Moreover, the disagreement between diffusion length lifetime and PCD lifetime in the p-type sample is consistent with trapping effects on the lifetime measurement, and it is of comparable magnitude as the discrepancies referred to above. Trapping is known to be more of a problem in p-type silicon than in n-type.

The difficulty with the trapping hypothesis is that one would not expect such a tight correlation of diffusion-length lifetime and bulk lifetime as is in fact observed. An alternative explanation which has been put forward[16] is injection-level effects on the lifetime measurements. (The discrepancies between device and bulk measurements in that radiation effects study were found to disappear when comparison was made at the same injection level.) The photoconductivity decay lifetimes are typically measured over a range of injection ratios of 10^{-3} to 10^{-4}. At earlier times in the decay curve, the lifetime is typically longer due to injection-level dependence. If the decay constant increases later in the decay transient due to the presence of traps, the resultant decay curve may simulate a simple decay constant over a sufficient range in between that an acceptable measurement of lifetime is indicated, when in fact the low-injection-level lifetime will not have been observed.

The presence of any fast trapping at all, then, would have the tendency to cause the lifetime to be overestimated as a result of its injection-level dependence. That a certain amount of such trapping was present in all of the bulk samples measured in the current program is demonstrated by the fact that considerable background light was required in all cases in order to fill traps in SSPC measurements. The injection-level dependence of lifetime could also be a factor in the absence of any significant trapping. For neutron-irradiated material, it has been shown[16] using device measurements that at injection ratios as low as 10^{-3}, lifetime varies quite slowly with injection level, and this dependence may extend to injection ratios as low as 10^{-5} or 10^{-6}. It is possible that photoconductivity decay curves are perceived as exponential under these conditions.

The above factor would appear to be relevant only to the particular case of PCD lifetime. In SSPC, the injection level induced by the chopped light is clearly sufficiently low for all practical lifetimes that the appropriate limit should be observed. On the other hand, the injection level which is induced by the steady-state background light is not known. If lifetimes are short, traps have to be kept filled to a high degree in order that the conductivity modulation rising from the recombination process dominates in the SSPC measurement. If the detrapping time is also short, then the background light intensity required to accomplish this may be sufficient to increase both minority-carrier and majority-carrier excess densities beyond low-injection conditions. In practice, the background light intensity is increased until a plateau, or minimum, is reached in SSPC lifetime, which may or may not correspond to the low-injection-level lifetime. So the situation is not fundamentally better in the case of SSPC than of PCD.

The above discussion has probably overemphasized the discrepancies that exist. To balance the picture, it should be said that lifetime measurements have been very fruitful in the past in the determination of recombination center parameters. The simplicity of the methods, and their applicability to bulk material, assure that they will continue to be relied upon. Comparison of the data taken on the large number of samples in this program with that of others should help to establish the domain of usefulness of the standard lifetime measurements for nonideal material

SECTION 4.0
EXPERIMENTAL RESULTS

4.1 LIFETIME AND DIFFUSION LENGTH MEASUREMENTS ON WESTINGHOUSE SAMPLES

Results of SSPC measurements on Westinghouse bulk samples are given in Table IV Shown are the effective lifetimes, in microseconds, obtained at a generation rate of 8.1×10^{16} cm^{-3}/sec^{-1}. These data should be comparable to the equivalent raw Westinghouse data, i e., without correction for surface recombination effects. We have also given the ratio of effective lifetime obtained at higher and lower generation rates to that obtained under standard conditions. The generation rate g_1 amounts to 50% of the standard value, or 4.05×10^{16} $cm^{-3}sec^{-1}$, and g_3 amounts to 1.93 of the standard value, or 1.56×10^{17} $cm^{-3}sec^{-1}$. (The ratios were only recorded initially to two or three significant figures, so the given normalized values imply a greater precision than is appropriate.) The ratios may be interpreted as follows if the ratios are monotonically increasing with higher g, then an injection-level effect on the measured value may be indicated, if the ratios for g_1 and g_3 are both larger than unity, then an appropriate background light level has been chosen for the measurement under standard conditions. The observation of a ratio larger than unity for g_1 would indicate residual trapping effects on the conductivity modulation, whereas the observation of a ratio larger than unity for g_3 would imply an injection-level dependence of the measured lifetime. The minimum in SSPC lifetime observed under standard conditions (g_2) would then be a "best value" in the presence of both trapping and injection-level effects. If, on the other hand, the measured ratios are monotonically declining with increasing injection level, then the available background light intensity was most likely insufficient to saturate the traps for a plateau value of SSPC lifetime to be observed. (It is also possible, however, to observe cases in which the lifetime decreases with increasing injection level, in which case no minimum, or plateau, value would be expected.)

Table IV. Lifetime data for Westinghouse bulk samples.

Sample Designation	(τ_{eff})-ratio g_1	g_2	g_3	τ_{eff} (μs)	s = 8.3 x 10^3 τ (μs)	L (μm)	s = 9 3 x 10^3 τ (μs)	L (μm)
W-002-00-000-1	1.006	1	0.992	1.53	2.80	95.1	2.86	95.9
W-002-00-000-2	1.006		1.002	1.41	2.62	91.9	2.69	93.3
W-002-00-000-3	1.000		0.998	1.47	2.83	95 5	2.91	96.9
W-002-00-000-4	1.006		0.981	1.45	2.78	94 7	2.84	95.7
W-014-00-000-1	0.995		1.002	1.61	3.41	105.0	3.49	106 0
W-014-00-000-2	1.004		0.992	2.26	5.65	135.0	6.10	140.0
W-014-00-000-3	1.014		1.012	1.98	4.48	120 0	4.78	124.0
W-014-00-000-4	.			.	.	.		.
W-019-Cu-003-1	1.016		1.004	1.19	1.97	79.8	2 02	80.6
W-019-Cu-003-2	1 004		1.000	1.34	2.46	89.1	2.58	91.2
W-019-Cu-003-3	1.002		1.002	1.66	3.63	108.0	3.72	110.0
W-019-Cu-003-4	1.010		1.002	1.21	2.03	80.8	2.07	81.7
W-020-00-000-1	1.013		1 011	1.43	2.71	93.5	2.77	94.5
W-020-00-000-2	1.008		0.982	1.77	3.47	106.0	3 76	110 0
W-020-00-000-3	1.004		0.991	2.05	5.19	129.0	5.64	135.0
W-020-00-000-4	1.002		0 998	2.29	5.66	135 0	5.82	137.0
W-004-Cr-001-2	1.017		0.989	0 038	0 038	11.2		.
W-004-Cr-001-end-3	1.016		0.995	0.035	0.036	10.7		
W-004-Cr-001-end-4	1.019		0.966	0 033	0 035	10.6		
W-005-Mn-001-tang-1	0.991		1.012	9.76				.
W-005-Mn-001-tang-2	1.000		1.003	9.89		.		.
W-005-Mn-001-cent-3	1.007		1.003	8.87				.
W-005-Mn-001-4	0.997		1.010	9 38			.	
W-006-Ni-001-cent-1	1.008		0.988	1.71	3.59	108.0	3.96	113.0
W-006-Ni-001-cent-2	1.005		1.003	1.51	2.97	97.9	3.07	99.5
W-006-Ni-001-tang-3	1.002		1.004	1.62	3 30	103.0	3.53	107.0
W-006-Ni-001-seed-4	0.997		1.007	1.72	3.59	108.0	4.01	114.0
W-007-Cu-001-cent-1	1.000		1 004	1.57	3.28	103.0	3.31	103.0
W-007-Cu-001-tang-3	0.995		0.998	1.51	2.91	96.9	3.07	99.5
W-007-Cu-001-seed-4	1.009		0.996	1.69	3.33	104.0	3.44	105.0
W-008-Ti-001-tang-1	1.095		1.038	0.180	0.196	25.1	.	
W-008-Ti-001-tang-2	0.998		1.002	0.170	0 183	24.3		
W-008-Ti-001-seed-3	0 966		1.009	0.184	0.199	25.3		.
W-008-Ti-001-seed-4	0.993		0.998	0 165	0.178	23.9	.	
W-009-V-001-seed-1	1.013		0.977	2.15	6.46	144.0	7 16	152.0
W-009-V-001-seed-2	0.975		0 954	2.27	7.61	157 0	8.61	167 0
W-009-V-001-tang-3	0.987		1.013	2.38	8.87	169.0	10.3	182.0
W-009-V-001-tang-4	0 965		0.987	2.34	8.36	164.0	9.61	176.0
W-010-Ni-002-seed-1	1 002		0 996	1 87	4.90	126.0	5.36	131.0
W-010-Ni-002-seed-2	1 005		0 989	1.90	4.68	123 0	5.18	129 0

Table IV. (Continued)

Sample Designation	(τ_{eff})-ratio g_1	g_2	g_3	τ_{eff} (μs)	s = 8.3 x 10^3 τ (μs)	L (μm)	s = 9.3 x 10^3 τ (μs)	L (μm)
W-010-Ni-002-tang-3	1.004	1	0.991	1.90	4.40	119.0	4.69	123 0
W-010-Ni-002-cent-4	1.009		0 985	2.42	7 35	154.0	8.13	162.0
W-011-Zr-001-tang-1	1.009		0.983	2.18	6.70	147 0	7 48	153.0
W-011-Zr-001-tang-2	1.034		1.015	2.14	6 35	143.0	7 06	151.0
W-011-Zr-001-cent-3	1.008		0.984	2 05	5.66	135 0	6.22	142.0
W-011-Zr-001-seed-4	1.014		0.980	1.79	3.64	108.0	3.85	111.0
W-012-Cr-002-seed-1	1.009		0.982	0.095	0.098	17 8		
W-012-Cr-002-seed-2	1.017		0.986	0.082	0 084	16 5		
W-012-Cr-002-tang-3	1 010		0 982	0.076	0.078	15.8		
W-012-Cr-002-tang-4	1.014		0.990	0.089	0 093	17 3		
W-013-Mn-002-tang-1	1.026		1.000	2.43	9 58	176 0	11.2	190.0
W-013-Mn-002-tang-2	1 002		0 989	2.31	8.02	161.0	9 16	172.0
W-013-Mn-002-seed-3	1.011		0.982	1.53	3.35	104.0	3 58	108.0
W-013-Mn-002-seed-4	1.015		1.000	2.44	9 72	177 0	11.4	192.0
W-015-Zn-001-tang-1	1 006		0 994	1 56	3.10	99 9	3 27	103 0
W-015-Zn-001-tang-2	0 998		1.007	1 54	3 02	98 7	3 19	101.0
W-015-Zn-001-cent-3	1 024		1 013	1 55	3.06	99 3	3 23	102 0
W-015-Zn-001-seed-4	1 009		1 000	1.50	2 86	96 1	3 27	103 0
W-016-Fe-001-tang-1	1 002		0 980	0.053	0 054	13 2		
W-016-Fe-001-tang-2	1 011		0 985	0 048	0 048	12.4		
W-016-Fe-001-cent-3	1.000		1.000	0 086	0 089	16.9		
W-016-Fe-001-seed-4								
W-017-Cu-002-tang-1	1 002		0 994	1.86	3.93	113.0	4 17	116 0
W-017-Cu-002-tang-2	0 998		0 993	1 67	3.54	107 0	3 76	110 0
W-017-Cu-002-tang-3	1 000		0 970	1.41	2.39	87 8	2.70	93 3
W-017-Cu-002-seed-4	1.019		0 981	1 50	2 88	96 3	3 03	98 8
W-018-Fe-002-tang-1	1.004		1.000	0 022	0 023	8 60		
W-018-Fe-002-tang-2	1.000		1.000	0 021	0 022	8 40		
W-018-Fe-002-cent-3	1 007		0 983	0.019	0.020	7 98		
W-018-Fe-002-seed-4	1.000		0.991	0 021	0 022	8 40		
W-021-Mg-001-tang-1	0 994		1.000	1.25	2.11	82.4	2 18	83.9
W-021-Mg-001-tang-2	1.019		1.000	1.47	2 77	94.6	2.91	96 9
W-021-Mg-001-cent-3	0 991		1 000	1.43	2.64	92.2	2 77	94 5
W-021-Mg-001-seed-4	0 998		0 990	1 53	2.98	98.1	3 15	101 0
W-022-00-000-cent-1	0 986		1.002	1 97	4.43	120 0	4.73	123 0
W-022-00-000-cent-2	0 993		0 996	1.93	4.24	117 0	5 28	130 0
W-022-00-000-cent-3	0 993		0 998	1 87	3.97	113 0	4.22	117 0
W-022-00-000-cent-4	0 987		1 006	2 26	6 10	140.0	6 66	147 0
W-023-00-000-tang-1	1 004		0 973	0 130	0 137	21.0		
W-023-00-000-cent-2	1 010		0 981	0 117	0.123	19 9		

Table IV. (Continued)

Sample Designation	(τ_{eff})-ratio g_1	g_2	g_3	τ_{eff} (μs)	s = 8.3 x 10^3 τ (μs)	L (μm)	s = 9 3 x 10^3 τ (μs)	L (μm)
W-023-00-000-cent-3	1.005	1	0.995	0.086	0.092	17.2		
W-023-00-000-seed-4	1.002		0.989	0.109	0.115	19.2		
W-024-Mg-002-tang-1	1.000		1.000	1.61	3 29	103 0	3 49	106.0
W-024-Mg-002-tang-2	0.941		1.059	1 38	2.48	89.5	2.59	91.4
W-024-Mg-002-seed-3	1.038		0.987	1.81	4.19	116.0	4.50	121 0
W-024-Mg-002-seed-4	0.974		1.026	1.50	2.88	96 3	3 03	98.8
W-025-00-000-tang-1	0 957		1.000	3 99	.		.	
W-025-00-000-cent-2	1.000		1.050	1.44	2.67	92.9	2.80	95.1
W-025-00-000-cent-3	0.988		1 012	1.82	3.44	105.0	3.60	108.0
W-025-00-000-seed-4	1.047		1 011	3.09	13.1	205.0	15.1	221.0
W-026-Mn-003-tang-1	0.950		1.017	1.29	2.21	84.5	2.30	86 2
W-026-Mn-003-tang-2	0.973		1.016	1.35	2.39	87 8	2.49	89.7
W-026-Mn-003-seed-3	0.880		1.019	1.32	2.51	89.9	2.65	92.3
W-026-Mn-003-seed-4	1 000		1 018	1.37	2 45	88 9	2.56	90 8
W-027-Mn/Cu-001-tang-1	0.986		1.007	8.18	.		.	
W-027-Mn/Cu-001-tang-2	1.071		1.000	8 30		.		.
W-027-Mn/Cu-001-cent-3	0 933		1.067	7 92				.
W-027-Mn/Cu-001-seed-4	0.993		1 000	7.92	.	.		.
W-028-Al-001-tang-1	0 994		1.017	0.820	1.14	60.6	.	
W-028-Al-001-tang-2	0.980		0 980	0.860	1.21	62.5	.	
W-028-Al-001-seed-3	1.000		1.000	0.880	1.25	63 6	.	
W-029-Cr-003-tang-1				-				
W-029-Cr-003-tang-2	1.000		1.000	0.480	0.57	42.9		.
W-029-Cr-003-seed-3	0.968		1.011	0.690	0.94	55.0		
W-029-Cr-003-seed-4	0.929		1.040	0.65	0.87	52.9		
W-030-Cr/Cu-001-tang-1	1.000		1.000	0.016	0.016	7.23		.
W-030-Cr/Mn-001-tang-2	1 125		1 250	0 019	0.020	7.98		
W-030-Cr/Mn-001-cent-3	0.976		1.065	0.024	0 025	9 04		
W-030-Cr/Cu-001-seed-4	0.900		1.100	0.019	0.020	7 99	.	
W-031-Cr/Mn-001-tang-1	1.022		0 955	1 40	2.54	90 6		.
W-031-Cr/Mn-001-tang-2	1.000		0 918	1.42	2.61	91 7	.	.
W-031-Cr/Mn-001-seed-3	1.004		1.004	5 06				.

Table IV. (Continued)

Sample Designation	(τ_{eff}) - ratio g_1	g_2	g_3	τ_{eff} (μs)	s = 8.3 x 10^3 τ (μs)	L (μm)	s = 9 3 x 10^3 τ (μs)	L (μm)
W-031-Cr/Mn-001-seed-4	1.125	1	1.213	5.11		.		
W-032-Mg-003-tang-1	1.016		1.000	1.65	3.45	106.0		
W-032-Mg-003-tang-2	1.000		1.011	2.30	7.89	160 0		
W-032-Mg-003-seed-3	1.033		1 025	2.85	13.0	205.0	14 9	219 0
W-032-Mg-003-seed-4	0.957		1.026	2.68	8.09	162.0	8 70	167 0
W-033-Ti-002-tang-2	1.014		1.029	0.62	0.795	50 6		
W-033-Ti-002-cent-3	1.012		1.023	0.72	0 930	54.9		
W-033-Ti-002-seed-4	1 000		1 022	0.71	0.920	54.3		
W-035-V-002-tang-1	1.029		1.029	0 670	0 850	52.4	.	
W-035-V-002-tang-2	1.019		1.038	0.880	1.21	62 3		.
W-035-V-002-seed-3	1.000		1.033	0 820	1.10	59 6		
W-035-V-002-seed-4	1.012		1.025	0.750	0.980	56 3		
W-036-Zr-002-seed-1	1.000		1.000	0.750	0.980	56 3		
W-036-Zr-002-seed-2	1.000		1.014	0.750	1.01	57 0		
W-036-Zr-002-tang-3	1.000		1 010	0 740	0 960	55 7		
W-036-Zr-002-tang-4	1.000		1.014	0 730	0.970	56 0		
W-037-Zr/Ti-001-tang-1	1.045		0 909	0 200	0 220	26 5		
W-037-Zr/Ti-001-tang-2	1.018		0 982	0.230	0 260	28.9		
W-037-Zr/Ti-001-seed-4	1.000		1 000	0.196	0.210	26 3	.	
W-038-Al-002-tang-1	0 984		1 016	0.280	0.310	31.8		
W-038-Al-002-tang-2	1.000		1 032	0 290	0.330	32.7		
W-038-Al-002-seed-3	1.058		1.033	0.350	0.396	35.7	.	
W-038-Al-002-seed-4	1.005		1.015	0.440	0 510	40 6		
W-039-Ni-003-tang-1	1.022		1 044	1 20	1.97	79 8	2 04	81.1
W-039-Ni-003-tang-2	1.043		1.043	1.72	3 38	104.0	3 55	107.0
W-039-Ni-003-cent-3	0.801		0 969	1.74	3.45	106.0	3 64	108.0
W-039-Ni-003-seed-4	1 086		1.012	2.34	8.37	164.0	9 62	176.0
W-040-Cr/Ni-001-1	0.968		1.000	0 025	0 026	9 07	.	
W-040-Cr/Ni-001-2	0.943		1.000	0.031	0.032	10.2		
W-040-Cr/Ni-001-3	1.000		1.053	0 033	0.036	10 7		
W-040-Cr/Ni-001-4	1 033		1.067	0.028	0 030	9.85		
W-041-Ni/Cr/Cu-001-1	1.125		1.075	0 039	0 042	11.7		
W-041-Ni/Cr/Cu-001-2	1.000		1 022	0.038	0 041	11.5		
W-041-Ni/Cr/Cu-001-3	1.054		1.054	0.034	0 037	10 9		
W-041-Ni/Cr/Cu-001-4	1 050		1.075	0 030	0 030	9 75		

Table IV. (Continued)

Sample Designation	(τ_{eff})-ratio g_1	g_2	g_3	τ_{eff} (μs)	s = 8.3 x 10^3 τ (μs)	L (μm)	s = 9.3 x 10^3 τ (μs)	L (μm)
W-042-Ti-003-1	1.040	1	1.000	0.169	0.184	24.3	.	
W-042-Ti-003-2	1.020		0.969	0.186	0.200	25.5	.	.
W-042-Ti-003-3	1.023		0.909	0.175	0.188	24.6	.	
W-042-Ti-003-4	1.042		0.833	0 183	0.198	25.2		
W-043-Fe/Ti-001-1	1.008		1.008	0.104	0.108	18.7	.	
W-043-Fe/Ti-001-2	1.000		1.000	0.103	0.108	18.7		.
W-043-Fe/Ti-001-3	0.951		0.982	0.086	0.094	17.5	.	
W-043-Fe/Ti-001-4	1.000		1 000	0.120	0.126	20.1		.
W-044-Fe-003-1	1.013		1.013	0.697	0.877	53.2	.	
W-044-Fe-003-2	1.032		1.048	0.504	0.615	44.5		.
W-044-Fe-003-3	1.000		1.014	0 659	0.820	51.4	.	.
W-044-Fe-003-4	1.032		1.032	0.741	0.968	55.9	.	.
W-045-Cr/Fe/Ti-001-1	1.009		1.000	0 092	0.101	18 05		.
W-045-Cr/Fe/Ti-001-2	1.000		0.982	0.101	0.105	18.4		
W-045-Cr/Fe/Ti-001-3	1.000		1.018	0.079	0.087	16 7		
W-045-Cr/Fe/Ti-001-4	1.025		1.008	0.092	0.101	18.1	.	
W-046-Fe/V-001-1	1.020		0.990	0.880	1.25	63.6		.
W-046-Fe/V-001-2	1.000		1.000	0.820	1.102	59.6		.
W-046-Fe/V-001-3	1.029		1.029	0 670	0.876	53.1		.
W-046-Fe/V-001-4	1.028		1.000	0.691	0 884	53.4		
W-047-Cu/Ni/Zr-001-1	1.022		1.022	1.15	1.85	77.1	1.91	78.4
W-047-Cu/Ni/Zr-001-2	1.022		1.022	1.22	1.91	78.4	1.97	79.6
W-047-Cu/Ni/Zr-001-3	1.000		1.000	1.35	2.39	87.8	2.49	89.7
W-047-Cu/Ni/Zr-001-4	0.989		0.995	1.38	2.31	86.3	2.39	87.8
W-048-Ti-004-1	1.040		1.040	0.450	0.540	41.7	.	
W-048-Ti-004-2	1.006		0.988	0.369	0.430	37 2		
W-048-Ti-004-3				-				
W-048-Ti-004-4				-				
W-049-V-003-1	1.000		1.000	0.169	0.181	24.1	.	.
W-049-V-003-2	1 000		0 987	0.192	0.211	26 1	.	
W-049-V-003-3	1 000		0.986	0.181	0 195	25 1	.	.
W-049-V-003-4	1.015		1.015	0.187	0.201	25 5		
W-050-Ti/V-001-1	1.013		1.000	0.571	0.718	48 1		
W-050-Ti/V-001-2	1.008		1.000	0.932	1.35	66.1		
W-050-Ti/V-001-3	1.012		1.000	0.575	0.722	48.2		

Table IV. (Concluded)

Sample Designation	(τ_{eff})-ratio g_1	g_2	g_3	τ_{eff} (μs)	s = 8.3 x 10^3 τ (μs)	L (μm)	s = 9 3 x 10^3 τ (μs)	L (μm)
W-050-T1/V-001-4	1.045	1	1.015	0.523	0.644	45.6		
W-051-Cu/T1-001-1	1.000		1.000	1.31	2.48	89 4	2.61	91.7
W-051-Cu/T1-001-2	0 977		0.931	1.71	3.71	109.0	3.96	113.0
W-051-Cu/T1-001-3	1.000		0.986	1.93	4.24	117 0	4.51	121.0
W-051-Cu/T1-001-4	1.013		0.973	1.88	4.57	121.0	4.93	126.0
W-052-N1-004-1	0.983		0.983	1.64	3.09	99.9	3.24	102 0
W-052-N1-004-2	1 017		1.000	1.81	4.19	116.0	4.51	121.0
W-052-N1-004-3	1 015		1.030	2.02	4.68	123.0	5.00	127 0
W-052-N1-004-4	1.011		1 000	2.00	4.56	121.0	4.87	125 0
W-055-Cu-004-1	1.020		0.990	2.09	4.47	120 0	4.74	124.0
W-055-Cu-004-2	1.026		1.009	2.38	5.95	139 0	6 39	144.0
W-055-Cu-004-3	1.000		0 983	2.31	5.55	134.0	5.94	138 0
W-055-Cu-004-4	1.027		1 014	1.95	4 33	118 0	4.62	122.0
W-056-Cu-005-1	1.015		1.000	2.14	5 31	131 0	5.72	136 0
W-056-Cu-005-2	1.015		1.007	2.78	11.8	195.0	13.8	211.0
W-056-Cu-005-3	1 025		1.000	2.20	4.97	127 0	5.30	131.0
W-056-Cu-005-4	1 029		1.029	1 81	4.20	116.0	4.52	121.0

The effective lifetime measured under standard conditions was corrected for surface recombination using the value s = 8 3 x 10^3 cm/s. The resulting value of bulk lifetime is given in Table IV along with the corresponding diffusion length. The latter is only approximate in that the conversion assumed a diffusivity of 32.2 for all of the samples even though they were characterized by some spread in resistivity. By virtue of the statistical analysis discussed in the Appendix, a second determination of lifetime was made using a slightly larger value of surface recombination velocity, s = 9 3 x 10^3 cm/s. Only the longer lifetimes, where the surface has a significant effect, were recalculated. The sensitivity of the bulk lifetime to assumptions about the surface is quite apparent.

For several samples no bulk lifetimes are shown. In these cases, the measured effective lifetime exceeded the expected surface lifetime under the assumed surface recombination velocity. This indicates the presence of severe trapping. Under these conditions, the ratios of effective lifetime would be expected to be monotonically declining with increasing injection level. This may or may not be the case due to the complication of sample heating in the course of the measurement, when the very highest background light intensities were used in an attempt to fill the traps.

Data are presented with a precision that is appropriate to the experimental resolution, not the putative accuracy. This was done for the purpose of any statistical studies or further treatment of the data which might yet be undertaken.

No data at all are shown for some samples. Some of these were not uniform in resistivity and could not be measured. Others, unfortunately, were casualties.

Diffusion length data taken on the Westinghouse 1 x 1 cm^2 solar cells test structures are given in Table V. Data were taken at three different generation rates $g_1 = 2.46 \times 10^{15}$ $cm^{-3}sec^{-1}$, $g_2 = 7.11 \times 10^{15}$ $cm^{-3}sec^{-1}$, and $g_3 = 1.61 \times 10^{16}$ $cm^{-3}sec^{-1}$. Diffusion length values are shown in μm, and no correction has been made for the depletion width, which is about 1 μm for these resistivities. Corresponding lifetimes have been indicated, although these are likewise calculated without correction for depletion width, and the assumption of D = 32.2 cm^2/s has been made throughout.

Calibration of the generation rate of the penetrating light apparatus was done in the Co^{60} source using the Westinghouse devices which were made from baseline material. Discussion of the data is reserved for Section 4.3.

Table V. Diffusion lengths determined at three generation rates for Westinghouse devices.

Sample Designation	g_1		g_2		g_3	
	L (μm)	τ (μsec)	L (μm)	τ (μsec)	L (μm)	τ (μsec)
W-004-Cz-001-1T$_1$	43 8	0 595	43 5	0 587	43 1	0 576
W-004-Cz-001-2T$_1$	48 7	0 736	48 0	0 715	47 5	0 700
W-004-Cz-001-4C	42 8	0 580	42 5	0 560	42 2	0 550
W-004-Cz-001-1S	52 2	0 845	52 0	0 840	51 8	0 830
W-005-Mn-001-1ET	33 1	0 339	33 1	0 340	33 0	0 340
W-005-Mn-001-3ET	34 2	0 363	34 2	0 360	34 1	0 360
W-005-Mn-001-2S	31 8	0 313	32 6	0 333	33 1	0 340
W-005-Mn-001-4S	28 5	0 250	30 2	0 280	31 3	0.300
W-006-Ni-001-2ET	120 0	4 49	143 0	6 33	159 0	7 79
W-006-Ni-001-3ET	122 0	4 58	143 0	6 33	157 0	7 61
W-006-Ni-001-5ES	48 9	0 740	66 3	1 36	84 4	2 21
W-006-Ni-001-8ES	70 6	1 55	94 2	2 75	116 0	4.18
W-007-Cu-001-1T	146 0	6 57	147 0	6 72	146 0	6 59
W-007-Cu-001-2T	171 0	9 07	179 0	9 96	180 0	10 1
W-007-Cu-001-2S	185 0	10 7	202 0	12 7	207 0	13 3
W-007-Cu-001-5C	165 0	8 44	168 0	8 73	168 0	8 73
W-008-Ti-001-1S	5 18	0 008	4 91	0 007	4 90	0 007
W-008-Ti-001-2S	5 18	0 008	5 16	0 008	5 11	0 008
W-008-Ti-001-1T	4 56	0 006	4 57	0 006	4 49	0 006
W-008-Ti-001-3C	5 05	0 008	5 04	0 007	4 08	0.008
W-009-V-001-3S	6 29	0 012	6 27	0 012	6 22	0 012
W-009-V-001-5C	6 29	0 012	6 19	0 012	6 13	0 012
W-009-V-001-3T	6 29	0 012	6 31	0 012	6 21	0 012
W-009-V-001-4T	6 29	0 012	6 27	0 012	6.24	0 012
W-010-Ni-002-1C	34 9	0 380	34 8	0 380	34 7	0 370
W-010-Ni-002-2T	33 8	0 350	33 6	0.350	33 6	0 350
W-010-Ni-002-3S	34 3	0 370	34 2	0 360	34.1	0 360
W-010-Ni-002-4S	35.4	0 390	35 3	0 390	35 2	0 380
W-011-Zr-001-1S	93 1	2 69	103.0	3 32	112 0	3 88
W-011-Zn-001-2S	79 1	1 94	89 7	2 50	99 9	3 10
W-011-Zn-001-3T	163 0	8 24	162 0	8 15	160 0	7.93
W-011-Zn-001-4C	174 0	9 34	176 0	9 58	176 0	9 58
W-012-Cz-002-1C	77.4	1.86	82.3	2 10	85.5	2.27
W-012-Cz-002-4ET	123.0	4 66	125 0	4.85	126.0	4.94
W-012-Cz-002-6ES	10.8	0 520	49 6	0 760	58 3	1 05
W-012-Cz-002-7ES	37 0	0 430	44 1	0 600	51.6	0 830
W-013-Mn-002-1S	74 7	1 73	88 4	2 42	101 0	3 15
W-013-Mn-002-2S	120 0	4 50	137 0	5 80	149.0	6 92
W-013-Mn-002-1T	123 0	4.66	128 0	5 01	130 0	5 24
W-013-Mn-002-4C	143 0	6 33	151 0	7 09	155 0	7.43
W-015-Zn-001-1T	164.0	8.32	207 0	13 3	239 0	17 7
W-015-Zn-001-2T	272 0	22 9	298 0	27 5	305 0	28 9
W-015-Zn-001-1S	34 8	0.380	42 5	0 560	54 2	0 910
W-015-Zn-001-4C	122 0	4 62	123 0	4 69	123 0	4 69
W-016-Fe-001-1S	153 0	7 25	154 0	7 38	153 0	7 28
W-016-Fe-001-3S	144 0	6.39	144 0	6 42	143 0	6 30
W-016-Fe-001-1T	76 0	1.80	77 7	1 87	78 6	1 92
W-016-Fe-001-4C	100 0	3 11	101 0	3 18	102 0	3 21
W-017-Cu-002-1T	208 0	13 1	203 0	12 7	196 0	11 9
W-017-Cu-002-2T	191 0	11.3	187 0	10 8	181 0	10 2

Table V. (Concluded)

Sample Designation	g_1		g_2		g_3	
	L (μm)	τ (μsec)	L (μm)	τ (μsec)	L (μm)	τ (μsec)
W-017-Cu-002-2S	113 0	3 96	131 0	5.30	144.0	6.40
W-017-Cu-002-3S	134 0	5.57	156 0	7 54	174 0	9 36
W-018-Fe-002-1S	20 5	0 130	20 4	0 130	20 4	0.130
W-018-Fe-002-2S	21 3	0 140	21.3	0 140	21 3	0 140
W-018-Fe-002-1T	47 3	0 690	46.8	0 680	47 3	0 690
W-018-Fe-002-4C	19.8	0 120	19.8	0.120	19 8	0 120
W-019-Cu-003-1T	200.0	12 4	201 0	12 5	197 0	12 0
W-019-Cu-003-2T	210 0	13.6	208 0	13.4	201.0	12 6
W-019-Cu-003-3S	186 0	10 7	190.0	11.2	190 0	11.1
W-019-Cu-003-4S	161.0	8 04	173 0	9.30	180.0	10.0
JPL #6 Baseline	346.0	37.1	338.0	35 4	327 0	33.2
JPL #7 Baseline-3B	165.0	8 46	174.0	9 40	176 0	9.64
W-021-Mg-001-1S	137 0	5.80	152 0	7.12	162.0	8.12
W-021-Mg-001-2S	158 0	7 71	169 0	8.85	175 0	9 53
W-021-Mg-001-3T	208 0	13.5	210 0	13.7	208 0	13 4
W-021-Mg-001-4T	258 0	20.6	257 0	20 5	248 0	19.0
W-024-Mg-002-1T	88.4	2.12	102.0	3.25	114 0	4.03
W-024-Mg-002-2T	143 0	6.33	171.0	9.08	194.0	11 7
W-024-Mg-002-2S	102 0	3 25	123.0	4 66	140 0	6.06
W-024-Mg-002-3S	41.4	0.530	52.2	0 850	64.4	1 29
W-026-Mn-003-1S	385 0	45.9	521 0	84.0	591 0	108 0
W-026-Mn-003-2S	437 0	59 3	487.0	73 4	467 0	67.6
W-026-Mn-003-3T	140 0	6.08	140.0	6.08	139 0	5.99
W-026-Mn-003-5C	126.0	4 92	126.0	4.92	125.0	4 85

Sample Designation	g_1		g_2		g_3	
	L (μm)	τ (μsec)	L (μm)	τ (μsec)	L (μm)	τ (μsec)
W-027-Mn/Cu-001-3T	29.7	0.270	30.3	0 290	30.5	0.290
W-027-Mn/Cu-001-6C	30 9	0.296	31 8	0.310	32.3	0 320
W-028-Al-001-1S	47.5	0.700	47 1	0.690	46 6	0 670
W-028-Al-001-2S	45.6	0 650	45.3	0 640	45 1	0.630
W-029-Cr-003-1S	213 0	14.1	220.0	15 1	220.0	15 1
W-029-Cr-003-2S	141 0	6 19	157.0	7.61	165 0	8 40
W-029-Cr-003-3T	167.0	8.62	181.0	10.1	186.0	10 7
W-029-Cr-003-4T	144.0	6.47	155 0	7 43	157.0	7 61
W-030-Cr/Cu-001-2S	41.3	0 530	40.9	0 520	40.7	0 510
W-030-Cr/Cu-001-3S	42.5	0.560	42 3	0.560	42.1	0.550
W-030-Cr/Cu-001-2T	32 4	0 330	32.3	0.320	32.1	0.320
W-030-Cr/Cu-001-3T	32.7	0.330	32 5	0 330	32.3	0 330
W-031-Cr/Mn-001-1T	13 6	0 057	13.3	0.055	13.2	0 054
W-031-Cr/Mn-001-2T	13.4	0.056	13 4	0.056	13 3	0 055
W-031-Cr/Mn-001-1S	15 4	0 074	15.4	0.074	15 3	0 073
W-031-Cr/Mn-001-3S	10 4	0.033	10 5	0 034	10.4	0 034

4.2 LIFETIME AND DIFFUSION LENGTH MEASUREMENTS ON MONSANTO SAMPLES

The SSPC lifetime and penetrating light measurements of diffusion length determined on Monsanto samples are given in Tables VI and VII, respectively. The format is the same as that used for the Westinghouse samples. In this case, however, lifetimes are calculated only for one value of surface recombination velocity, $s = 8.3 \times 10^3$ cm/s, since the Monsanto samples tended to be thicker and the surface has a less dramatic effect. Diffusion lengths in Table VII were converted to lifetime using a diffusivity of 22 in all cases, corresponding to the mean resistivity for the Monsanto cells.

The bulk samples were furnished as 2×2 cm^2 solar cell blanks and it was necessary to cut these in half to fit our SSPC sample holder. A diamond saw with a vacuum chuck was used for the purpose After sawing, the samples were cleaned using organic solvents and DI water, prior to the application of the contacts. A similar solvent treatment had been found to have no discernible effect on lifetime measurements made on Westinghouse samples.

Calibration of the generation rate for the 2×2 cm^2 solar cells was compelled to be indirect due to the fact that all of the Monsanto cells had solder reflow metallization, which made the Co^{60} method inapplicable due to unquantifiable dose enhancement effects. Calibration was done by means of conventional solar cells Since most of the Monsanto cells did not have an AR coating, the AR coatings were also removed from the standard cells to equalize the surface reflection. Some of the Monsanto cells did have an AR coating, however, and the enhancement of generation rate which this implied was determined by removal of the AR coating from one of the cells and comparing pre- and post-measurements The difference in generation rates was found to be only about 11 - 12%, which may seem low However, it must be considered that this refers only to bandedge radiation, or about 1.06 μm, for which the AR coating is not optimized

Generation rates were slightly different for the Monsanto cells than for the Westinghouse measurements $g_1 = 2.05 \times 10^{15}$, $g_2 = 5.92 \times 10^{15}$, and $g_3 = 1.34 \times 10^{16}$ cm^{-3}sec^{-1}.

Table VI. Lifetime data for Monsanto bulk samples.

Sample Designation	(τ_{eff})-ratio			τ_{eff} (μs)	s = 8.3 x 10^3	
	g_1	g_2	g_3		τ (μs)	L (μm)
MON-2-0-00-014-D-1	0.926	1	1.056	2.25	3.96	93 4
MON-2-0-00-016-D-1	1.024		1 048	2.95	6.49	120.0
MON-2-0-A-012-D-1	1.025		0 950	0.036	0.039	9.25
MON-2-0-A-016-D-1				0.023	0.024	7 32
MON-2-0-C-010-D-1	0.971		0.989	1.54	2.34	71.7
MON-2-0-C-012-D-1	1.034		1.000	1.39	1 90	64.6
MON-2-0-E-006-D-1	1.570		0.941	0 091	0.10	14.8
MON-2-0-E-012-D-1	1.000		0.933	0.100	0.110	15.6
MON-2-0-F-006-D-1	1.017		1.025	2.67	4.94	104.0
MON-2-0-F-008-D-1	1.049		1.033	2.37	4.32	97.5
MON-2-0-G-002-D-1	1.516		0 703	0.180	0.190	15.3
MON-2-0-G-004-D-1	1 765		0.971	0.186	0.197	15.7
MON-2-0-I-001-D-1	1.045		0.982	1.95	3.16	83.4
MON-2-0-I-007-D-1	1.096		1.017	2.43	4.51	99.7
MON-2-0-J-010-D-1	1.035		0.965	3.52	8.46	137.0
MON-2-0-J-014-D-1	1.058		1.029	0.331	0.365	28.4
MON-2-J-014-D-1	0.934		1 009	0 305	0.331	27.0
MON-2-J-016-D-1	1 083		0.988	0.295	0.319	26.5
MON-2-0-006-D-1	1 038		1.000	3.09	8.53	153.0
MON-2-0-008-D-1	1.059		1.044	3.05	8.42	154.0
MON-2-B-010-D-1	1.144		0.992	3.41	8.97	141.0
MON-2-B-012-D-1	1.030		1 020	3.17	7.57	129 0
MON-2-E-002-D-1	1.207		0.948	0.089	0 097	14.6
MON-2-E-006-D-1	1.119		0.963	0.098	0.107	15.4
MON-2-G-010-D-1	1.075		1.000	2.18	4.40	98.5
MON-2-G-012-D-1	1.041		1.014	2.70	6 03	115.0
MON-2-H-014-D-1	1.198		0.937	0.089	0.100	14.7
MON-2-H-016-D-1	1.095		0.869	0.074	0.081	13.5
MON-2-I-012-D-1	0.963		0.950	2.17	3.74	90.7
MON-2-I-016-D-1	1.000		1.018	2.56	4.95	104.0
MON-2-K-012-D-1	1.009		0.991	3.53	9.79	147.0
MON-2-K-016-D-1	1.037		0.971	3 33	8.47	137 0
BC6BD (3)-1	1.029		1.007	3.38	8.78	139.0
BC6BD (4)-1	1.057		1.011	2.16	3 71	90.4
BC9BD (1-1)-1	1.044		1.000	3 69	25.7	277 0
BC9BD (2-1)-1	1.023		1.023	2.79	7.19	147 0
BC11BD (1-1)-1	1.000		0 929	0 070	0 076	12 9
BC11BD (3-1)-1	1.318		0.955	0 060	0.065	12.0
BC12BD (1-3)-1	1.016		1.031	1.65	2.48	73 8
BC12BD (4-3)-1	1.032		1.016	1.68	2 54	74.8

Table VI. (Concluded)

Sample Designation	(τ_{eff}) - ratio			τ_{eff}	$s = 8.3 \times 10^3$	
	g_1	g_2	g_3	(μs)	τ (μs)	L (μm)
BC13AD (6-1)-1	0 994	1	1.006	23.5		.
BC13AD (8-1)-1	1.000		1.021	19.5		.
BC14AD (1-1)-1	1.014		1.013	12.3		
BC14AD (2-1)-1	1.024		1.012	13.6		
BC15BD (1-3)-1	1.046		1.015	1.78	2.90	79.9
BC15BD (2-3)-1	1.057		1.038	1 41	2.06	67.4
BC16BD (1-1)-1	1.027		1.009	0.940	1.22	51.8
BC16BD (1-2)-1	1.033		1.000	0.935	1.21	51.6
BC17BD (1-1)-1	1.042		1.017	0 990	1.30	53.5
BC17BD (2-1)-1	1.035		1.000	0.990	1.30	53.5
B-M3BD-3-1	1.043		1.000	1.14	1 48	57 1
B-M3BD-4-1	1.035		1 021	4.23	13 5	173 0
B-M9BD-3-1	1.034		1.014	4 37	19 3	206.0
B-M9BD-4-1	1.027		1 018	3 51	11.6	160 0
B-M11BD-4-1	0.974		1.034	1.04	1.34	54.3
B-M11BD-5-1	1.015		0.992	1.04	1.31	53 7
B-M13AD-4-1	1.000		1.012	14.9		.
B-M13AD-5-1	0.984		1 016	11.6		
B-M14BD-4-1	1.005		1.027	18.1		.
B-M14BD-5-1	0.987		0 996	21 3		
B-M15BD (1-1)-1	1.000		1.000	5.82		
B-M15BD (2-1)-1	1.113		1.035	3 65	10.7	153 0
B-M16BD-3-1	0.944		1.016	3.52	8 46	137 0
B-M16BD-4-1	1.029		1.000	3.80	10 1	149.0
B-M17BS-3-1	0.512		1.706	8 05	.	
B-M17BS-5-1	0.950		1.000	9.35		
B-M19BD-3-1	1.078		1.009	2.01	3.13	74.4
B-M19BD-4-1	1.043		1.000	1.84	2.73	70.0
B-M31BD-3-1	1.079		1.022	5.05	43.1	308 0
B-M31BD-4-1	1.026		1 053	5.06	43 7	310.0
B-M32BD-3-1	1.000		0 857	0 060	0.065	11.9
B-M32BD-4-1	1.091		0.836	0.037	0 040	9.37

Table VII. Diffusion lengths determined at three generation rates for Monsanto solar cells.

Sample Designation	g_1		g_2		g_3		Sample Designation	g_1		g_2		g_3	
	L (μm)	τ (μsec)	L (μm)	τ (μsec)	L (μm)	τ (μsec)		L (μm)	τ (μsec)	L (μm)	τ (μsec)	L (μm)	τ (μsec)
C1AD-1-2	51 7	1.21	52.6	1 26	53 0	1 27	C7BD-1-3	5 04	0.0115	5 04	0 0115	5.04	0 0115
C1AD-1-3	52.3	1 24	53.7	1 31	54 6	1 35	C7BD-2-1	4 86	0.0107	4.95	0 0111	4 95	0 0111
C1AD-2-1	46 5	0 980	48 3	1 06	49 2	1.10	C7BD-2-3	4 92	0.0110	4.92	0.0110	4 92	0.0110
C1AD-3-1	36.3	0 600	38 1	0 660	38.7	0 680	C8BID-2-3	27.0	0.331	28.5	0 369	29 4	0.392
C2BID-2-1	52 2	1.24	53.7	1 31	54 0	1 32	C8BID-2-4	32 7	0.486	34.2	0.531	35.1	0.599
C2BID-2-2	53 7	1,31	55 2	1 38	55 8	1.41	C8BID-3-1	33 0	0 494	34 8	0.550	35 4	0.569
C2BID-2-3	50 7	1 17	52 5	1 25	52 8	1 27	C8BID-3-4	27.9	0 353	29 7	0 400	30 6	0 425
C2BID-2-4	51 3	1 20	52.8	1 27	53.1	1 28	C9BID-2-1	56.5	1.45	54 2	1.33	53.5	1,299
C3AD-2-1	38.7	0 680	39.9	0 720	40 5	0 740	C9BID-3-3	52.2	1 24	53 1	1 28	53.4	1 30
C3AD-2-2	38.1	0 660	39.3	0 700	39 6	0 710	C9BID-3-4	51 9	1 22	53 1	1.28	53.1	1.28
C3AD-4-1	37 2	0 630	38 4	0.670	38 7	0 680	C9BID-4-1	61.9	1 74	64 2	1.87	64 8	1.91
C3AD-3-4	48 9	1 09	50 7	1 17	51.3	1 20	C10BID-3-2	2.64	0 00316	2 46	0.00274	2.40	0.00260
C4BD-1-4	35 4	0 570	36.0	0 590	36 3	0.600	C10BID-3-2	2.46	0.00218	2 22	0.00224	2 22	0.00224
C4BD-2-1	36.0	0 590	37.0	0 620	37 2	0 630	C10BID-4-1	2 46	0.00275	2 46	0.00275	2.43	0 00268
C4BD-2-2	34 2	0 530	35.1	0 560	35 4	0,570	C10BID-4-2	3 18	0.00459	2 52	0 00228	2.31	0 00242
C4BD-2-3	34.8	0 550	35.4	0 570	35 7	0.580	C11BID-2-2	3 00	0 00409	3 09	0.00434	3.09	0 00434
C5BD-2-1	33 3	0 500	34.5	0.540	35 1	0 560	C11BID-2-3	3 06	0.00425	3.12	0.00442	3.09	0 00434
C5BD-2-2	33 9	0 520	35 1	0 560	35 7	0 580	C11BID-2-4	3.15	0 00451	3 18	0.00459	3 15	0 00451
C5BD-3-2	31 8	0 460	33.0	0 490	33.3	0.500	C11BID-4-3	67 7	2 08	70 6	2 26	71 3	2 31
C5BD-3-3	31.8	0 460	32.7	0 490	33 0	0 490	C12BD-1-4	10.4	0 0492	11.97	0 0651	13 8	0 0861
C6BD-1	64 5	1 89	66 1	1 98	66 7	2.02	C12BD-2-1	11 6	0 0615	13 4	0 0813	15 4	0 107
C6BD-4	62.5	1 77	63.8	1 85	64.2	1 87	C12BD-2-3	11 1	0.0559	12 9	0 0756	14.9	0 0100
C6BD-5-1	92 9	3 92	96 5	4 23	97.1	4 28	C12BD-3-1	10.2	0 0473	11.7	0 0622	13 2	0 0791
C6BD-5-3	68.6	2 14	67.4	2 06	57 4	1.49	C13BD-2-3	36 0	0 589	36.9	0 618	36 9	0 618
C7BD-1-2	5 01	0 0114	5.01	0 0114	5 04	0 0115	C13BD-2-4	34.5	0.541	34 8	0 550	34.8	0 550

Table VII. (Continued)

Sample Designation	g_1		g_2		g_3	
	L (μm)	τ (μsec)	L (μm)	τ (μsec)	L (μm)	τ (μsec)
C13BD-3-1	35 9	0 584	36 3	0 598	36 3	0 598
C13BD-3-2	32.4	0 477	33 3	0.504	33.6	0.513
C14AD-2-2	37 8	0 649	38 7	0 680	39 6	0 712
C14AD-2-3	32 7	0.486	35 1	0 560	35 7	0 579
C14AD-4-1	35 1	0.560	37 5	0 639	38 1	0 659
C14AD-5-2	100 0	4.56	102 0	4 75	103.0	4 83
C15BD-1-1	45.0	0 918	47 9	1 04	49 4	1.11
C15BD-1-4	46,0	0 961	49.0	1.09	50 6	1.16
C15BD-3-1	45.3	0 932	48.3	1.06	50.1	1.14
C15BD-4-1	63.8	1 85	66 2	1 99	66 8	2 03
C16BID-2-1	4 65	0 00982	5 01	0 0114	5 22	0 0124
C16BID-3-1	6 75	0.0207	4 68	0 00995	1.11	0 00767
C16BID-3-2	4 26	0 00824	4.35	0 00859	4 44	0 00895
C16BID-3-4	3 99	0 00723	4 20	0 00797	4 33	0 00851
C17BD-1-2	22 6	0 232	22 7	0 234	22 7	0 234
C17BD-2-1	20.1	0 184	20 4	0.189	20 1	0 190
C17BD-3-2	21 0	0 200	21 2	0 205	21.2	0.205
C17BD-3-3	20 4	0 189	20 7	0 195	20 7	0 195
M1BD-1	122 0	6 70	124.0	6 93	129 0	7 53
M1BD-3	97 7	4 33	99.0	4 45	99 0	4 46
M1BD-5	101 0	4 64	102.0	4 76	102 0	4 75
M1BD-6	95 8	4 17	97.4	4 31	97 1	4 28
M2BD-2	42 8	0.830	43 4	0 855	43 6	0 862
M2BD-3	26 4	0 317	26 7	0 324	26.7	0 324

Sample Designation	g_1		g_2		g_3	
	L (μm)	τ (μsec)	L (μm)	τ (μsec)	L (μm)	τ (μsec)
M2BD-4	32.7	0 486	33 0	0 495	33.3	0 504
M2BD-6	33 6	0 512	33.9	0.523	34.1	0 527
M3BD-3	111 0	5.61	112.0	5 74	114.0	5 86
M3BD-4	242 0	26.7	252 0	28.9	246,0	27.5
M3BD-5	108,0	5 25	110,0	5 49	111.0	5.57
M3BD-6	113 0	5.82	117.0	6 18	117 0	6 19
M4BID-3	110 0	5 49	112,0	5 65	111,0	5 57
M4BID-5	102 0	4 73	103 0	4.83	103.0	4 83
M4BID-6	99 7	4.51	101 0	4 67	101.0	4 63
M4BID-7	96 2	4 20	96 5	4 23	96 8	4,26
M5BID-3	5 73	0.0149	5.79	0 0152	5 79	0 0152
M5BID-4	6.24	0 0177	6 36	0 0184	6 36	0.0184
M5BID-5	6.36	0 0184	6 42	0.0187	6.42	0 0187
M5BID-6	5 73	0 0149	5 79	0 0152	5 76	0 0151
M6BD-3	47.1	1.01	48.9	1 09	50 1	1 14
M6BD-4	51 9	1 22	52.8	1 27	53 4	1.30
M6BD-5	54 6	1.35	55 97	1 42	56 5	1 45
M6BD-6	51 3	1.20	52.5	1 25	53.4	1 30
M7BD-3	80.9	2 97	84 3	3 23	86 96	3.43
M7BD-5	57.7	1 51	60 7	1 67	63 2	1 81
M7BD-6	52.0	1 23	55 5	1 40	58 5	1.55
M7BD-7	59 1	1 59	62 9	1 80	66.2	1 99
M8BD-1	6.24	0 0177	6 18	0 0173	6 15	0.0172
M8BD-2	6 24	0 0177	6 30	0.0180	6 30	0 0180

Table VII. (Concluded)

Sample Designation	g_1		g_2		g_3	
	L (μm)	τ (μsec)	L (μm)	τ (μsec)	L (μm)	τ (μsec)
M8BD-3	6 45	0 0189	6.51	0.0193	6.51	0.0193
M8BD-5	6.57	0 0196	6 42	0 0189	6.33	0.0182
M9BID-2	47.1	1.01	48 9	1 09	49 8	1 13
M9BID-3	41 7	0 789	43 5	0 859	44.7	0 907
M9BID-4	111 0	5 57	107 0	5.18	105.0	5.04
M9BID-5	48 6	1 07	49 8	1 13	50.7	1 17
M10BD-2	70.6	2.26	72.3	2 37	73.0	2.42
M10BD-4	78 1	2.77	79.6	2 88	80.0	2.91
M10BD-5	76.5	2.66	75.6	2.60	75.6	2.60
M10BD-6	91 2	3 78	91.7	3 82	91 2	3.78
M11BD-2	113 0	5.82	115 0	6 00	115.0	6.00
M11BD-3	115.0	6.00	114.0	5.91	114.0	5.86
M11BD-4	141.0	9.00	144 0	9.35	143 0	9.27
M11BD-5	116.0	6 09	118 0	6 33	118.0	6.29
M13AD-2	54 8	1.36	55.7	1 41	55.7	1.41
M13AD-3	42 2	0.809	42.9	0 836	42.9	0.837
M13AD-4	45.3	0.932	45 6	0 914	45 5	0.942
M13AD-6	62.1	1 75	63.2	1.82	63 2	1.81
M14BD-2	44.4	0 895	45.3	0 932	45.3	0 932
M14BD-5	61.6	1.72	62 4	1.77	62.4	1 77
M14BD-6	58.0	1 53	58 5	1.55	58 3	1 54
M14BD-7	54 3	1.34	55 8	1.41	55.9	1.42
M15BD-2	88 2	3.53	93.5	3.97	97.1	4 28
M15BD-3	75 6	2 60	80 2	2.92	83 3	3.15
M15BD-4	80 2	2.92	85.3	3.30	89 0	3.60
M15BD-5	85 2	3.30	89 8	3 66	92.9	3.92
M16BD-2	78.7	2.81	82 6	3.10	86.0	3 36
M16BD-3	72.3	2 37	76.3	2.64	79.6	2.88
M16BD-4	75.6	2.60	79 2	2 85	81.7	3 03
M16BD-5	74 1	2 49	77 5	2 73	77 7	2.74
M17BD-3	33.6	0.513	34 0	0.523	34.0	0 526
M17BD-4	29.7	0.401	30.0	0.407	30 0	0.406
M17BD-5	21.0	0 199	23 4	0.248	21.0	0 261
M17BD-6	28.5	0 368	28.8	0.376	28.7	0 375
M19BD-2	204.0	1.89	214 0	2.09	216 0	2 12
M19BD-3	101.0	4.61	102.0	4.76	104 0	4.87
M19BD-4	115.0	6 00	112.0	5 69	111.0	5.57
M19BD-5	138 0	8.60	141.0	9.00	144 0	9 35
M31BD-2	113 0	5 82	115 0	6.00	116 0	6.09
M31BD-4	116 0	6.09	118.0	6.28	117.0	6.18
M31BD-5	123.0	6.86	126.0	7.15	125.0	7 04
M31BD-6	123.0	6 81	125.0	7 04	126 0	7.15
M32BD-2	48.7	1 08	48 9	1 08	48 8	1 08
M32BD-3	45.9	0 957	46 5	0 982	46.5	0 982
M32BD-4	48 3	1.06	48.9	1 09	48 7	1 08
M32BD-5	50.4	1.15	50,9	1.17	50.8	1 17

4.3 DISCUSSION OF RESULTS

The bulk lifetime data obtained on Westinghouse/Dow Corning samples are summarized graphically in Figure 4-1, where lifetimes are shown as a function of concentration of the secondary impurity as determined by Dow Corning.[6] The concentration values are reproduced in Table VIII. These data confirm the extreme sensitivity of lifetime to the presence of moderate concentrations of titanium, chromium, iron, and possibly zirconium. The cases of iron and chromium appear to be particularly well-behaved in that the concentration dependence approximated the expected (-1)-slope. In the case of vanadium, manganese, and magnesium, trapping effects on the lifetime measurements are indicated since the apparent lifetimes are larger for the more heavily doped specimens. The lifetime appears to be considerably less sensitive to the presence of aluminum, nickel, and copper. In the case of nickel, and possibly aluminum, this may be due to the low fraction of the concentration which is expected to be electrically active.

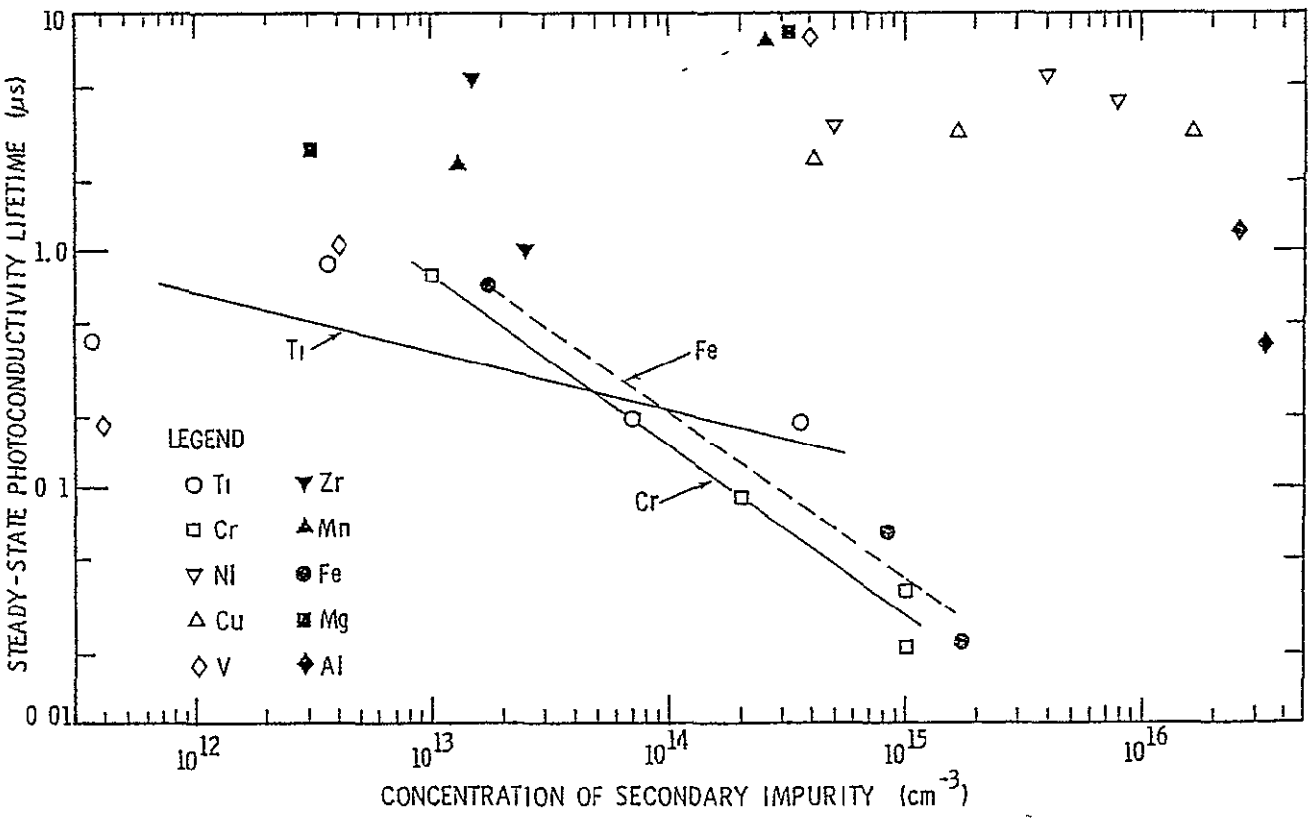

Figure 4-1. Summary of lifetime data for Westinghouse boron-doped, 3 - 5 Ω-cm material with various concentrations of secondary dopants.

Table VIII. Best estimates of impurity concentrations as determined by Dow Corning and Westinghouse. Data are taken from Appendix 3 of Ref. 6.

Ingot Identification	Best Estimate of Impurity Conc. (10^{15} atoms/cm)	Ingot Identification	Best Estimate of Impurity Conc. (10^{15} atoms/cm)
W002-00000	--	W029-Cr003	0 01
W003-00000	--	W030-Cr/Cu001	1 0/1 7
W004-Cr001	1.0	W031-Cr/Mn001	1 0/1 3
W005-Mn001	1 3	W032-Mg003	0.32
W006-Ni001	0 5	W033-Ti002	0 0036
W007-Cu001	1 7	W034-0000	--
W008-Ti001	0 36	W035-V002	0.004
W009-V001	0 4	W036-Zr002	<0.025
W010-Ni002	4 0	W037-Zr/Ti001	<0.015/0.40
W011-Zr001	<0.015	W038-Al002	34
W012-Cr002	0 2	W039-Ni002	8
W013-Mn002	0 26	W040-Cr/Ni001	0 8/3 5
W014-00000	--	W041-Ni/Cr/Cu001	3/0 8/1 7
W015-Zn001	<0.001	W042-Ti003	0 07
W016-Fe001	0 85	W043-Fe/Ti001	0 56/0 06
W017-Cu002	17	W044-Fe003	0 017
W018-Fe002	1 7	W045-Cr/Fe/Ti001	0 65/0 43/0 06
W019-Cu003	0 4	W046-Fe/V001	0 56/0 07
W020-00000	--	W047-Cu/Ni/Zr001	1.7/0.75/<0.015
W021-Mg001	0 003	W048-Ti004	0 00036
W022-00000	--	W049-V003*	0 0004
W023-00000	--	W050-Cu/V001	0 00036/0.0004
W024-Mg002	0 03	W051-Cu/Ti001*	1 7/0 36
W025-00000	--	W052-Ni004	7 5
W026-Mn003	0 013	W055-Cu004	0 05
W027-Mn/Cu001	1 3/1 7	W056-Cu005	65
W028-A001	26		

*Evidence exists that a mixup may have occurred between these ingots, or samples derived therefrom, in the course of their routing history.

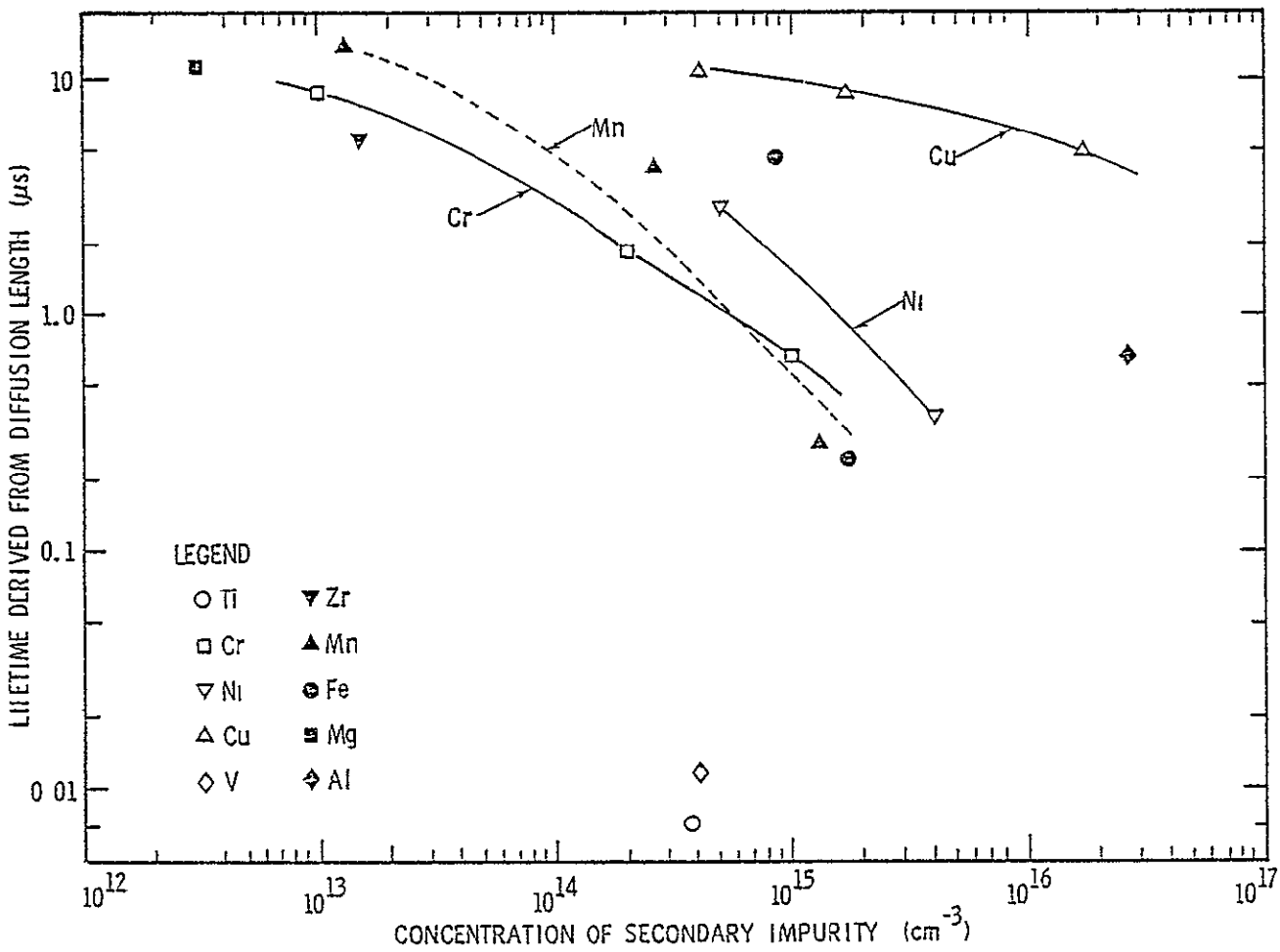

Figure 4-2. Summary of lifetime data derived from diffusion length measurements made on cells of the same material as illustrated in Figure 4-1

The device lifetime data obtained on the Westinghouse/Dow Corning samples are summarized graphically in Figure 4-2, where lifetimes derived from diffusion length are shown as a function of concentration of the secondary impurity. These data indicate that the lifetime is most sensitive to the presence of titanium, vanadium, iron, chromium, manganese and nickel. A much lesser sensitivity is indicated for aluminum and copper. Insufficient data are available to make a judgment with respect to zirconium and magnesium.

The data indicate somewhat greater sensitivity to the presence of chromium, titanium, and nickel than was observed in the bulk samples. In the case of titanium, this may be due to the effect of trapping on the bulk lifetime at higher concentrations, and in the case of nickel, it may be due to a change in the fraction of electrically active impurities. The sensitivity to the

presence of iron was found to be considerably reduced in the device data. This is understandable on the basis of the very high diffusivity of iron, in conjunction with a low solid solubility, at processing temperatures.

In general terms, the bulk and device data confirm the conclusions already drawn by Westinghouse with regard to the sensitivity of lifetime to the presence of these various impurities. The use of different experimental techniques in our study, however, did lead to certain quantitative differences which may affect decisions as to the level of a particular impurity which is tolerable in boron-doped material. A more detailed comparison of our respective sets of data was deemed to be of interest, and this is given in Appendix B.

In the case of the Monsanto samples, the device data are the most extensive, and we have focused on these for the purposes of a preliminary analysis. Sample identifications and lifetimes derived from diffusion length measurements are given in Table IX. A graphical summary of these data is given in Figure 4-3 as a function of the secondary impurity concentration, as determined by Monsanto using spark source mass spectrometry. Only the data for the boron-doped samples are included. In those cases in which the concentration could not be determined in this way, the data points are plotted at the detection limit. Data for both Czochralski and float-zone ("Mon-X") material are shown. The data are qualitatively consistent with those of Westinghouse in terms of the hierarchy of impurities with respect to their lifetime-degrading effectiveness. Data are also provided for carbon and sodium. Zirconium is more unambiguously established as one of the critical impurities. Certain ingots containing nickel, manganese, and magnesium were found by Monsanto to exhibit efficiencies in excess of those found for the baseline ingot and the possibility was raised that these impurities might in fact improve the lifetime. These tendencies have been confirmed in our lifetime measurements. Thus, the higher efficiencies indeed appear to result from higher base lifetimes in these ingots, rather than from changes in junction properties, for example. We prefer to believe that the enhancement is

Table IX. Monsanto sample identifications.
Data were taken from Tables 21 and 22 of Ref 18

Sample Designation	Primary Dopant	Secondary Dopant	Concentration of Secondary Impurity ($\times 10^{16}$ cm^{-3})	Mean Device Lifetime (μs)	Standard Deviation (μs)
C1A	B	—	—	1.01	0.30
C2B1	B	C	10.	1.23	0.061
C3A	B	Fe	.21	0.765	0.22
C4B	B	Cr	.41	0.560	0.026
C5B	B	Mn	1.2	0.485	0.030
C6B	B	Ni	7.1	2.43	1.0
C7B	B	V	.07	0.011	0.370
C8B1	B	Zr	≤.06	0.416	0.086
C9B1	B	Mg	.12	1.41	0.24
C10B1	B	Al	200.	0.00317	0.0010
C11B1	B	Ti	.06	0.00428	0.00021
C12B	B	C/Ni	2.9/4.7	0.0535	0.0065
C13B	P	—	—	0.548	0.052
C14A	P	C	5.3	0.565	0.082
C15B	B	Na	.021	1.17	0.46
C16B1	B	P-comp	22.	0.0115	0.0062
C17	P	Ti	.095	0.201	0.022
M1B	B	--	—	4.96	1.18
M2B	B	Fe	≤.16	0.536	0.21
M3B	B	Mn	.15	5.56	0.29
M4B1	B	Ni	.62	4.73	0.550
M5B1	B	V	.05	0.016	0.0018
M6B	B	Zr	≤.03	1.200	0 140
M7B	B	Mg	.01	1.83	0.78
M8B	B	Ti	≤.01	0.0185	0.00094
M9B1	B	C	—	2.11	2.31

Table IX. (Concluded)

Sample Designation	Primary Dopant	Secondary Dopant	Concentration of Secondary Impurity ($\times 10^{16}$ cm^{-3})	Mean Device Lifetime (μs)	Standard Deviation (μs)
M10B	B	Al	40.	2.87	0.65
M11B	B	Ni/Mn/Mg	1.8/.24/≤.011	6.73	1.52
M13A	P	--	--	4.00	0.430
M14B	P	C	8.6	1.37	0.353
M15B	B	Na	≤.013	3.09	0.411
M16B	B	P-comp	1.6	2.57	0.187
M17B	P	Ti	≤.013	0.370	0.130
M19B	--	Al only		5.28	2.80
M31B	B	Cu	≤.024	6.40	0.520
M32B	B	Cr	.26	1.06	0.080

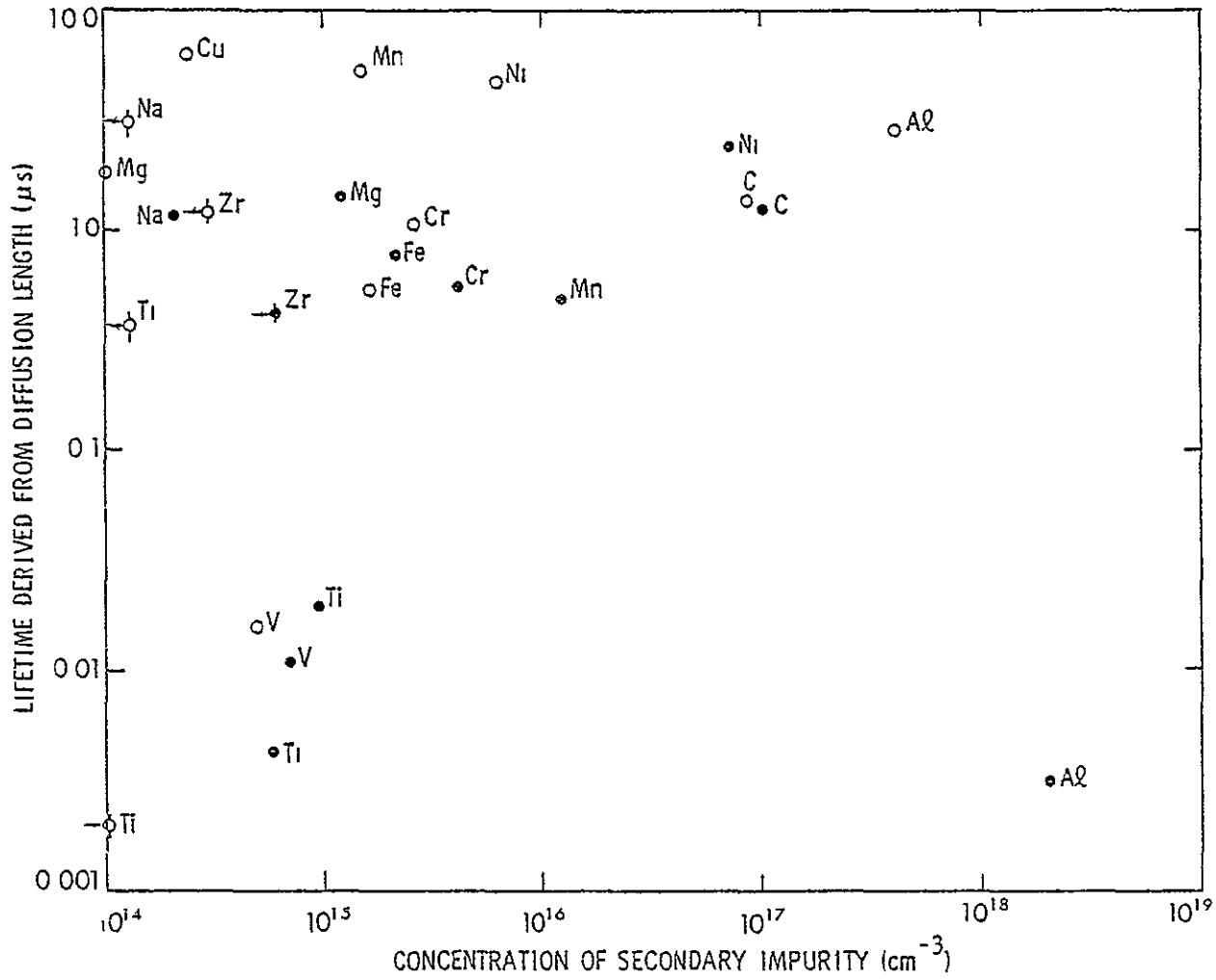

Figure 4-3. Summary of lifetimes derived from diffusion length measurements as a function of concentration of secondary impurities for boron-doped material. Closed circles refer to Czochralski material while open circles refer to float-zone ("Mon-X").

observed only because the baseline ingots (in the case of Czochralski) for some reason did not yield a particularly good lifetime. Nevertheless, the lifetime in nickel-doped solar cells was found to be considerably higher for Monsanto devices than for Westinghouse samples.

We have given the data only the most cursory survey above. Clearly, the data are capable of yielding considerably more information with more detailed analysis. However, this is beyond the scope of the present study.

Our recommendation would be that further studies of this kind be performed on samples which are thicker than these by a factor of two or three so that surface effects are only a perturbation on the measurement rather than a major determinant. This is particularly desirable when trapping is involved. The photoconductivity methods have to discriminate against the effects of trapping and this is considerably easier when the recombination process is not dominated by the surface lifetime.

In studies of the kind undertaken here, a balance must be struck in which the accuracies with which the impurity concentrations and the lifetimes may be obtained are mutually optimized. If the impurity concentration is too low, conventional methods are not adequate to determine the concentrations accurately. On the other hand, lifetime measurements are not as reliable when the lifetimes are short. Fewer ambiguities arise when the concentration of recombination centers is small, and trapping is less likely to be important. From the standpoint of the lifetime measurements, therefore, it would be desirable in the future to target the impurity concentrations so that the lifetime is is reduced just to the point at which solar cell performance is affected, i.e., on the order of 0.5 - 1 μs.

For purposes of mutual comparison among different contractors, standard conditions of measurement, in terms of generation rate and sample temperature, should be established. With regard to the latter, measurements at slightly elevated temperature, say 40°C, are to be preferred. This would correspond more closely to the mean operating temperature of flat-plate arrays, and it would reduce any effect of trapping on the measurements

With respect to generation rate, several comments are in order. It has been the objective in this study to obtain the low-injection level limit of lifetime, short of characterizing the full injection level dependence of lifetime. The generation rates employed in the SSPC lifetime and penetrating light diffusion length methods are appropriate to this purpose. For example, at a 1-μsec lifetime, the 8×10^{16} $cm^{-3} sec^{-1}$ generation rate of the SSPC method yields an injection ratio in 3 Ω-cm material of 2×10^{-5}, which is almost

certainly sufficiently low On the other hand, the background light intensity adds an additional, unquantified amount to the prevailing generation rate (estimated to be typically $\geq 10^{17}$ $cm^{-3}sec^{-1}$).

The question may be raised as to whether these generation rates are relevant to actual solar cell operating conditions. Since the generation rate which prevails under solar illumination is a strong function of depth into the cell, the appropriate analog in terms of uniform generation in a laboratory environment is not obvious. A suitable choice would appear to be the generation rate which prevails at a distance of one diffusion length from the junction Since injection-level effects are most prominent for the longest diffusion lengths (under conditions of constant generation rate), it is most appropriate to calculate the relevant generation rate for such long diffusion lengths, say 200 μm. We have calculated the generation rate which prevails at a distance of 200 μm from the junction, under AM(1) conditions and assuming zero reflection loss, to be about 6×10^{17} $cm^{-3}sec^{-1}$ This is quite comparable to the generation rate which prevails in the SSPC experiment, if both the modulated and background light intensity are taken into account. Therefore, the generation rate employed in these experiments is in fact appropriate to solar cell operating conditions, while simultaneously satisfying low-injection conditions for typical lifetimes observed in this program, as discussed above

The most significant results of this investigation have been as follows· Firstly, consistency of results among the very different experimental methods of measuring lifetime and diffusion length have been verified. Secondly, the SSPC lifetime method has been established for measurements to about 10 ns, and under adverse conditions with respect to minority-carrier trapping and surface recombination. Finally, the extreme sensitivity of lifetime to the presence of certain impurities has been established, and general correspondence with the results of others in terms of the hierarchy of impurities to which the lifetime is sensitive has been found.

APPENDIX A
STATISTICAL ANALYSIS OF THE DATA

In the discussion of the determination of the SSPC generation rate in Section 2.5, a crude test of the validity of the lifetime data was mentioned, namely the requirement simply that all of the measured lifetimes be less than the surface-limited lifetime. This was indeed found to be the case for the vast majority of the samples. In those cases where this condition was violated, there was usually independent evidence of domination by trapping. When the highest available background light intensities were used, and a plateau such as that in Figure 2-4 was still not observed, it was apparent that trapping was dominating the results.

A more refined test is available, however, to check the quality of the data. If the generation rate and the surface recombination velocity are properly chosen, and if there were no random error in the measurements, one would expect to find no correlation of the sample lifetime with sample thickness. We undertook to test this with both the Westinghouse and Monsanto data. Results are shown graphically in Figures A-1 and A-2 for the two sets of data. The logarithm of the lifetime is plotted for convenience of presentation. A correlation of lifetime and sample thickness appears to exist in the case of the Westinghouse samples, whereas in the case of the Monsanto specimens, the sample is not sufficiently large as to give a firm impression.

The correlation which is observed, for those samples having lifetimes greater than 1 μs, could arise either from an underestimate of the surface recombination velocity or from an overestimate of the generation rate. It is of course possible that a true, or inherent, correlation between sample thickness and lifetime exists. It could be that the "better" silicon (lower impurity concentration, etc.) yielded larger ingots, causing more generous slices to be taken in those cases. We can only suppose, for the sake of discussion, that such a correlation did not in fact exist. The existence of random errors would likewise cause a correlation of the data to be observed, but in this case the thinner sample would tend to show the larger lifetimes, so that the correlation

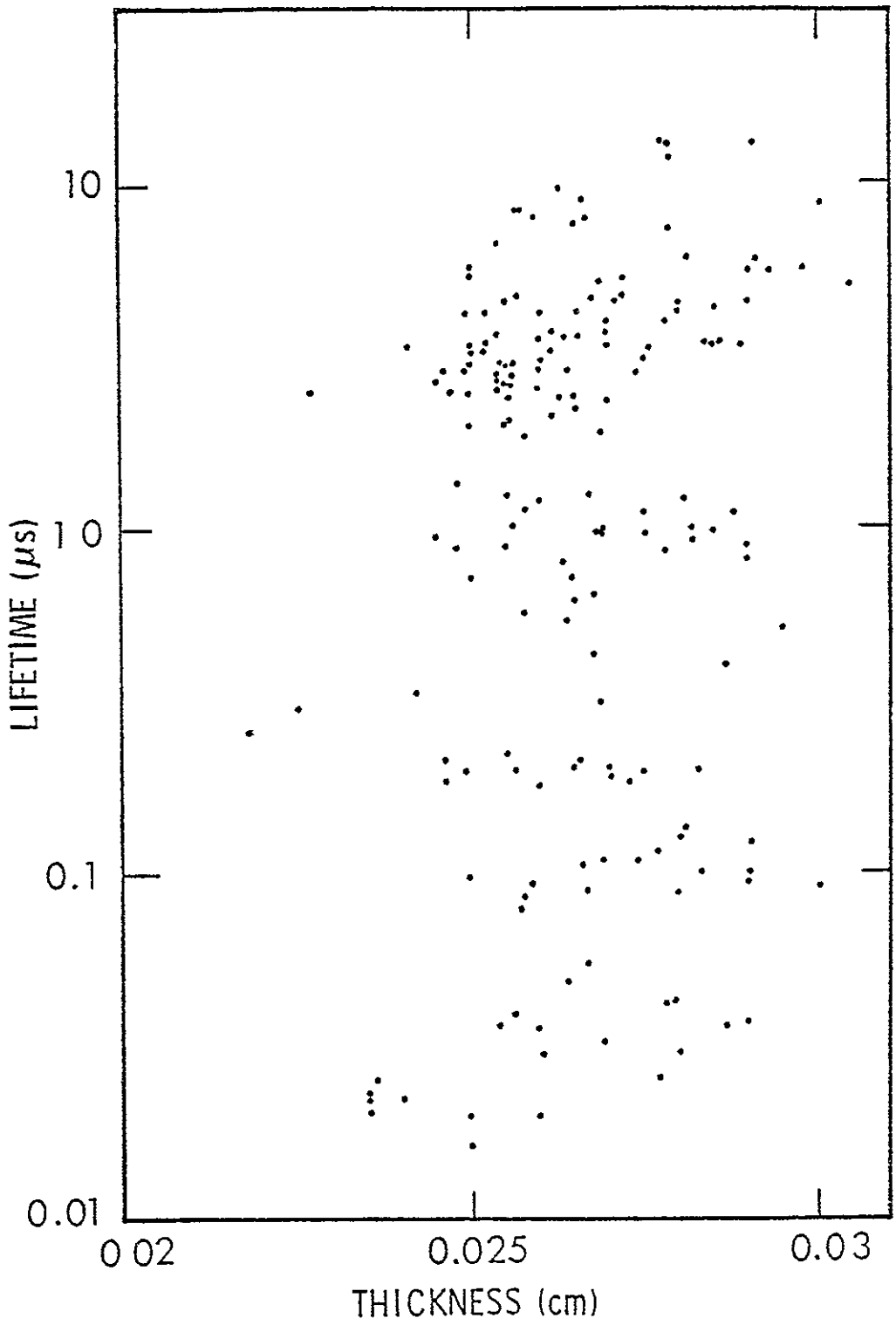

Figure A-1. Distribution of calculated lifetimes for Westinghouse bulk samples, as a function of sample thickness. Lifetimes were calculated under the assumption of s = 8 3 x 10^3 cm/sec.

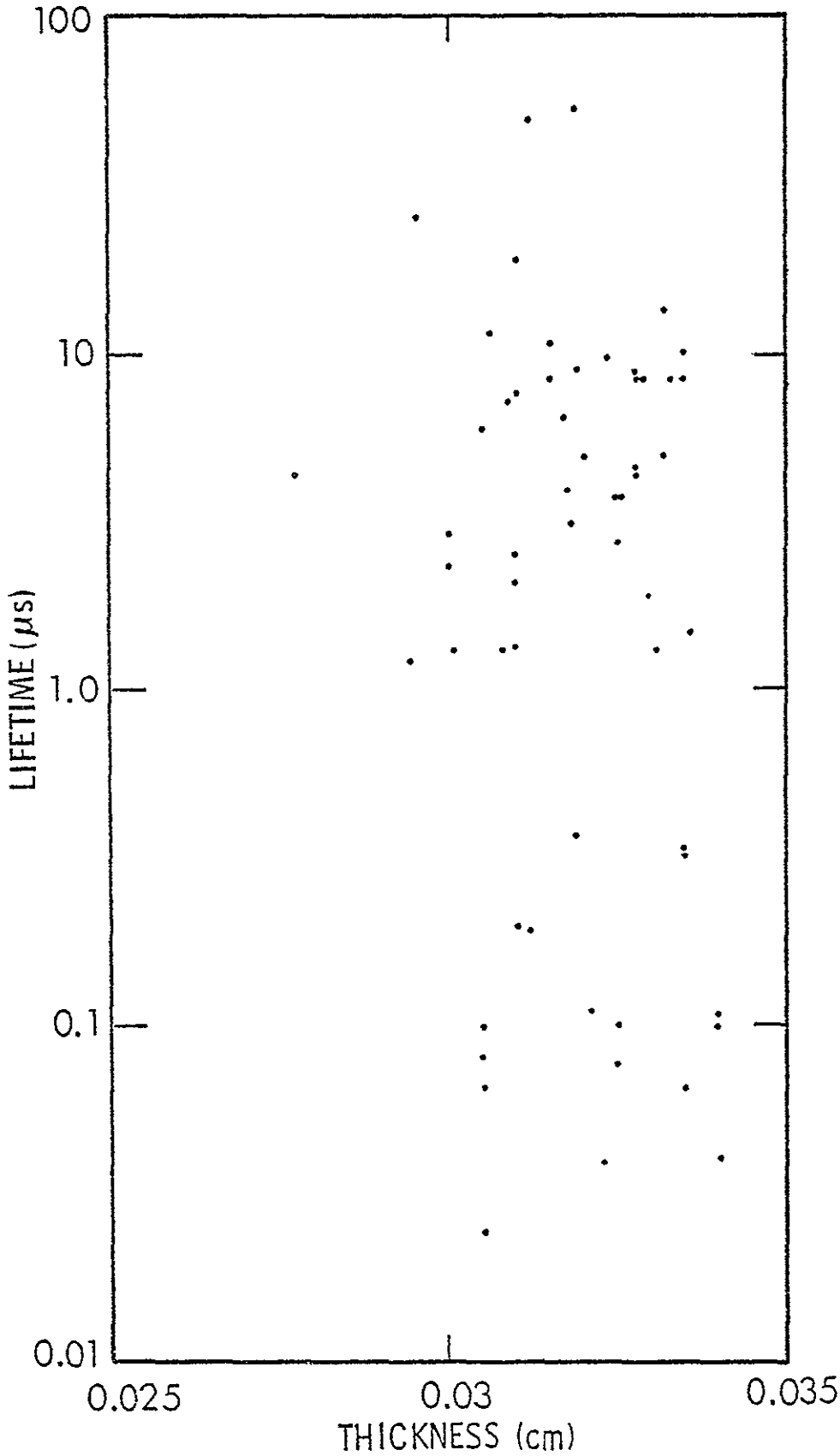

Figure A-2 Distribution of calculated lifetimes for Monsanto bulk samples, as a function of sample thickness. Lifetimes were calculated under the assumption of $s = 8.3 \times 10^3$ cm/sec.

would be opposite in sign to what we observe. Trapping should also be independent of sample thickness, thus yielding a calculated bulk lifetime which would be larger for the thinner samples, again leading to the opposite correlation from that we observe.

The implication of the above is that either the chosen value of surface recombination velocity was too low, or the generation rate was in fact lower than what was determined. Since the surface recombination velocity is the more uncertainly defined quantity, values of lifetime were recalculated for a higher s in the case of the Westinghouse samples in order to observe the sensitivity of the observed correlation to choice of s. Results are shown in Figure A-3. The correlation does not appear markedly reduced as a result of the 12% change in assumed value of s.

The subjective impressions may be confirmed by analytical treatment. The correlation coefficient for two random variables x and y is defined by the equation

$$P_{xy} = \frac{\frac{1}{n}\sum_{i=1}^{n}(x_i - \bar{x})(y_i - \bar{y})}{\sigma_x \sigma_y} \qquad (13)$$

where $\bar{x}$ and $\bar{y}$ are the mean values of the distribution of x and y, and σ_x and σ_y are the standard deviations. For all of the Westinghouse lifetime data in which lifetimes exceed 0.5 μs, a correlation coefficient of 0.76 was found. A reasonably strong correlation is seen to exist. The Monsanto data, by contrast, show a correlation coefficient of 0.25 (all of the Monsanto lifetime data were included in this calculation). The evidence for a correlation here is considerably weaker, possibly due to the fact that the mean sample thickness tends to be about 20% greater. For the Westinghouse data which were recalculated with a larger surface recombination velocity, a correlation coefficient of 0.80 was determined. This is higher than that determined for the lower surface recombination velocity, but it should be kept in mind that the earlier

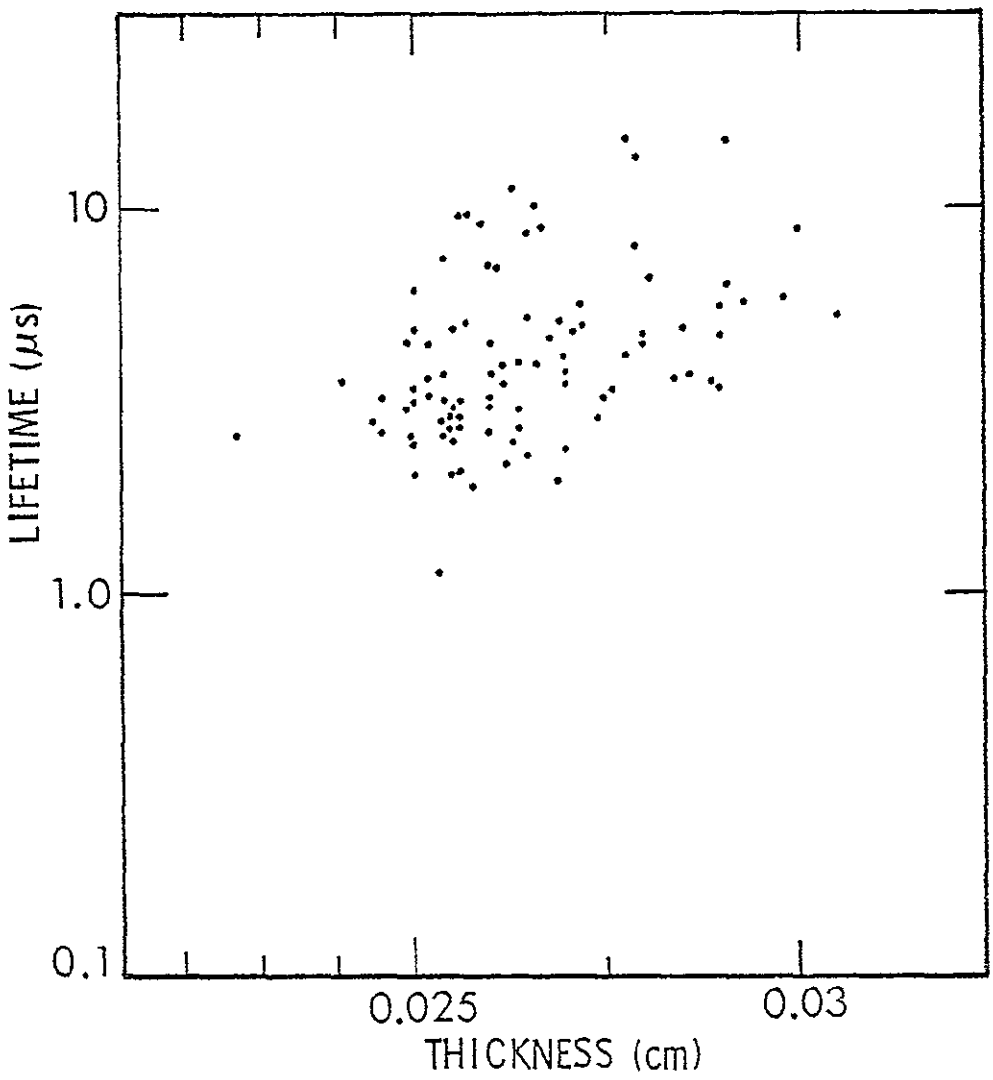

Figure A-3. Distribution of lifetimes calculated with s = 9.3 x 10^3 cm/sec for Westinghouse bulk samples. Only those samples with lifetimes in excess of 1.5 μs were recalculated.

calculation included a larger data set. For the recalculated data, the correlation does appear to be reduced, as seen by comparing Figures A-1 and A-3.

In view of the strong correlation that is observed, it would be of interest to make a direct determination of the generation rate as well as a direct determination of the surface generation velocity, rather than the indirect determinations which we felt compelled to make. If such a determination continues to yield a correlation of lifetime with sample thickness, then perhaps the conclusion would be justified that the correlation is either "accidental" or a "true" correlation, unrelated to any systematic errors in the measurement.

APPENDIX B
COMPARISON OF LIFETIME AND DIFFUSION LENGTH MEASUREMENT METHODS

The bulk samples for which lifetimes were determined in this program were obtained from ingots which were also characterized by other contractors. The devices on which diffusion lengths have been determined have likewise been studied by other methods. This affords a good opportunity, therefore, to assess the correlation among the various techniques for the purpose of establishing a range of usefulness for each of the methods. We have hence undertaken a comparison of our measurements with those of the Westinghouse group.

A graphical comparison of Westinghouse photoconductivity decay (PCD) lifetime results and Northrop steady-state photoconductivity (SSPC) data is shown in Figure B-1. A general tendency for the Westinghouse lifetime values to be the larger is observed. This is quite possibly due to the fact that the Westinghouse PCD measurements were carried out at somewhat higher

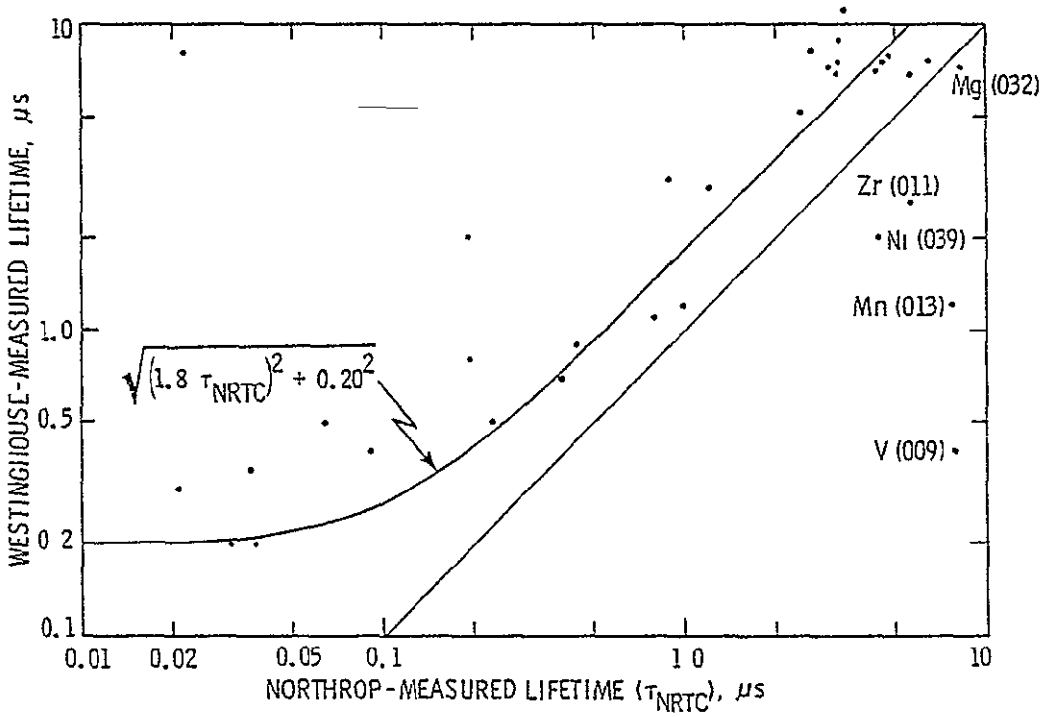

Figure B-1. Comparison of Westinghouse PCD lifetime and Northrop SSPC measurements.

injection levels than the Northrop SSPC measurements, in which the objective was to determine the low-injection-level limit of lifetime. On the one hand, it is difficult to obtain very low injection-level PCD lifetimes at short lifetimes, and at moderate-to-low resistivities, and, on the other hand, it can be argued that the higher injection-level measurements are more appropriate in any case to solar cell operation. Our rationale in determining the low-injection-level limit of lifetime is that this quantity is the most relevant for analytical purposes.

It is also observed that in a few cases, the Northrop lifetime values are significantly higher than the Westinghouse values. In these cases, which have been identified in the figure with the secondary impurity and ingot number, trapping was so severe in the SSPC measurements that a legitimate lifetime measurement was not possible. That is, true plateau values were not reached as the background light intensity was increased. The data were nevertheless recorded as being our best values. In the event of very severe trapping, PCD may therefore yield a value of lifetime which is more accurate than the SSPC value. In the presence of a modest amount of trapping, however, the SSPC method yields better values. The distinction between these cases is always directly apparent in the SSPC measurements. Since trapping was found to be ubiquitous in the measured samples, it is likely that trapping is also responsible for the general tendency for the Westinghouse PCD lifetimes to be larger than the SSPC lifetimes.

At the shortest lifetimes measured, Westinghouse data were limited instrumentally to about 200 ns, presumably due to the finite decay time of the LED pulse used for excitation. In Figure B-1 we have shown an empirical curve which expresses the observed relationship between the data sets, taking into account the instrumental limitation, and weighting the long-lifetime data in the comparison. An approximate ratio of 1.8 between the respective sets of lifetime values is indicated. We have also shown a curve which would be obtained if the data corresponded precisely It should be kept in mind that the samples used in the respective measurements were not identical, but only

derived from the same ingots, many of which exhibited considerable variation in lifetime over their length. The Northrop lifetime values given in Figure B-1 are averages over all of the samples from a particular ingot.

Device measurements of lifetime are compared in Figure B-2. Shown are Westinghouse measurements of open-circuit decay (OCD) lifetime and lifetimes derived from Northrop measurements of diffusion length, performed on the same devices. A curve is shown which would have been observed if the data corresponded precisely. In fact, the same tendency of the transient data to yield larger lifetimes than steady-state methods as was seen in Figure B-1 is also noted here. This tendency appears not to be sustained at long lifetime, but this is so only because the Westinghouse lifetime values were not corrected for recombination at the back surface. At short lifetimes, an instrumental factor appears to be limiting the measured transient lifetimes to something in excess of 100 ns. Again, the sets of data seem to be related by a scale factor of about 2, which is ascribed (as before) to trapping effects on the transient lifetimes and to the fact that the transient measurements were undoubtedly conducted at somewhat higher injection level than the steady-state diffusion length measurements.

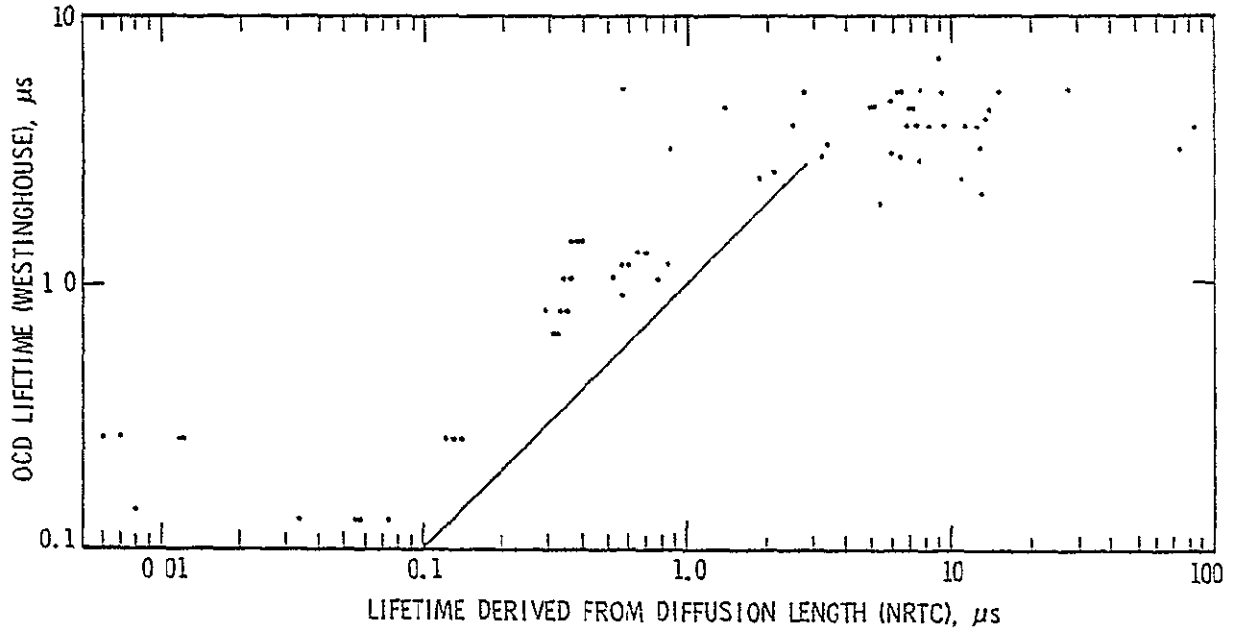

Figure B-2. Comparison of Westinghouse measurements of OCD lifetime and lifetime derived from Northrop diffusion length measurements.

A comparison of Westinghouse measurements of short-circuit current under broadband (AM(1)) illumination and Northrop measurements of diffusion length is shown in Figure B-3. In the range of diffusion lengths where this parameter is expected to be determinative for short-circuit current, excellent correlation is indeed observed. At longer diffusion lengths, the short-circuit current ceases to be sensitive to the diffusion length.

A similar comparison of cell efficiency and measured diffusion length is shown in Figure B-4. Again, reasonable correspondence is observed in that region in which cell efficiency is expected to be dominated by the diffusion length. It is also clear from this figure that cell efficiency is not as sensitive a measure of material quality as is the diffusion length itself. Over a factor of 2 range in cell efficiency, the diffusion length varies by a factor of about 8. It is also apparent that cell efficiency, as well as short-circuit current under broadband illumination, is insensitive to base material quality in the range of 100 μm in diffusion length, whereas one would generally wish to extend the range to at least 300 μm. It is therefore both desirable and necessary to go beyond measurements of cell parameters under broadband illumination conditions. The simple expedient of using filtering to produce highly penetrating irradiation permits one to make short-circuit current measurements of diffusion length using the same station ordinarily used for cell parameter measurements, provided that signal-recovery circuitry is sufficiently sensitive, and given the availability of a suitable calibration solar cell of optical properties identical to those of the test devices.

The comparisons presented above among measurements made using a variety of experimental techniques generally show the degree of correspondence which is to be expected under the given experimental conditions In our estimation, the preference of a steady-state method of lifetime measurement over a transient method appears to be demonstrated for relatively poor material which is characterized by trapping, except when the latter is very severe. Short lifetimes are more easily measured, and the effect of traps is observed

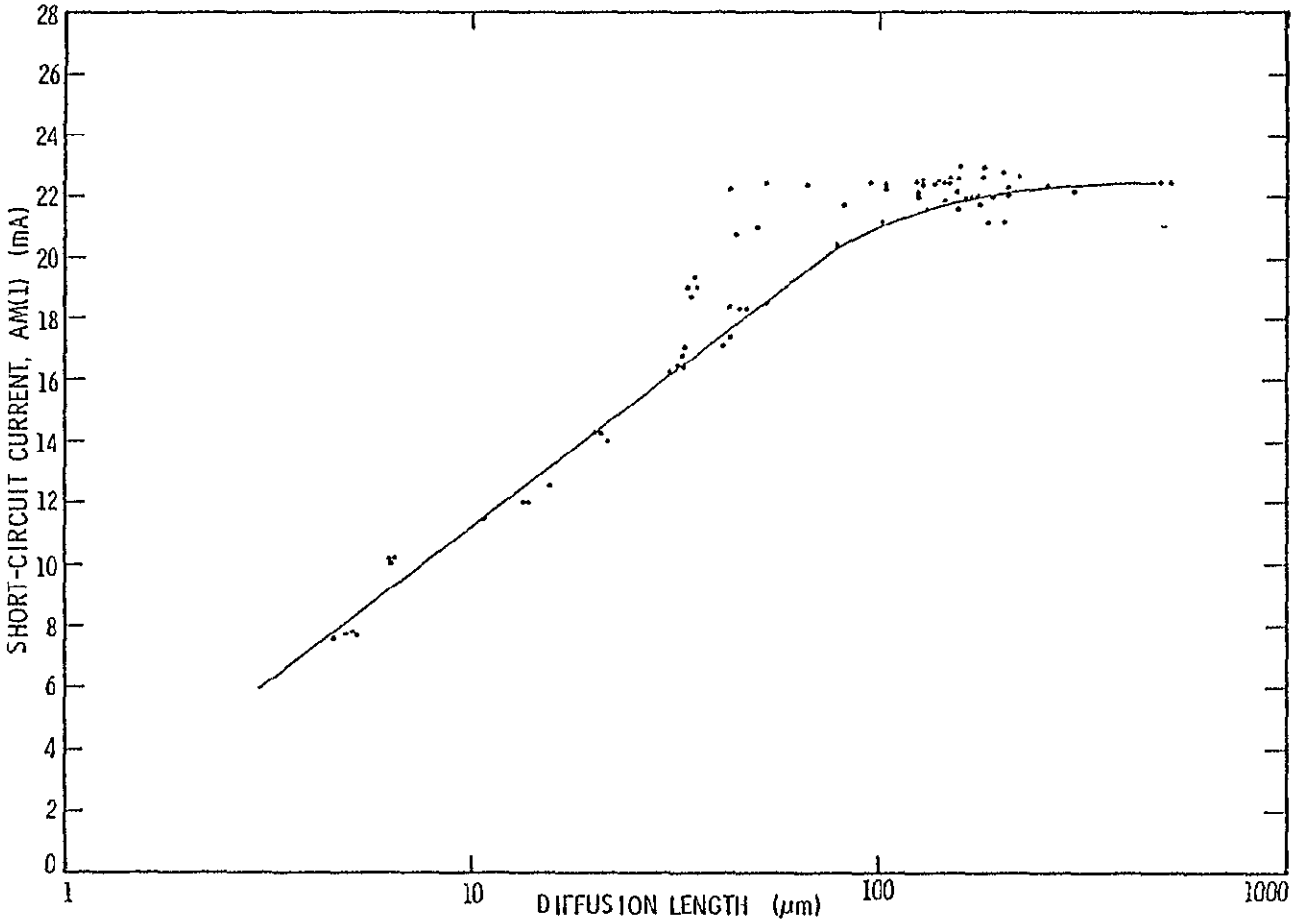

Figure B-3 Comparison of Westinghouse measurements of short-circuit current and Northrop measurements of diffusion length.

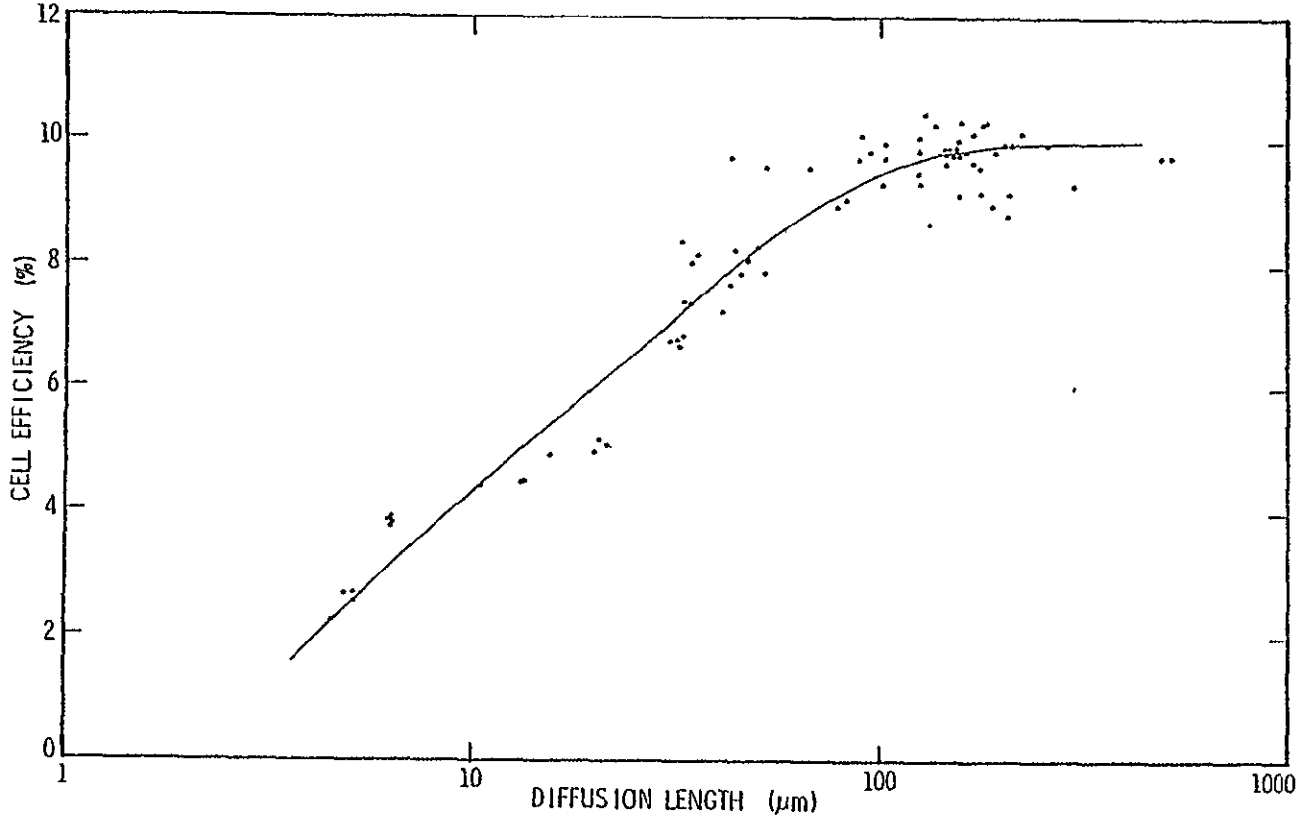

Figure B-4. Comparison of Westinghouse cell efficiency measurements with Northrop diffusion length measurements.

directly. With respect to device measurements, the desirability of making steady-state measurements of diffusion length rather than transient measurements of lifetime is apparent, in view of the susceptibility to trapping of the latter. Whenever base material quality is being studied, such a determination is also preferable to conventional measurements of cell parameters.

REFERENCES

1. J.R. Srour, S. Othmer, K.Y. Chiu, IEEE Trans. Nucl. Sci. 22, 2656 (1975).

2. J.R. Srour, S. Othmer, K.Y. Chiu, and O.L. Curtis, Jr., "Damage Coefficients in Low-Resistivity Silicon," NASA CR-134768 (1975).

3. W.W. Gartner, Transistors, Principles, Design, and Applications, (D. VanNostrand Co., Inc., Princeton, 1960).

4. O.L. Curtis, Jr., Phys. Rev. 172, p.773 (Aug. 1968).

5. A. Many, Y. Goldstein, and N.B. Grover, Semiconductor Surfaces, (North Holland Publishing Co., Amsterdam, 1965), p. 259.

6. R.H. Hopkins, J. R. Davis, P. Rai-Choudhury, P. D. Blais, J. P. McHugh. R.G. Seidensticker, and J. R. McCormick, Fifth Quarterly Report, Silicon Materials Task, ERDA/JPL-954331-77/1, p. 24.

7. A. G. Milnes, Deep Impurities in Semiconductors, (Wiley, New York, 1973), p. 167.

8. W. Rosenzweig, Bell System Tech. J. 41, 1573 (1962).

9. J.H. Reynolds and A. Meulenberg, Jr., J. Appl. Phys. 45, 2582 (1974).

10. J.A. Wall and E.A. Burke, "Gamma Dose Distributions at and near the Interface of Different Materials," IEEE Trans. Nucl. Sci. 17, 305 (1970).

11. E.A. Burke, J.R. Cappelli, L.F. Lowe, and J.A. Wall, "Solar Cell Radiation Response near the Interface of Different Atomic Number Materials," NASA TM X-2440 (1972).

12. J.A. Wall and E. A. Burke, "Dose Distributions at and near the Interface of Different Materials Exposed to Cobalt-60 Gamma Irradiation," AFCRL-TR-75-0004 (1974).

13. S. Othmer and O.L. Curtis, Jr.,"Scanning Electron Microscope Measurements of Diffusion Length in Neutron-Irradiated Silicon," IEEE Trans. Nucl. Sci. 20, 204 (Dec. 1973).

14. W.H. Hackett, Jr., J. Appl. Phys. 43, 1649 (1972).

15. R.F. Bass and O.L. Curtis, Jr.,"Effects of Impurities on Carrier Lifetime in Bulk Solar Cell Material," Report NCL-69-29R, p. 21 (1969).

16. J.R. Srour, "Stable Damage Comparison for Neutron-Irradiated Silicon," IEEE Trans. Nucl. Sci. 20, 190 (Dec. 1973).

17. V.G. Weizer and C.W. Andrews, Scanning Electron Microcopy 1, 183 (1977).

18. H. Gutsche, D E. Hill, Final Report, Silicon Materials Task, ERDA/JPL-954338-76, pp. 61-62.